Radiation tolerant fiber optic humidity sensors for High Energy Physics Applications

Dottorato di Ricerca in “Ingegneria dell’informazione”
XXVII Ciclo
Universita’ degli Studi del Sannio
Dipartimento di Ingegneria

2015, December 15th

Tutors
Prof. Andrea Cusano
Ing. Paolo Petagna
Co-tutor
Dr. Marco Consales

Candidate
Gaia Maria Berruti

ABSTRACT

This work is devoted to the development of fiber optic humidity sensors to be applied in high-energy physics applications and in particular in experiments currently running at CERN.

The high radiation level resulting from the operation of the acce - lerator at full luminosity can cause serious performance deterioration of the silicon sensors which are responsible for the particle tracking. To increase their lifetime, the sensors must be kept cold at temperatures below 0 °C. At such low temperatures, any condensation risk has to be prevented and a precise thermal and hygrometric control of the air filling and surrounding the tracker detector cold volumes is mandatory.

The technologies proposed at CERN for relative humidity monitoring are mainly based on capacitive sensing elements which are not designed with radiation resistance characteristic. In this scenario, fiber optic sensors seem to be perfectly suitable. Indeed, the fiber itself, if properly selected, can tolerate a very high level of radiation, optical fiber transmission is insensitive to magnetic field and electromagnetic noise and it is perfectly suited for read-out over very long distances. Although many different approaches to humidity measurements through optical fibers have been reported in literature, no commercial sensor of this family is available on the market, and only a few approaches have proved really conclusive performances for a practical application out of the laboratory environment.

In 2011, our multidisciplinary research group has been involved in the development of new generation of relative humidity fiber optic-based sensors at CERN.

Investigations were originally concentrated on polyimide-coated Fiber Bragg Gratings and gave for the first time the experimental demonstration of the possibility to use them at low temperatures as well as in presence of strong ionizing radiations. For this reason, this platform has been selected for the hygrometric control of the air in critical areas of the Compact Muon Solenoid experiment: 72 fiber optic-based thermo-hygrometers, organized in arrays, have been installed in the detector and are currently providing a full map of temperature and humidity in front of the tracker volume.

Furthermore, a second generation of high-sensitivity titanium dioxide-coated Long Period Grating-based humidity sensors has been recently proposed. Preliminary results are very encouraging and are evidencing the strong potentialities of the proposed technology in light of its application in the particles tracking detectors of the future.

KEYWORDS

Relative humidity monitoring, thermo-hygrometers, fiber optic sensors, Fiber Bragg Grating, Long Period Grating, radiation tolerance, Compact Muon Solenoid, CERN.

SOMMARIO

Oggetto di questo lavoro di tesi è lo sviluppo di sensori in fibra ottica per il monitoraggio dell'umidità in ambienti della fisica ad alta energia, con particolare riferimento a uno dei quattro esperimenti principali dell'acceleratore del CERN di Ginevra, quale il Compact Muon Solenoid.

L'elevato livello di radiazioni dovuto all'intensa attività dell'acceleratore potrebbe danneggiare i sensori in silicio, responsabili della tracciatura delle particelle. Al fine di mitigare tali effetti e incrementarne la durata della vita, tali sensori sono raffreddati a temperature al di sotto di 0 °C. Tuttavia, a basse temperature, è necessario prevenire fenomeni di condensazione che potrebbero compromettere il corretto funzionamento di tutta l'elettronica disponibile in situ. Da qui deriva l'esigenza di implementare un costante controllo igrometrico della qualità dell'aria nel volume del tracciatore dell'esperimento.

Le tecnologie proposte in passato al CERN per il monitoraggio di umidità relativa si basano essenzialmente su sensori commerciali capacitivi, non qualificati per operare in ambienti ad alta radiazione.

In questo scenario, i sensori in fibra ottica appaiono come un'ottima alternativa: infatti, se opportunamente selezionata, la fibra ottica è in grado di resistere a elevati livelli di radiazione; la trasmissione in fibra è insensibile a campi magnetici e rumore elettromagnetico ed è perfettamente idonea per read-out su lunghe distanze.

Diversi tipi di sensori in fibra ottica sono stati proposti in letteratura negli ultimi vent'anni per il monitoraggio di umidità relativa. Tuttavia nessun sensore di questo tipo è disponibile sul mercato e solo pochi approcci hanno fornito risultati conclusivi sull'utilizzo di tali dispositivi in ambienti reali, al di fuori delle condizioni controllate, tipiche di un laboratorio sperimentale.

Nel 2011, il nostro gruppo di ricerca interdisciplinare è stato coinvolto nel progetto di sviluppo di una nuova generazione di sensori di umidità per gli esperimenti attivi al CERN.

Le nostre attività di ricerca si sono concentrate inizialmente sui reticoli di Bragg rivestiti di un sottile strato di poliimmide. Con i risultati collezionati, abbiamo dimostrato per la prima volta in letteratura che questi dispositivi sono in grado di lavorare correttamente a basse

temperature, anche a seguito di ripetute esposizioni ad elevate dosi di radiazioni ionizzanti.

Per questa ragione, questa piattaforma tecnologica è stata selezionata come soluzione del problema del controllo igrometrico dell'aria in aree critiche dell'esperimento CMS: 72 termo-igrometri in fibra ottica, organizzati in array, sono attualmente installati nel rilevatore, e forniscono una mappa puntuale e precisa della temperatura e dell'umidità all'interno del volume del tracciatore.

Inoltre, nell'ambito della stessa collaborazione, è stato recentemente lanciato lo sviluppo di una seconda generazione di sensori di umidità, altamente sensibili, basati sulla tecnologia dei reticoli a passo lungo. I risultati preliminari sono molto incoraggianti: la tecnologia proposta, infatti, sta mostrando delle grandi potenzialità in termini di sensibilità all'umidità e resistenza a radiazione, proponendosi come candidata al controllo igrometrico nei rilevatori di particelle del CERN del futuro.

PAROLE CHIAVE

Monitoraggio di umidità relativa, termo-igrometri, sensori in fibra ottica, reticolo di Bragg, reticolo a passo lungo, tolleranza a radiazioni, Compact Muon Solenoid, CERN.

ACKNOWLEDGMENTS

This work could not have been possible without the great support that I received from many people over the years.

First of all I would like to thank my thesis director, Prof. Andrea Cusano, who gave me the opportunity to start this adventure in 2011, welcoming me in his amazing research group in University of Sannio and introducing me to new people, new concepts and new technologies. His experience, his advices and his intuitions have successfully guided my work in the last years, even at thousands kilometers away, and made me grow up from both personal and professional points of view.

Many many (and many more) thanks to Paolo Petagna, my CERN supervisor, who gave me the chance to join his working group and to become part of the coolest Cooling Team ever. Thanks Paolo, for the time, guidelines and resources spent for our project and for my training! Thanks for always listening to me, answering to my doubts, trusting and motivating my work from the first day I arrived at CERN!

I am also grateful to my supervisor-colleague-friend Marco Consales, who knows me since the time of High schools, for all the time spent on Skype or in the office discussing about data analysis and papers reviews and submissions. Thank you, Marco, for always reacting to my SOS signals.. and thanks for all the coffees together, for which you never let me pay!

My deep gratitude goes to Salvatore Buontempo, helpful tutor and friendly guide along these years at CERN. With his "propagating" enthusiasm and optimism, he has always been a source of precious suggestions for me.

I also would like to acknowledge Dr. Michele Giordano and Dr. Anna Borriello from the Institute for Polymers Composite and Biomaterials (CNR Naples) and Prof. Gianluca Breglio from University Federico II of Naples for the their technical and scientific support.

I am also indebted to the team of OptoSmart s.r.l., and in particular to Armando Laudati, for providing technical assistance whenever I needed, and for the procurement and assembly of the FBG-based sensors arrays for the CMS experiment.

I am grateful to the full Detector Technology group of the Physics Department at CERN. In particular, thanks to Mar Capeans Garrido and Andrea Catinaccio, for welcoming me into the group and supporting the project; thanks to Veronique, who has always had the correct answer to each administrative/organizational issue and to Raphael Dumps and Jerome Noel for their technical support in the laboratory.

Thanks to the Hungarian crew installed at CERN, represented by Zoltan, Noemi and Alajos (simply Ali' for me), for all the time spent together splicing fibers and checking gratings. Thanks for the efforts made in designing and implementing the optical fiber sensors acquisition system which we are using in CMS and for being always at my disposal, whenever I was calling.

A special mention goes to Francesco Palmonari and Alexander Kaminskiy for the help provided during the installation of the thermo-hygrometers in the CMS experiment.

Thanks to the old and new "Cool-ing" colleagues and friends, Paola, Lukasz, Bart, Alessandro, Maciej & Ala, Andrea, Kacper, Michal, Piotr, Claudio, Dina, Nicola, Riccardo and Tiago for all the time spent together inside and outside the working hours. And sorry if I am forgetting someone. We are many!

I also would like to mention the guys of the Optoelectronic group from University of Sannio, who have often hosted me in the lab. Thanks to Alberto, Antonio, Francesco, Angelo, Giuseppe and all the others!

Thanks to my "extended" family in Geneva for making my stay abroad enjoyable and for cheering me up when I needed. Grazie Raffaello, Marco, Tessa, Tiziana, Aniello, Camille, Francesco, Cheryl, Vincent, and Stefano! It has been a privilege to share this amazing experience with you!

Huge thanks go to Jerome, Pietro and Giulia, the "pillars" of my days at work, and not just this! Guys, I know that it has been difficult to survive against my noise and my loud voice.. You managed, without too many complains! Thank you! Thanks for always being there and for having adopted me! And Giulia, I really thank you very much! My experience in Geneva would not have been the same without you!

Grazie ad Antonella, compagna di avventure e sventure da 18 anni. Ce l'abbiamo fatta anche questa volta, insieme!

Grazie a Marco, che con affetto mi ha supportato e soprattutto sopportato ogni giorno, con il suo buonumore e con la sua spiccata ironia, soprattutto nei momenti piu' difficili.

Un ringraziamento speciale va alla mia famiglia, che mi ha seguito, sostenuto e incoraggiato giorno dopo giorno, non facendomi mai sentire sola, e a Salvatore, per il suo grande amore, per la sua costante presenza e per la sua immensa pazienza.

Grazie a Gioia, Giovanni e Sara, i miei tre splendidi portafortuna.

Finally, I would like to acknowledge the CMS experiment and University of Sannio, who co-financed my Doctoral Student Program at CERN, together with the Detector Technology group of the Physics Department.

Thanks, Merci, Grazie!

Geneva, December 2015

CONTENTS

LIST OF FIGURES

LIST OF TABLES

PREFACE

Relative humidity monitoring has a significant impact in various application fields and many sensing schemes and solutions have been proposed according to the specific applications over the years. In this work we concentrate our attention about the use of fiber optic sensors for humidity monitoring in high energy physics environments, such as the Compact Muon Solenoid, one of the main experiments of the accelerator running at CERN in Geneva.

In particular, in 2011, our multidisciplinary research group has been involved in the development of a new generation of fiber optic-based relative humidity sensors at CERN.

Investigations originally concerned polyimide-coated Fiber Bragg Gratings and gave for the first time the experimental demonstration that this innovative technology may be a robust alternative to standard commercial hygrometers. After a few years of development, 72 optical thermo-hygrometers organized in multi-sensors arrays, have been installed in CMS in December 2013 and they are currently providing constant monitoring of temperature and relative humidity. However, experience in operation has shown some limitations of the coated FBG-based sensors, which will be fully detailed in this work.

To overcome these limitations, we recently proposed an innovative class of optical relative humidity optical sensors, based on high-sensitivity titanium dioxide-coated Long Period Grating. Preliminary results collected at CERN from 2013 in collaboration with University of Sannio and the Institute for Polymers Composite and Biomaterials (National Research Council in Naples) on samples produced in-house are very encouraging, evidencing the great potential of TiO_2-coated LPG sensors, in terms of high relative humidity sensitivity, high accuracy in the low relative humidity range and tolerance to strong γ-ionizing radiations.

In this thesis, our developments and studies on optical devices based on both the FBG and LPG technologies for applications of relative humidity monitoring are presented.

THESIS OUTLINE

After a brief introduction about the European Organization for Nuclear Research, the main motivations for a precise thermo-hygrometric control of the air in the experiments running at the accelerator in Geneva as well as the technical specifications that any humidity sensors should satisfy in order to be installed in such harsh environments are specified in Chapter 1.

In Chapter 2, the fiber optic sensing technology is introduced, with a particular focus on the so-called Fiber Bragg Grating-based sensors, which we found to have a strong potential in applications of relative humidity monitoring, as a good alternative to the traditional commercial sensing devices.

In Chapter 3 results of our deep investigations concerning the use of coated FBGs for relative humidity monitoring in high radiation environments are presented, with the sensors fully characterized in terms of sensitivity, repeatability, hysteresis and time response, before and after their exposure to high γ-ionizing radiation doses.

The results of the first months of operation of 72 FBG-based thermo-hygrometers installed in the CMS experiment from 2013 are provided in Chapter 4; the limits and the benefits of this technology in view of our on-field experience are also discussed.

In order to overcome the limitations of the FBG technology, we propose in Chapter 5 a new generation of optical high sensitivity metal oxide-coated Long Period Grating-based sensors. The main differences and advantages of LPG-based sensors compared to the FBG technology are also provided.

Finally, general conclusions and perspectives for this research work are discussed in Chapter 6.

1 RELATIVE HUMIDITY SENSORS FOR HIGH RADIATION EXPERIMENTS AT CERN

In this chapter we provide an overview of the main experiments running at the CERN accelerator in Geneva and we give the main motivations for a precise hygrometric control of the air in the particles detectors as well as the technical specifications that each new humidity sensor should comply with in order to be used in this context.

In particular, a careful analysis of the main features of standard electronic hygrometers available on the market is presented, demonstrating that no commercial device is suitable for applications in harsh radiation environments. This has addressed our investigations in this research field with the aim to design, develop and characterize a novel generation of relative humidity sensors based on optical fibers.

1.1 CERN AND THE LARGE HADRON COLLIDER

The European Organization for Nuclear Research [1] operates the world's leading laboratory for particle physics.[1] It was founded in 1954 [2] and it has become a prime example of international collaboration, with currently 21 member states. Additional nations from around the globe also contribute to and participate in the research program.

Research at CERN focuses on fundamental physics, finding out what the Universe is made of and how it works. The instruments used to carry out this kind of investigations are purpose-built parti-

1 The name CERN is derived from the acronym for the French "Conseil Européen pour la Recherche Nucléaire", a provisional body founded with the mandate of establishing a world-class fundamental physics research organization in Europe. Originally, the physics research was concentrated on understanding the inside of the atom, hence the word "nuclear". Today, the understanding of matter goes beyond the nucleus, and CERN main area of research is particle physics that is to say the study of the fundamental constituents of matter and the forces acting between them. For this reason the laboratory operated by CERN is often referred to as the European Laboratory for Particle Physics.

2 The European Organization for Nuclear Research was founded by the Convention for the Establishment of a European Organization for Nuclear Research that was signed on 1 July 1953 by 12 European States - Belgium, Denmark, Federal Republic of Germany, France, Greece, Italy, Netherlands, Norway, Sweden, Switzerland, United Kingdom, Yugoslavia - and came into effect on 29 September 1954.

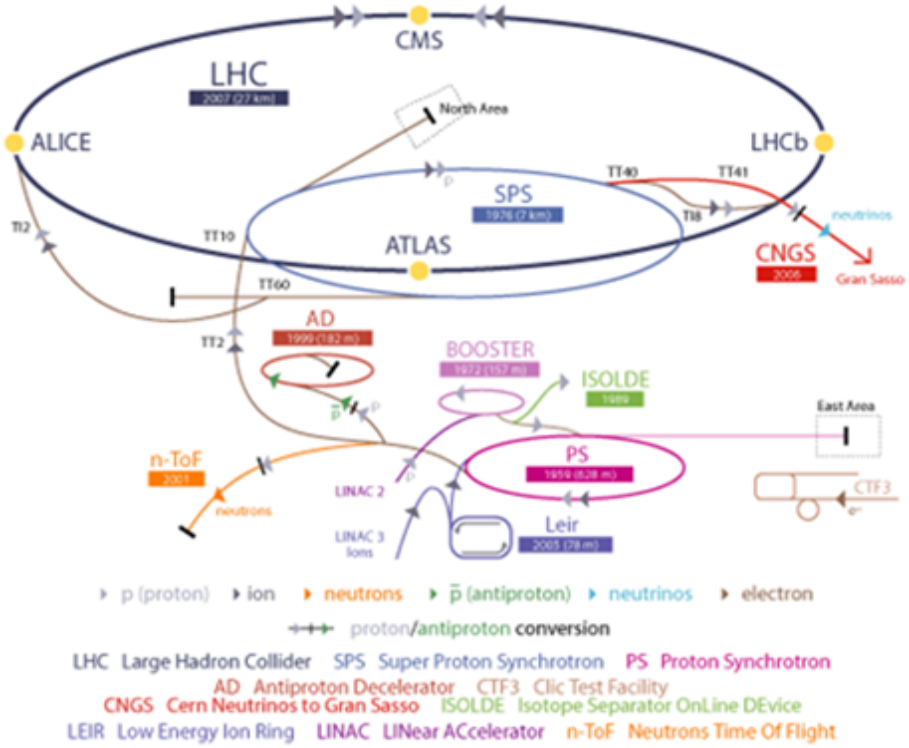

Figure 1.1: CERN's accelerators complex

cle accelerators and detectors: accelerators boost beams of particles to high energies before collisions; detectors observe and record the results of these collisions. As a matter of fact, the accelerator complex at CERN is a succession of machines that accelerate particles to increasingly higher energies. Each machine boosts the energy of a beam of particles, before injecting the beam into the next machine in the sequence. The proton source is a simple bottle of hydrogen gas and an electric field is used to strip hydrogen atoms of their electrons to yield protons.

Fig. 1.1 shows the scheme of the beam circulation in the complex apparatus of accelerators at CERN. First, the protons are introduced in the Linear Accelerator, which accelerates them up to 50 Mev of energy. The beam is then injected into the Proton Synchrotron Booster, where the particles are sped up to 1.4 Gev and later introduced in the Proton Synchrotron. The Proton Synchrotron pushes the protons up to 25 Gev and packs them in bunches separated by 25 nanoseconds each. The Super Proton Synchrotron is responsible to accelerate the beams up to 450 Gev.

The last element of the chain is the Large Hadron Collider [3] [2], housed in a 27 kilometers long tunnel, located between 45 and 170 meters below the surface, crossing the border between France and Switzerland, which is the largest and most powerful particle accelerator of the world. [4]

In particular the protons are transfered to the LHC in two separated vacuum beam pipes: in one pipe the beam circulates clockwise while, in the other, it circulates anticlockwise.

The protons are kept on orbit during the acceleration by a strong magnetic field maintained by superconducting electromagnets which are cooled using liquid helium at 1.9 K. Thousands of magnets of different varieties and sizes are used to direct the beams around the accelerator. These include 1232 dipole magnets, 15 meters in length, which bend the beams,and 392 quadrupole magnets, from 5 to 7 meters long each, which focus the beams.

Picture shown in Fig. 1.2 reports the view of LHC's main tunnel.

Seven experiments have been constructed at the LHC, located underground in large caverns excavated at the Interaction Points [5]. They are run by collaborations of scientists from institutes all over the world and use their own detectors to analyze the particles produced by collisions in the accelerator.

The biggest LHC experiments are ATLAS and CMS, which use general-purpose detectors to investigate the largest range of physics possible [6]. ALICE and LHCb have detectors specialized for focusing on specific phenomena. [7]

3 The accelerator complex also includes the Antiproton Decelerator for studies of antimatter and the Online Isotope Mass Separator facility for the systematic study of atomic and nuclear properties and exotic decays far from the line of stability. It also feeds the CERN Neutrinos to Gran Sasso project and the Compact Linear Collider test area, as well as the neutron time-of-flight facility. Protons are not the only particles accelerated in the LHC. Lead ions for the LHC start from a source of vaporized lead and enter LINAC3 before being collected and accelerated in the Low Energy Ion Ring. They then follow the same route to maximum energy as the protons.

4 The first research run of LHC took place from 30 March 2010 to 13 February 2013 at an initial energy of 3.5 teraelectronvolts (TeV) per beam, rising to 4 TeV per beam from 2012. It took 4 minutes and 20 seconds to fill the LHC ring, and 20 minutes for the protons to reach their maximum energy of 4 Tev. After an almost two years shutdown period for planned upgrades and re-commissioning, collisions have restarted in the upgraded collider on 5 April 2015, reaching the full specified operating energies of 7 TeV per beam on 20 May 2015. In a such configuration, it takes less than 90 microseconds for a proton to travel once around the main ring with a speed of about 11000 revolutions per second and interactions between the two beams takes place at discrete intervals, mainly 25 nanoseconds apart.

5 The region at the center of the experiment, where the particle beams accelerated in the LHC are brought into collision is conventionally called the "Interaction Point".

6 CMS and ATLAS experiments have the same scientific goals but they use different technical solutions and a different magnet-system designs.

7 The three smallest experiments are TOTEM, LHCf and MoEDAL.

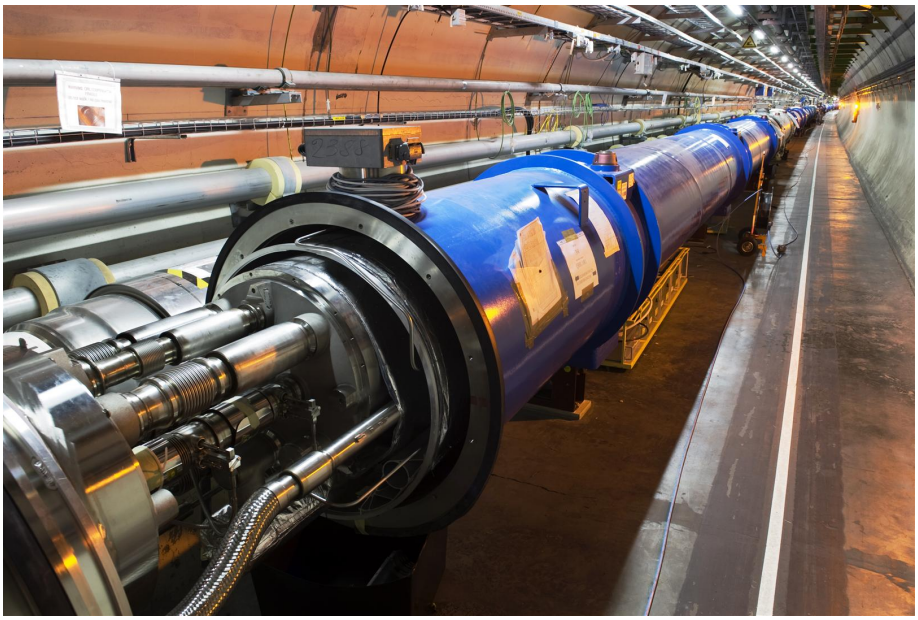

Figure 1.2: view of the LHC's main tunnel

Fig. 1.3 shows the location of the LHC across the French and Swiss border and the four access points corresponding to the main four experiments. Fig. 1.3 reports the real pictures of the four main experiments running at CERN.

1.2 THE COMPACT MUON SOLENOID

The Compact Muon Solenoid [3] is a general-purpose experiment, as its research program includes most of the physics at the LHC accelerator, ranging from the Standard Model measurements to the Higgs Boson and new physics researches concerning the dark matter.

The full CMS detector is 20 meters long and 15 meters in diameter and weighs 14000 tons. [8] It takes its name from the superconducting solenoid generating an internal magnetic field of 3.8 Tesla, which allows a compact design of the detector, and from the muon system located outside the solenoid, which ensures excellent muon triggering and identification.

Like mostly modern detectors linked to particles accelerators, CMS has a layered "onion" structure, as shown in Fig. 1.5: as a matter

8 The CMS experiment is located in an underground cavern at Cessy in France, just across the border from Geneva.

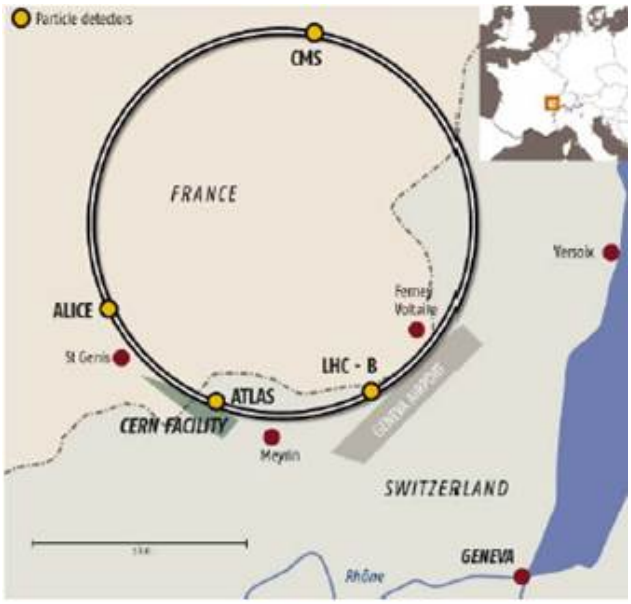

Figure 1.3: Location of the LHC accelerator across the French and Swiss border and the main four LHC experiments

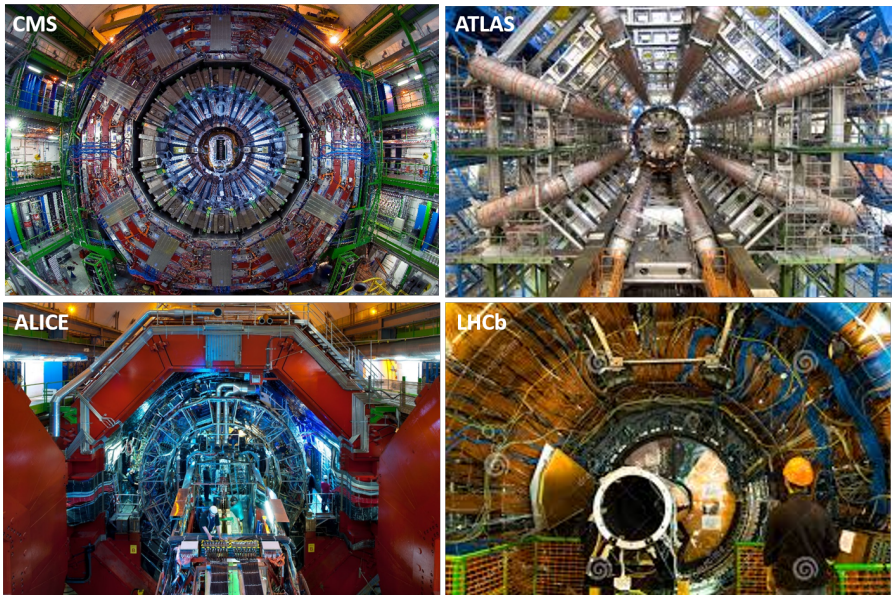

Figure 1.4: Pictures of the four main experiments running at the LHC accelerator

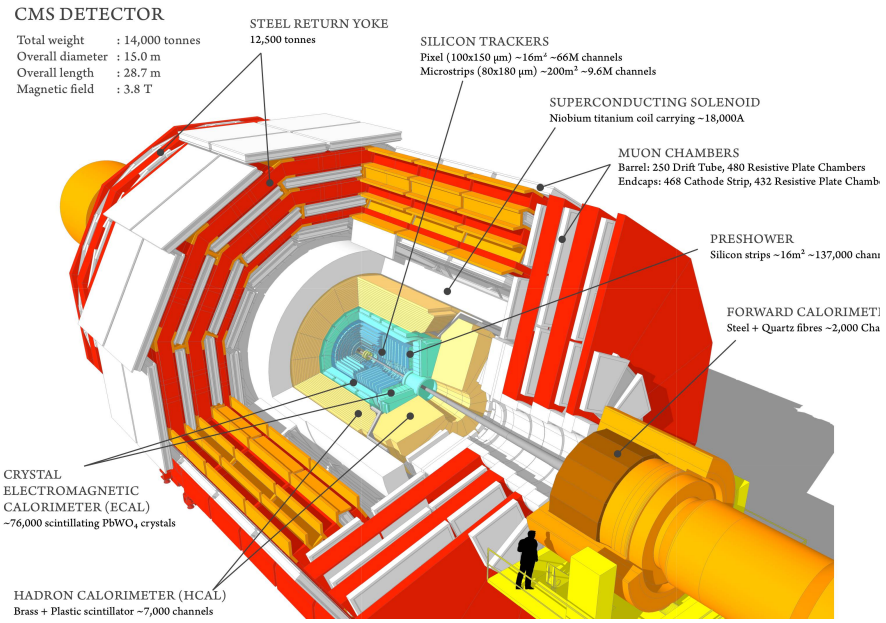

Figure 1.5: Schematic view of the CMS detector at LHC

of fact different types of detectors, in a cylindrical form, are nested within one another, like a series of Russian matrioshka dolls. [4] [9]

1.2.1 Detector overview

A particle emerging from the collision and traveling outwards first encounters the CMS tracking system. It is made of silicon pixels and silicon strip detectors which accurately measure the positions of passing charged particles allowing physicists to reconstruct their tracks and to measure their momentum, as it will be discussed in the next section.

The energies of the particles are measured in the next layer of the detector, the so-called calorimeters. In particular, the first calorimeter is the Electromagnetic Calorimeter, which measures the energy of photons and electrons; on the other hand the Hadron Calorimeter is designed principally to collect and measure the energy associated to any particle made up of quarks.

The outer part of the detector, the iron magnet "return yoke", confines the magnetic field and stops all remaining particles except for muons which are tracked further outside, in dedicated muon chamber detectors.

9 An unusual feature of the detector is that instead of being built in-situ underground, like the other giant detectors of the LHC experiments, it was constructed on the surface, before being lowered underground in several sections and reassembled.

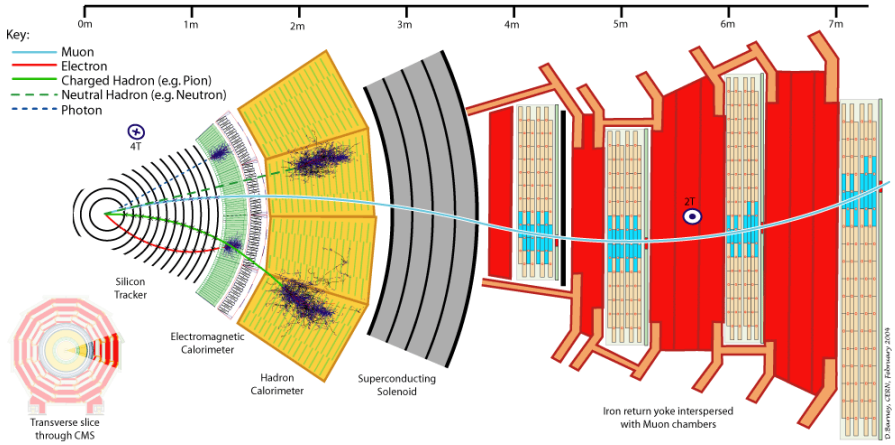

Figure 1.6: Trasversal view of CMS depicting the detector's components and the response of each layer to different types of particles

Each consecutive detector layer in the experiment is more voluminous and more massive. This comes quite naturally, as the Tracker, which is the innermost part, measures the precise particle tracks without influencing them, while the calorimeters absorb the particles to measure their energy.

A transversal view of CMS experiment depicting the "signature" of different types of particles detected in each layer is shown in Fig. 1.6.

1.2.2 The tracking system

The inner tracking system of CMS [5, 6] is designed to provide a precise and efficient measurement of the trajectories of charged particles emerging from their collisions. It surrounds the Interaction Point and has a length of 5.8 m and a diameter of 2.5 m. The full volume is enclosed in the superconducting solenoid generating a homogeneous 4 T magnetic field.

At the LHC design luminosity [10] of $10^{34}\,\mathrm{cm}^{-2}\mathrm{s}^{-1}$, reached for the first time in 2015 and corresponding to a total integrated luminosity over one year of about $40\,\mathrm{fb}^{-1}$, about 1000 particles from more than 20 overlapping proton-proton interactions traverse the Tracker for each bunch crossing, about every 25 ns. Therefore these features require fast response and lead to a high number of channels, implying detection electronics with high power density, which in turn requires

10 Luminosity is one of the most important parameters of an accelerator. It is a measurement of the number of collisions that can be produced in a detector per centimeter-squared per second. The bigger is the value of the luminosity, the bigger is the number of collisions.

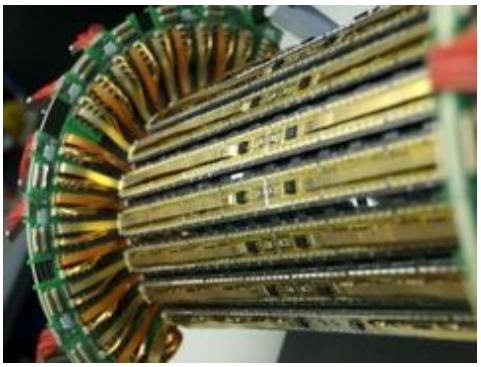

(a)

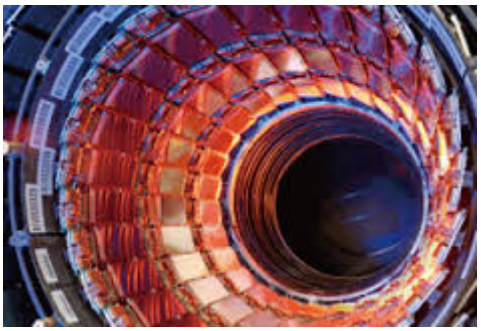

(b)

Figure 1.7: (a) Half shell of the pixel detector and (b) silicon strips detectors in CMS Tracker

efficient cooling. These specifications have to be balanced against the aim of keeping the amount of the Tracker material to a minimum in order to limit undesirable phenomena, such as multiple scattering which corresponds to interaction of particles with detector materials. Furthermore, the intense particle flux leads to high radiation levels which may cause severe radiation damage to the tracking system environment. With this in mind, the main challenge in the design of the tracking system was to develop detector components and service systems able to operate in this harsh environment for an expected lifetime of 10 years.

The requirements on granularity, speed and radiation hardness lead to a Tracker design entirely based on silicon detector technology. In fact the final design of CMS Tracker is composed of a pixel detector, which is the closest part to the Interaction Point, and the strip detector, both using silicon sensors:

With about $200\,m^2$ of active silicon area the CMS Tracker is the largest silicon tracker ever built. [7]

- The pixel detector contains 65 million pixels, allowing it to track the paths of particles emerging from the collision with extreme

accuracy. In Fig. 1.7a, a picture of the half shell of the CMS pixel detector is reported.

- After the pixels and on their way out of the Tracker, particles pass through ten layers of silicon strips detectors, shown in Fig. 1.7b, reaching out to a radius of around 120 cm. Silicon sensors are highly suited to receive many particles in a small space due to their fast response and good spatial resolution.

1.3 THE NEED OF HUMIDITY MONITORING IN THE CMS TRACKER

The high radiation dose resulting from the LHC operation at full luminosity can cause loss of performance of the silicon sensors of the CMS Tracker, due to their close proximity of the Interaction Point, and, as a consequence, it induces an increase of the leakage current which is a source of detector noise and heat generation. As such leakage currents linearly increase with the radiation dose and exponentially decrease with the inverse of temperature, all tracker sub-detectors are cooled by circulating fluids at low temperature and the CMS Tracker operates under the condition that the warmest point on the surface of each silicon sensor is below $-10\,^{\circ}\mathrm{C}$. To fulfill this requirement, a typical coolant temperature of $-20\,^{\circ}\mathrm{C}$ is chosen as the lower limit of the operation range, while the in-detector cooling design ensures a temperature difference less than around $-10\,^{\circ}\mathrm{C}$ between the sensors and the coolant. [8]

To avoid water vapor condensation, which would damage both the sensors and the complex and expensive readout electronics of the silicon modules, the volume needs to be kept dry. The safe target point for the atmosphere in the Tracker has been set to a dew point temperature of $-35\,^{\circ}\mathrm{C}$. Such conservative dew point accounts for possible changes in the bulk fluid temperature and for the uncertainty in the relative humidity measurement.

While industrial solutions favor baking in order to achieve low humidity values, this technique cannot be used for the LHC silicon trackers, since it would damage the sensors and readout electronics. The dry environment required is therefore achieved only by flushing dry gas, such as nitrogen, with a guaranteed dew point temperature at the delivery point of $-70\,^{\circ}\mathrm{C}$. During maintenance periods, dry air of similar dew point is used instead of the nitrogen. The dry gas flushing

must be continuous, as the services needed for the thousands of silicon sensors operation require that the Tracker volume is penetrated by thousands of pipes, cables and optical fibers in very complex geometrical arrangements, thus making impossible to achieve a perfect sealing of the volume. [9] Furthermore, while the experiments are designed for an operational life of the order of 10 years, the possibilities of maintenance access to the area surrounding the Tracker are extremely limited, and those inside the volume are virtually impossible.

Under these conditions, a continuous, correct and long-term reliable monitoring of the humidity levels is extremely important both inside the Tracker and in the surrounding region, in order to prevent any possible deterioration of the operational conditions of the whole experiment.

1.4 ENVIRONMENTAL SENSORS SPECIFICATIONS FOR CMS

Any humidity sensor to be introduced in the CMS detector volume should ideally comply with the following requirements:

- Radiation resistance to doses from 10 kGy up to 1 MGy [11], depending on the installation position and in particular on the distance from the Interaction Point ;
- Insensitivity to magnetic field (up to 4 Tesla);
- Small dimensions (few mm size, typically) in order to be easily integrated in the Tracker environment;
- Low mass;
- Correct operation at temperature down to $-20\,^{\circ}\mathrm{C}$ at least ;
- Response to the full range of relative humidity, from 0 %RH to 100 %RH;
- High long term stability and/or possibility of an easy remote recalibration ;

11 The Gray is a derived unit of ionizing radiation dose in the International System of Units, defined as the absorption of one joule of radiation energy by one kilogram of matter. As an alternative, the absorbed radiation dose may be expressed in rad, where 1 rad corresponds to 0.01 Gray.

- Reliable reading across long distances, as the powering and read-out stations are several tens of meters away from the measurement points;
- Reduced number of wires for operation, as many single measurement points are needed.

A rather complete review of possible transduction techniques available for relative humidity sensors is presented in [10].

Nowadays electronic humidity sensors represent the dominant technology on the world-wide market. Indeed the demand for low and compact sensors for humidity monitoring has driven the development of miniaturized electronic sensors. The capacitive and the resistive-based sensors are the most commonly proposed, with the capacitive-based sensors dominating and making up nearly 75 % of the commercial market. [12]

Several miniaturized commercial sensors have been investigated and used over the years in the CMS experiment, but none of them really satisfies the above mentioned full list of requirements.

For example, commercial sensors such as the $HIH-3610$ [11] and $HIH-4030$ [12] series produced by Honeywell (Fig. 1.8a and Fig. 1.8b respectively), have been proposed for the experiment as they are small, inexpensive and fast responding. They are mainly based on polymer capacitive sensing elements with on-chip integrated signal conditioning that needs at least three wires and an adequate voltage supply for each measurement point. Furthermore a measure of the local temperature has to be performed as the output of these hygrometers is affected by temperature (typically four more wires have to be introduced for each standard commercial thermometer). In addition these devices are critically damaged when exposed to irradiation, as they are not designed with radiation hardness characteristic. [13] Beside all the above mentioned problems, detailed analyses performed

12 Capacitive-based sensors operate on the basis of dielectric changes of a thin hygroscopic film upon exposure to moisture; resistive-based sensors rely on the transduction mechanism involving the change in conductivity caused by the absorption of moisture in a hygroscopic material such as conductive polymers.

13 The $HIH-4030$ sensors have been integrated in the Tracker Bulkhead area of the experiment during the first long shutdown of the LHC machine, started in February 2013 and consisting in a 2 years period of stop of the complex machine for maintenance and upgrade. These sensors have been read out using Arduino microcontrollers [13]. Even if these sensors are not expected to survive long once operation with beam starts -depending on their distance from the Interaction Point- they have been integrated in the experiment as they could provide cross-checks for the readings of other hygrometers and help to get a more fine-grained understanding of the humidity situation in the various volumes of the experiment during the $LS1$ phase. [14]

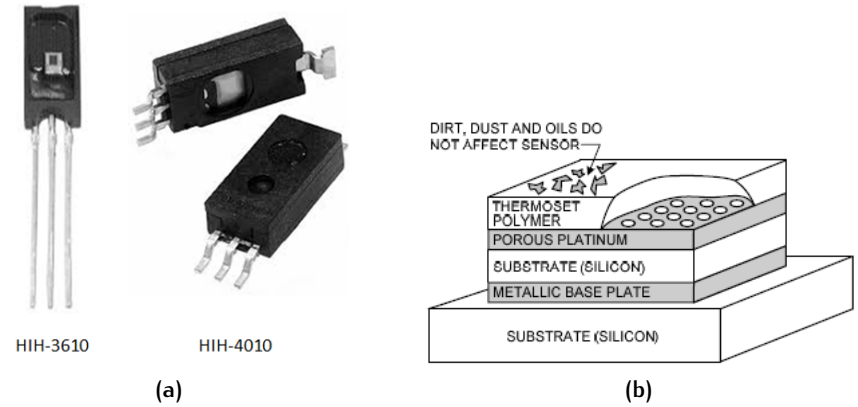

Figure 1.8: (a) $HIH-3610$ and $HIH-4010$ humidity sensors produced by Honeywell and (b) their scheme of the elements

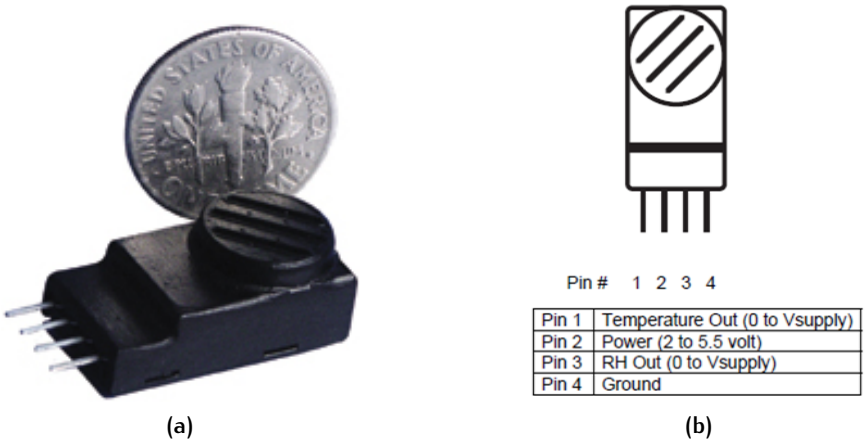

Figure 1.9: (a) Precon $HS2000$ and its (b) pin diagram (front view)

at CERN [15, 16] showed that the uncertainty of these sensors in the relative humidity measurement has an estimated absolute error at room temperature not lower than ± 2 %RH, even after individual calibration of each sensor. This absolute error rises up from ± 3 %RH to ± 5 %RH, when one takes into account the operation at temperatures below 0 °C.

Other capacitive-polymer technology-based sensors of newer generation are the Precon $HS-2000$ [17], shown in Fig. 1.9a. They integrate the relative humidity and the temperature measurements on the same small electronic chip, thus providing a direct reading of the dew point, eliminating the need of temperature correction by the user and reducing to four the total number of wires needed for each measurement point (Fig. 1.9b). However studies at CERN conducted in 2012 have shown that Precon $HS-2000$ are not resistant to radiation and they are sensitive to magnetic field. [18]

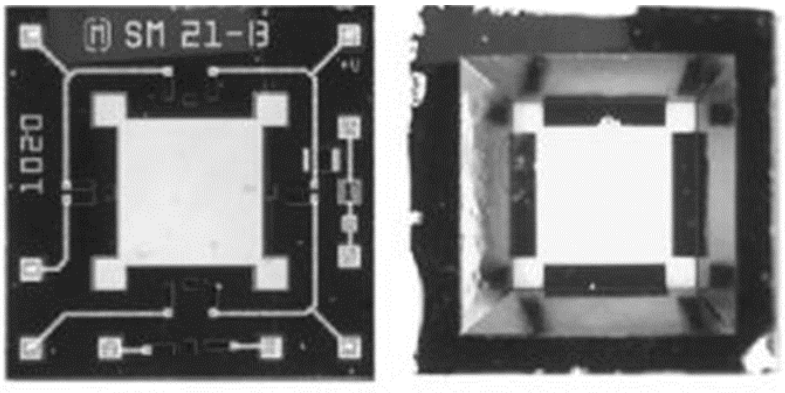

Figure 1.10: Front and backside pictures of an unpackaged *HMX*2000 sensor

Finally, Hygrometrix *HMX*2000s have been selected for the relative humidity monitoring in CMS. Front and backside pictures of an unpackaged sensor are presented in Fig. 1.10. *HMX*2000 is a resistive sensor where four polymeric resistive elements, which modify their size under the effect of humidity, are arranged to be the arms of a Wheatstone bridge. [14] Studies conducted at CERN in 2005 demonstrated that these devices, provide a non linear response characterized by long-term drifting and an extremely low response ($0 \div 100$ %RH in 100 mV), thus requiring a complex chain of amplification and powering in order to be operated and read-out over long distance. Moreover they have been found to be insensitive to strong magnetic fields and with good radiation tolerance characteristic. [9] For these reason,16 *HMX*2000 sensors have been integrated in 2012 inside and in proximity of the Tracker Bulkhead area of the CMS experiment (eight per each side of the detector), as reported in [18], coupled to standard miniaturized analog *PT*100 temperature sensors, thus requiring 4+4 wires to provide a dew point temperature reading for each measurement point. However the demonstration of the correct operation of these hygrometers, which are not available in the market anymore, in the CMS detector as well as the validity of their calibrations and readings have never been documented over the years.

14 The sensor is a piezoresistive device approximately 2 mm square and consists of four cantilever silicon beams, fabricated and connected to realize a Wheatstone Bridge. Each beam, fabricated as piezoresistor, where the electrical resistance is proportional to the mechanical strain experienced by the beam, is coated with a polymeric material. During operation, ambient water vapor molecules are absorbed onto the sensing film surface, resulting in bulk dimensional changes in the sensing film and, consequently, straining the beams and changing the resistance of the piezoresistors.

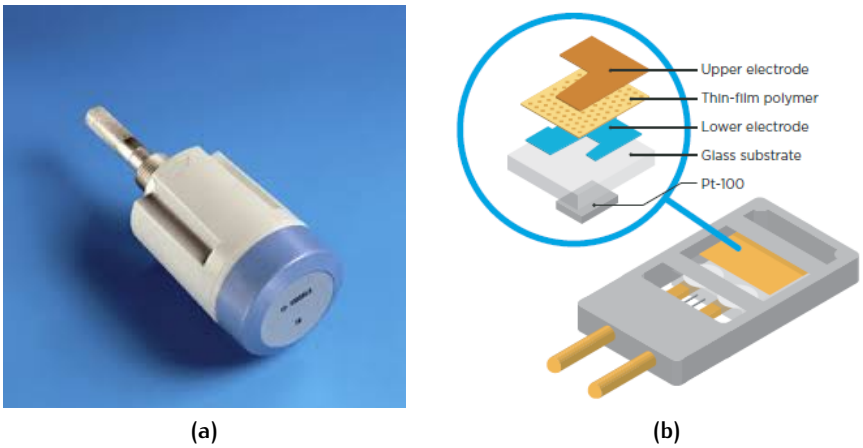

Figure 1.11: (a) Vaisala *DMT*242 dewpoint transmitter; (b) Vaisala dew point sensor based on thin film polymer technology

In order to have a completely decoupled system of humidity measurements in the tracker area of the experiment, a sniffer system with a total of 26 sniffing lines has also been introduced (20 lines have been recently added, during the last long shutdown of the accelerator, 6 lines were already existing in the volume before). This system extracts gas from different positions inside the Tracker, outside the Tracker and fully outside of the Tracker seal and transfers these air samples to a gas analysis rack located in the underground service cavern. [14] Here the analysis of the dew point is performed using 26 industrial Vaisala *DMT*242 dew point transmitters [15] [19], as the type of the one shown in Fig. 1.11a, which are renowned for their reliable performance, even in very dry environments.

The number of sniffer points to be added in the CMS Tracker is clearly limited due to space limitation, complexity of piping to reach the service cavern and economic reasons. Consequently, distributed sensing with the "sniffing" solution, which are able to provide only time-averaged dew point measurements, is not foreseen at all.

15 The *DMT*242 incorporates a thin film polymer sensor, shown in Fig. 1.11b, which absorbs or releases water vapor as the surrounding humidity increases or decreases, thus inducing a variation of the capacitance of the sensor itself. The capacitive sensor is bonded together with a temperature sensor in order to provide a dew point measurement.

(a) (b)

Figure 1.12: (a) SHT25 from Sensirion and (b) BME280 from Bosch environmental sensors

1.5 NEW TRENDS IN THE HYGROMETRIC SENSORS MARKET

The experience deriving from the design and production of the first generation of tracking detectors at LHC has clearly shown the lack of miniaturized relative humidity sensors well-suited for local, distributed monitoring inside harsh and virtually inaccessible environments. As a matter of fact, commercial humidity sensors available on the market are typically designed to operate at ambient temperature and technical specifications on their behavior are very often provided referring to the nominal working temperature (such as 20 °C or 25 °C).[20] Moreover, the tolerance to radiations and the insensitivity to magnetic interference, which are key-features for their possible application in high energy physics, are in most of the cases not documented or even not demonstrated, as already anticipated in the previous section.

Today, the benchmark in the market is represented by the sensors *SHT*25 (in Fig. 1.12a) and *BME*280 (in Fig. 1.12b), developed by the companies Sensirion [21] and Bosch [22], respectively, which are considered as the high-end model of new generation of digital relative humidity and temperature sensors in terms of performance.

As to the *SHT*25 sensor, the recommended operating range [16] does not cover the whole relative humidity interval at each temperature values, as shown in Fig. 1.13

The declared uncertainty of the Sensirion sensors in the relative humidity measurement is of around ± 2 %RH at 25 °C in the range

16 According to the data sheet, the sensor works stable within the recommended Normal Range. Long term exposure to conditions outside the Normal range may temporarily offset the relative humidity measurements.

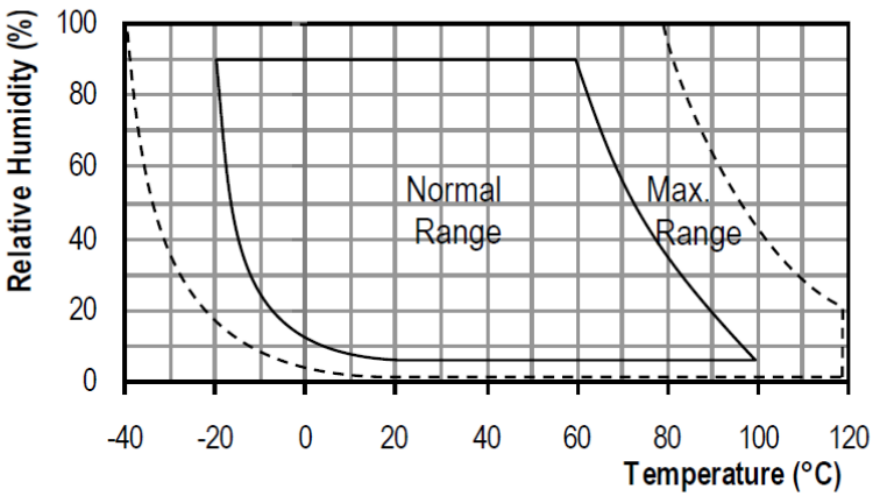

Figure 1.13: Operating recommended range of *SHT*25 from Sensirion

between 10 and 70 %RH. This error, which does not include hysteresis and long term drift, can even rise up to ±3 %RH, outside this range. The accuracy of the RH measurement at temperatures below 0 °C is not even specified in the data-sheet [21], as shown in Fig. 1.14a. Moreover, the temperature measurement presents a declared error of ±0.2 °C between 5 and 60 °C, increasing up to ±0.5 °C when operation temperatures below 0 °C or above 60 °C are approached, as reported in Fig. 1.14b.

Even in case of *BME*280 from Bosch, the company provides a limited operation range of the sensor [22], as reported in Fig. 1.15. Moreover, an accuracy of ±3 %RH (including the declared hysteresis error of ±1 %RH) at 25 °C for relative humidity measurements and of ±1 °C between 0 and 65 °C for temperature measurements are declared in the technical specifications of these sensors.

Taking in account these uncertainty values, it is possible to estimate the expected dew point error for both *SHT*25 and *BME*280 sensors when measuring a dew point of −30 °C at different environmental temperatures.

Results reported in Tab. 1.1 and Tab. 1.2 show that even with last-generation hygrometers, the above-mentioned errors in the temperature and relative-humidity measurements propagate in the dew point measurements resulting, for the typical range of interest for our application, in high errors up to ∼ ±15 °C in case of *SHT*25 and ∼ ±18 °C in case of *BME*280 when measuring at 20 °C.

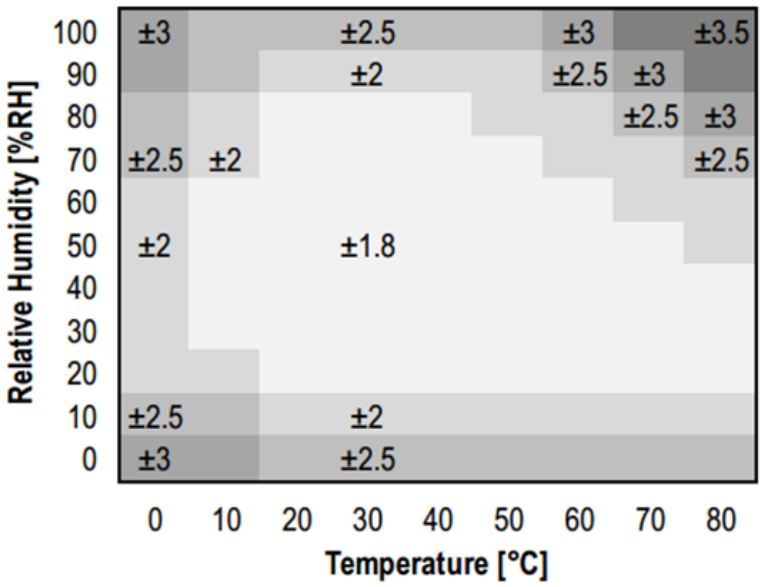

(a)

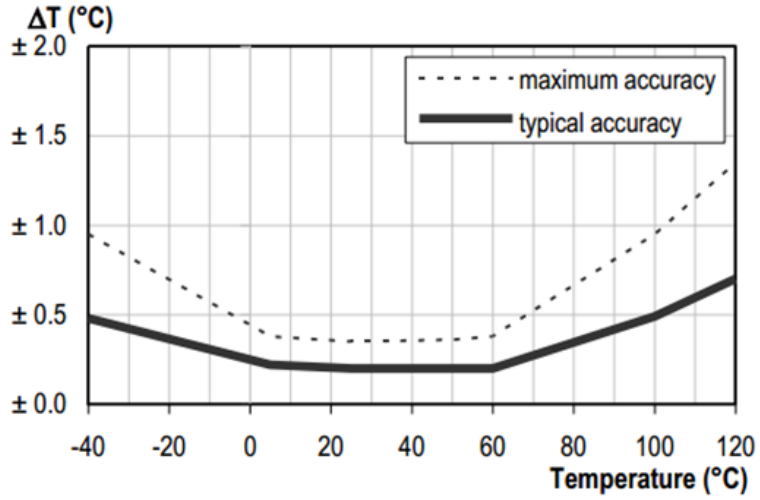

(b)

Figure 1.14: (a) Typical relative humidity and (b) temperature accuracy limits of the *SHT*25 sensor from Sensirion

Table 1.1: Expected dew point error using SHT25 from Sensirion

Reading	Uncertainty	Expected Dew Point	Dew Point Error
20 °C 1.63 %RH	±0.20 °C ±2.5 %RH	−30 °C	±14.8 °C
10 °C 3.10 %RH	±0.20 °C ±3.0 %RH	−30 °C	±9.3 °C
0 °C 6.23 %RH	±0.25 °C ±3.0 %RH	−30 °C	±4.6 °C

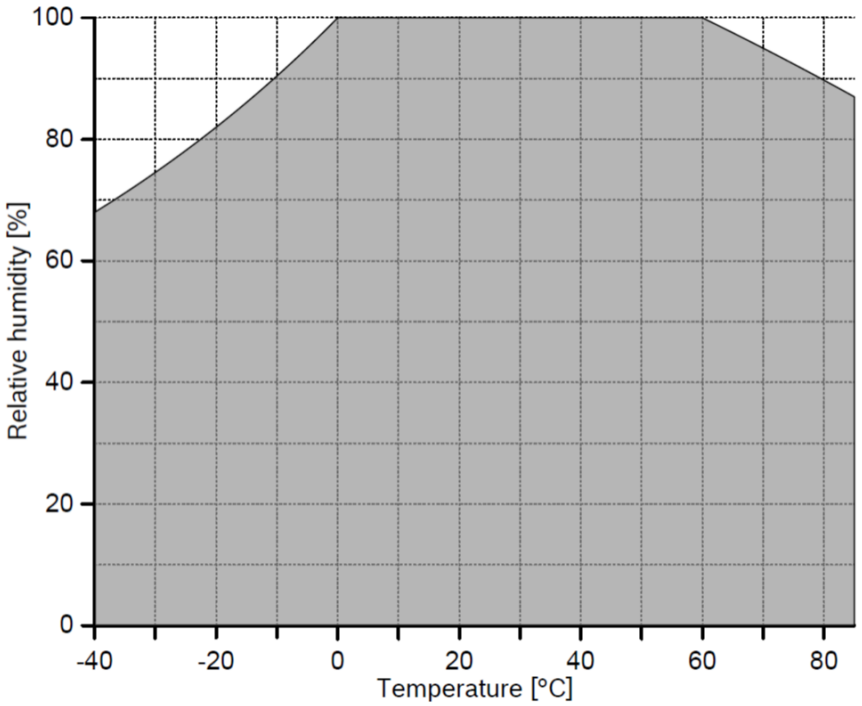

Figure 1.15: Operating range of *BME*280 from Bosch

Table 1.2: Expected dew point error using *BME*280 from Bosch

Reading	Uncertainty	Expected Dew Point	Dew Point Error
20 °C 1.63 %RH	±1 °C ±3 %RH	−30 °C	±17.7 °C
10 °C 3.10 %RH	±1 °C ±3 %RH	−30 °C	±9.3 °C
0 °C 6.23 %RH	±1 °C ±3.0 %RH	−30 °C	±4.7 °C

1.6 CONCLUSIONS

As largely discussed in the previous sections, commercial miniaturized relative humidity sensors are generally not suitable to be employed in harsh and complex environments, such as the experiments running at CERN, and also in situations where requirements in terms of tolerance to radiations, immunity to electromagnetic interference, multi- sensors operation, in situ and remote monitoring are required. On the contrary, fiber optics offer a new approach to this new measurement problem.

On this line of argument, the goal of this research is to design, develop and characterize in realistic conditions the performances of very promising relative humidity fiber optic sensors and to give the very first demonstration of their application inside high energy physics environments as well as of their strong potential as industrial and commercial products.

2 FIBER OPTIC SENSING TECHNOLOGY

Sensing has become a key enabling technology in several areas. In many advanced applications where miniaturization, sensitivity and remote measurements even in harsh environments are vital, optical fiber-based sensing techniques can provide novel solutions. As a result of this, optical fiber sensing technology is developed as a powerful technology that is currently being implemented in a wide variety of applications.

After a brief introduction about the fiber optic sensors properties and advantages, the attention will be focused here about the so-called optical fiber grating-based sensors. An overview of this innovative technology will be given and its application in the relative humidity sensing applications will be detailed.

2.1 WHY FIBER OPTIC SENSORS?

Modern optical fiber sensors owe their development to two important scientific advances made in 1960's, as the introduction of the first working laser - in 1960- and of the modern low-loss optical fiber- in 1966. Anyway, it was the development of the first experiments with low-loss optical fibers in the early 1970s which has represented the real transition from the experimental stage to practical applications.

From that moment the field of FOS has continued to progress and developed enormously [1]: for instance, fiber-optic sensors have been installed in bridges and dams to monitor the performance and structural damage, or some of them have been used to monitor the conditions within oil wells and pipelines, railways, wings of airplanes and wind turbines. Decades of research led to the development of

1 It was the steep growth of telecommunication industry in the 90's that fueled the research and development in fiber optic technology and led to availability of less costly, efficient and more sophisticated components. However, the cost of fiber optic sensor technology still needs to be reduced significantly to offer a compelling incentive to sensors industry for adoption of the newer technology. The prices of fiber optic and optoelectronic components such as laser diodes and fibers themselves have seen a steep decrease by a factor of around hundred-folds over the last 30 years. It is likely that this downward trend in prices will continue as the technology matures further, and this may open up newer possibilities for optical fiber sensor technology. [23]

accurate optical fiber measuring instruments, including gyroscopes, hydrophones, temperature probes and chemical monitors.

In comparison with conventional sensors, FOS exhibit a number of advantages which make them really attractive and of which the electronic counterpart lacks.

As a matter of fact, fiber optic sensors:

- are non-electrical devices;
- require small cable sizes and weights;
- enable small sensor sizes;
- allow access into normally inaccessible areas or in hostile media;
- permit remote sensing;
- offer immunity to radio frequency interference and electromagnetic interference;
- do not contaminate their surroundings and are not subject to corrosion;
- offer sensitivity to multiple environmental parameters.

Moreover, the dual role for optical fibers as sensor and pathway for sensing signals makes sensing architecture much simpler, in comparison to the conventional ones, especially when multi-point and distributed sensing is required.

The technology is still growing and several new types of fiber sensors are progressively emerging to measure a wide variety of physical properties, such as chemical changes, magnetic fields, rotation, radiation and much more. Some of them had also reached a mature state and have been commercially produced and industrialized [2]. [25]

2.2 FIBER OPTIC SENSORS CLASSIFICATION

The general structure of an optical fiber optic sensors-based system is shown in Fig. 2.1 and consists of three main components such as

2 The analysis of the global fiber optic sensors marketplace has been deeply covered by the business opportunity report from BCC Research in 2014. In particular the report has been focused on the markets and opportunities for fiber optic sensors in oil and gas exploration and drilling, medical, and industrial markets. According to this study, which takes also in account future opportunities for new application markets, the global market for fiber optic sensors reached nearly 1.7 billion in 2012 and 1.8 billion in 2013 and is expected to increase up to 2.2 billion by 2018 [24].

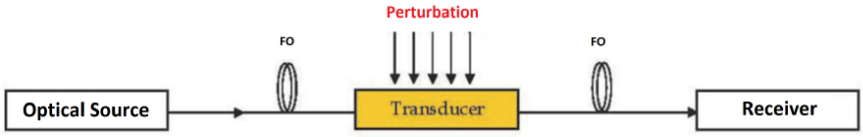

Figure 2.1: Basic components of an optical fiber-based sensing system

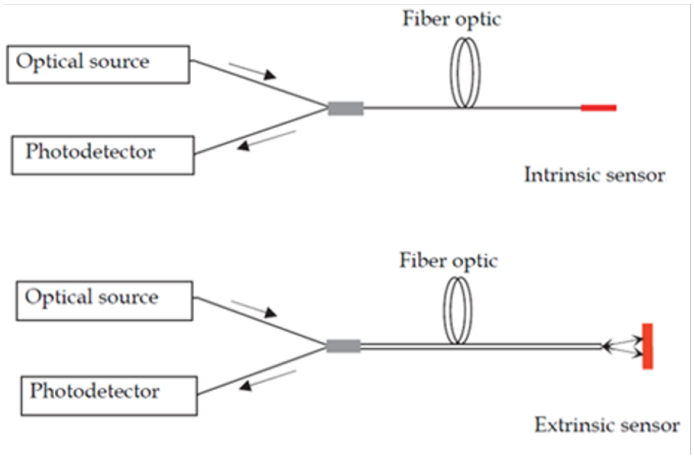

Figure 2.2: Intrinsic and extrinsic fiber optic sensors

source, transducer and detector. Lasers, diodes and LEDs are generally used as the optical source, optical fibers or doped fibers or bulk materials are employed as transducers and, at the output of the system, a photodetector is used to detect the variation in the optical signal that has been caused by the physical perturbation of the system.

As optical fiber sensors operate by modifying one or more properties of light passing through the fiber, they can be broadly classified as extrinsic or intrinsic, as shown in Fig. 2.2.

Intrinsic optical sensors directly employ an optical fiber as the sensitive material and also as the medium to transport the optical signal with information of the perturbation environment to be measured. In this case the light does not leave the fiber to perform the sensing function, except at the detection end of the sensor.

In case of extrinsic sensors, on the other hand, the optical fiber is simply used as mean to carry light to and from a location at which an optical sensor head is located. The sensor head is external and usually is based on optical components which are designed to modulate the properties of light in response to changes in the environment with respect to the physical perturbations of interest.

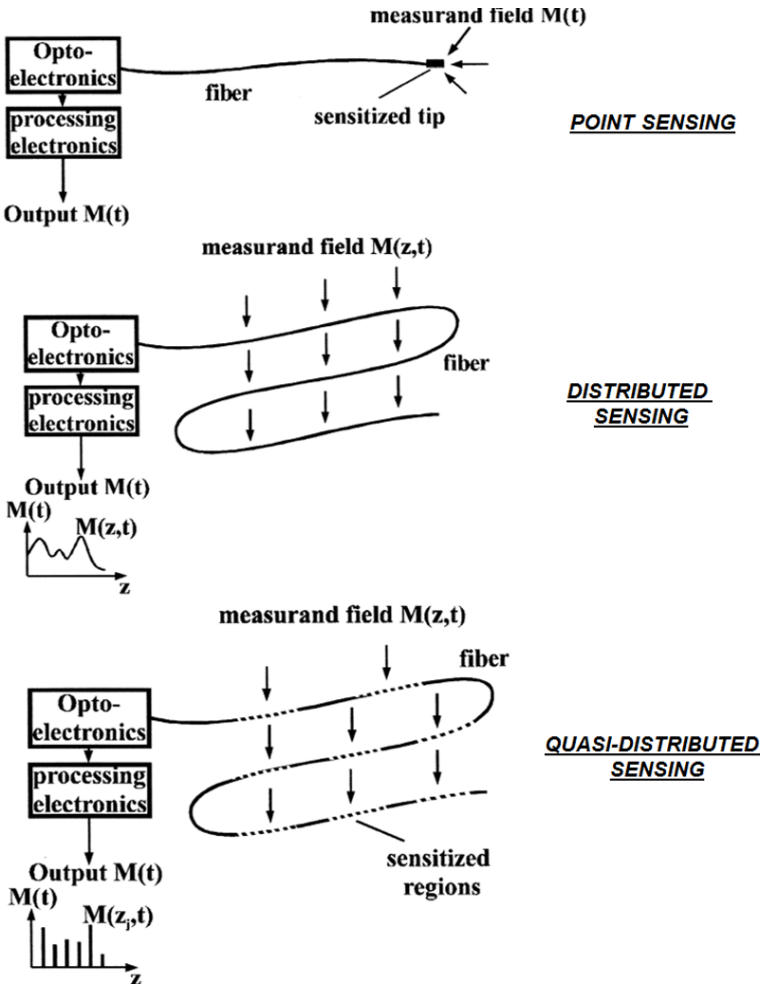

Figure 2.3: Point, distributed and quasi-distributed optical fiber- based sensing

The intrinsic fiber sensor types are more attractive and widely researched as this scheme has many advantages compared to extrinsic, such as their in-fiber nature and the flexibility in the design of the fiber sensor head. [25]

Optical fiber sensors can also be further classified according to their spatial positioning. For example, a point sensor can be used to sense measurands from discrete points while distributed fiber sensors provide spatial and temporal information of the measurand from any point along a single fiber with a certain resolution. A style of sensor that is "in between" these two configurations is represented by the quasi-distributed scheme, where the measurand information is obtained at particular and pre-determined points along all the length of a fiber network. [26]

A schematic of the three major sensing schemes - point, distributed and quasi-distributed - is illustrated in Fig. 2.3.

2.3 FIBER OPTIC SENSORS FOR HUMIDITY DETECTION

With the advent of optical fiber technology, a considerable effort of research has been focused on the development of fiber optic-based techniques for humidity sensing to be applied in a wide range of applications. For example the measurement of relative humidity is an important factor in various industries such as food and storage process, medical and biomedical, chemical, structural health monitoring, ecological and atmospheric weather conditions monitoring as well as for fuel and aerospace applications. [27, 28]

So far, electronic humidity sensors have covered the main part of the sensors market as their fabrication technology is well established. However at the present time there exist many applications where optical fiber humidity sensor technology can advantageously compete with the traditional ones. As mentioned in the previous section, FOSs use optical fiber to guide a light signal which, in case of humidity sensor, is modulated with the ambient humidity. Thanks to the low attenuation and large wide-band of the fiber it is possible to transmit large sensor data quantities over kilometer distances. There are also a high number of applications where the possible electric hazard produced by the electronic sensor itself or the electromagnetic interferences of the surrounding harsh environment makes difficult the utilization of electronic humidity sensors. In some fields it is also needed a measurement of humidity where the accessibility is limited in space and where an electronic sensor could be more difficult to locate. The small dimensions and simple geometries of optical fiber make possible the implementation of light-weight systems that can be easily embedded into constructions materials. Moreover the light weight and low mass facilitate drying after their use.

All these elements together form the main motivations that has driven the research activities in the field of fiber optic- based humidity sensing. [29]

To deal with the spread of the above mentioned applications of humidity monitoring and to allow for the different requirements, a wide range of technical approaches to fiber optic humidity sensors have been proposed in literature. Of course there is no “right answer” when it comes to designing an optical fiber sensor for humidity and no one technology offers absolute superiority over another one.

What is critically important is that there is a range of sensors from which to choose and the selection has to take place taking in consideration the response of the sensors and the specific application. [28]

The various fiber optic-based humidity sensing technique proposed and reported in literature, with design covering both extrinsic and intrinsic sensor types, can be further classified according to general schemes that highlight the operating principles being used. [30] Since the silica fiber can hardly presents obvious response to humidity, the implementation of the sensors typically relies on the deposition of functionalized coatings onto the fiber surface.

Generally speaking, the optical fiber-based technique for humidity sensing applications include direct spectroscopy [3], evanescent wave [4], interferometric methods [5] and in-fiber gratings.

3 The spectroscopic method is widely used in chemical analysis and it is usually a popular choice of method for many fiber optic-based chemical sensors. It examines the optical signal obtained by the measurements and relates absorption or fluorescence-based measurements to the concentration of the target analyte. The typical configuration of humidity sensing are based on the optrode design where appropriate moisture sensitive reagents are attached to the tip of the sensing fiber. [31, 32, 33].

4 Light traveling through a step index optical fiber is guided within the fiber itself as a result of the total internal reflection, for a certain critical angle of incidence. At each point, the interference between the incident and reflected signals, at the core/cladding interface generates the so-called evanescent wave which extends beyond the core of the optical fiber and penetrates the cladding region. The amplitude of the evanescent wave decades exponentially with the distance away from the core/cladding interface. For the case of relative humidity sensors, the physically deformed structure of the fiber, which is used to obtain evanescent wave absorption in an external medium, is coated with a specific overlay that reacts to humidity variations. A recent example of this approach may be found in the work by Corres et al. in [34].

5 Optical interferometry is a powerful and versatile tool that is applied in optical fiber sensing to yield high performance FOS. The sensing mechanism relies on the perturbation of the properties of the light signal traveling in the optical fiber introduced by an external environment.
For example, one of the first interferometric FOS for humidity measurements was demonstrated by Mitschke and consisted of a thin film Fabry-Perot cavity formed at the tip of the optical fiber, created by a layer of TiO_2 sandwiched in between two partially reflecting mirrors [35]. The interference between the optical signals reflected by the mirror at both ends of the cavity gives rise to a spectral response which gives a maximum intensity output (resonance) at specific wavelengths. As the refractive index of the cavity material has a dependence on humidity, the resonance was found to shift in response to humidity changes and was detected by performing intensity measurement at a fixed wavelength.
In 2011 our research group has proposed a novel fiber optic humidity sensor based on the near-field Fabry-Perot configuration for high radiation experiment at CERN. [36] The proposed device was realized depositing a particles layer of tin oxide onto the distal end of cleaved optical fibers. Even if the sensor provided very promising results such as high sensitivity, low response time and limits of detection below 0.1 % in the low humidity range $0 - 10$ %RH, it was found to be limited in terms of multiplexing capability due to the impossibility of integration of multiple sensors on the same fiber. For this reason this configuration has been discarded and the interest moved towards more innovative fiber optic sensors-based solutions.

Among them, we decided to concentrate our attention on the in-fiber grating sensors which belong to a class of intrinsic FOS that has gained widespread popularity in recent years.

In particular we focused the initial effort on the so-called Fiber Bragg Grating technology, which is largely discussed in the next section while the application of FBGs in applications of relative humidity sensing is presented in 2.5.

2.4 FIBER BRAGG GRATING TECHNOLOGY

A Fiber Bragg Grating is formed by photoinduced modulation of the refractive index in the core of a single mode optical fiber. [6] The structure formed within the fiber behaves as a wavelength selective filter, which reflects the light signal at a certain wavelength, named as Bragg wavelength (λ_B). [37]

This means that if broadband light travels in the core of an optical fiber, the incident energy at such a resonant frequency will be reflected back to the optical fiber, with the remaining optical spectra unaffected, as illustrated in Fig. 2.4.

The Bragg wavelength is strictly dependent on the fiber effective refractive index n_{eff} and the pitch of the grating Λ, according to the so-called Bragg condition:

$$\lambda_B = 2n_{\text{eff}}\Lambda \tag{2.1}$$

Both the refractive index and the grating pitch can be affected by strain and temperature, thus making FBGs very popular for strain and temperature sensing applications. [38, 39, 40]

As a matter of fact, an axial strain in the grating changes the grating spatial period, as well as the effective refractive index and results in a shift of the Bragg wavelength due to the elastic behavior and elasto-optic effect. Similarly, the change of ambient temperature induces a

6 Fiber Bragg gratings are created by "inscribing" systematic variation of refractive index into the core of a special type of optical fiber using an intense ultraviolet source such as a UV laser. Two main processes are used: interference and masking. The method that is preferable depends on the type of grating to be manufactured. Normally a germanium-doped silica fiber is used in the manufacture of fiber Bragg gratings, as it is photosensitive, which means that the refractive index of the core changes with exposure to UV light. The amount of the change depends on the intensity and duration of the exposure as well as the photosensitivity of the fiber. However, standard fibers can be used if the photosensitivity is enhanced by pre-soaking the fiber in hydrogen.

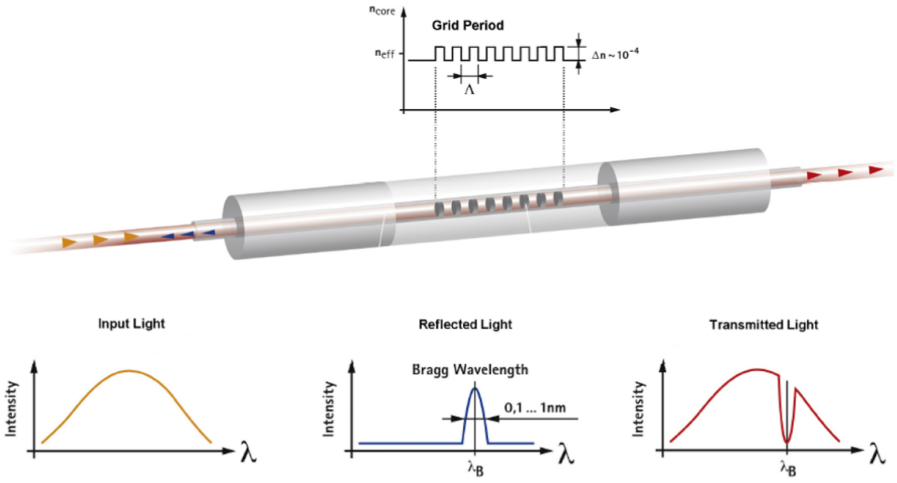

Figure 2.4: Fiber Bragg grating structure

similar effect on the grating, due to the thermal expansion and the thermo-optic effect.

Consequently, the Bragg wavelength shift ($\Delta\lambda_B$) due to the change in strain ($\Delta\epsilon$) and thermal effects (ΔT) can be expressed as follows:

$$\frac{\Delta\lambda_B}{\lambda_B} = (1 - P_e)\,\epsilon + \Big[(1 - P_e)\,\alpha + \zeta\Big]\Delta T \tag{2.2}$$

where P_e is the photo-elastic constant, ϵ is the strain induced on the fiber, α and ζ are the thermal-expansion and thermo-optic coefficients of the fiber, respectively.

In other words, the first addendum of the second term in Eq. (2.2) represents the longitudinal strain effect on the FBG, while the second addendum corresponds to the thermal effect, which comprises a convolution of the thermal expansion of the material and the thermal-optic effect.

As the grating is intrinsically sensitive to both temperature variations and strain, the application of proper methods to decouple the effect of temperature and strain on the FBG readings needs to be foreseen in order to get precise strain measurements. This is what is generally referred to as temperature compensation. [38]

A range of techniques has been proposed in literature to achieve this goal and they consist in measuring strain and temperature simultaneously. The most common solution uses two separated Fiber Bragg Gratings that is to say a strain-free temperature FBG-based sensor located in the same thermal environment as the strain FBG-based sensor. The error caused by the temperature variation on the FBG-

based strain sensor can be compensated just subtracting the wavelength shift induced by temperature variation (measured with the strain-free FBG) from the total wavelength shift obtained by the strain FBG sensor.

2.4.1 Why Fiber Bragg Gratings- based sensors?

Fiber Bragg Grating-based sensors have been subject to continuous and rapid development since they were first demonstrated for strain and temperature measurement about 25 years ago [41].

The main reason is represented by the fact that FBGs are simple intrinsic sensing elements, photo-inscribed into silica fiber, having a number of distinguishing advantages over other implementations of fiber-optic sensors [38, 42]:

- Resistance to harsh environments: FBG-based sensors are completely passive and do not use any electronic components. As a result, they are capable of operating under extreme operating conditions (e.g from cryogenic temperatures to several hundred degrees centigrade) and offer long-term survivability in most environments where electronic sensors are unable to operate.

- Electrical immunity: they are totally immune to electrostatic and electromagnetic interference. This allows them to be installed in locations characterized by severe electrical noise such as power generation and transmission plant. Furthermore they are 100 % intrinsically safe and can be used in the most hazardous explosive environments.

- Remote sensing: as the optical fiber is a very efficient signal carrier, the electrical interrogation unit can be sited many tens of kilometers away from the sensing location, whereas conventional electrical sensors require regular amplification to avoid signal to noise degradation.

- Wavelength encoding: the measurement signals are encoded in the wavelength shift of the reflection spectrum and, consequently, they are independent on power fluctuations.

- Long-term stability: being a passive sensor, a Fiber Bragg Grating has zero drift and can be used for many years without performing recalibration.

- Miniature size: the fiber into which FBGs are written is tiny, thus ensuring very little intrusion into the structures/environments where it is applied.

- Multiplexing: many tens of gratings can be written on the same optical fiber, and several hundreds can be simultaneously interrogated by one multi-channel instrument. This permits to use FBGs-based arrays to arrange a simple sensing system with a high number of sensing points distributed along a wide area [7].

- Multi-parameter sensing: indeed it is possible to develop sensors for measurements of pressure, vibrations, chemical and biological analytes, magnetic fields, weight and so on using the Fiber Bragg Grating technology [8].

For all these reasons, Fiber Bragg Grating-based sensing has proved to be a very fertile research area and FBG-based sensors have been developed over the years for a wide variety of sensing applications.

The traditional fields of application of FBG-based sensors include monitoring of civil structures (highways, bridges, buildings, dams, etc.), smart manufacturing and non-destructive testing (composites, laminates), remote sensing (oil wells, power cables, pipelines, space stations), smart structures (airplane wings, ship hulls, buildings, sport equipment), as well as traditional strain, pressure and temperature sensing and new developments are expected to continue over the next years. [42]

The principal applications of FBG-sensors are illustrated in Fig. 2.5 (adapted from [42]).

In the CMS experiment our research group has been installing a network of FBGs for both structural and temperature monitoring from 2010. The full network of temperature and strain optical fiber-based sensors, which up to now counts around 800 sensors, is fully proving the applicability of FBG technology even in harsh environments such as experiments running in the accelerator in Geneva. [43, 44, 45]

7 The only limitation in the realization of FBG arrays are imposed by the bandwidth of the acquisition system and the spectral minimum spacing between sensors. These two elements clearly put a constraint on the maximum numbers of sensors that can be integrated on a single channel.

8 As explained before, the Fiber Bragg Grating is intrinsically sensitive to strain and temperature. Integrating the grating with an appropriate material sensitive to physical, chemical and biological parameters, it is possible to develop physical, chemical and biological FBG-based sensors

Figure 2.5: Main application fields of FBG-based sensors (adapted from [42])

2.5 FBG-BASED RELATIVE HUMIDITY SENSORS

Bare silica fibers are insensitive to relative humidity. Nevertheless it is possible to develop a Fiber Bragg Grating-based relative humidity sensor by coating the grating itself with an appropriate hygroscopic material.

When exposed to the surrounding relative humidity change, the volume expansion of the moisture sensitive polymer due to absorption or desorption of water molecules, induces strain effect on the grating (the so-called swelling effect) and this results in a shift of the Bragg wavelength. Similarly a Bragg wavelength shift occurs in presence of temperature variations, due to the intrinsically dependence of λ_B to temperature, as explained before.

A simple schematization of a FBG-coated relative humidity sensor is given in Fig. 2.6.

In order to apply Eq. (2.2) in applications related to humidity sensing, a slight modification is required to consider the strain effect induced on the grating by the swelling of the moisture sensitive coating.

Indeed, in case of relative humidity sensor based on FBG technology, the Bragg wavelength shift due to temperature and relative humidity variations, can be expressed as follows:

$$\frac{\Delta\lambda_B}{\lambda_B} = (1 - P_e)\,\alpha_{RH}\Delta RH + \left[(1 - P_e)\,\alpha_T + \zeta\right]\Delta T \qquad (2.3)$$

where α_{RH} and α_T are the moisture expansion coefficient and the thermal expansion coefficient of the coated FBG.

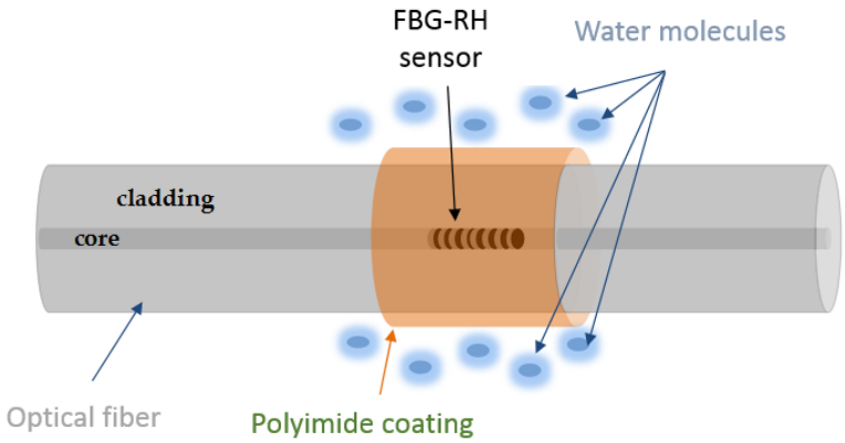

Figure 2.6: Schematization of FBG-coated relative humidity sensors

The Eq. (2.3) can be further simplified to

$$\frac{\Delta\lambda_B}{\lambda_B} = (1 - P_e)\,\epsilon_{RH} + (1 - P_e)\,\epsilon_T + \zeta\Delta T \tag{2.4}$$

which relates the shift in the Bragg wavelength to three main components such as the strain effect induced on the FBG due to moisture and to the thermal expansion (ϵ_{RH} and ϵ_T, respectively) and the thermo-optic effect.

It was demonstrated in literature [46] that the response behavior of a polymer-coated FBG is a linear superposition of relative humidity and temperature effects. This means that, in presence of temperature and relative humidity variations (ΔT and ΔRH, respectively), the Bragg wavelength shift of a FBG coated with an hygroscopic material can be expressed in linear assumption as:

$$\frac{\Delta\lambda_B}{\lambda_B} = S_{RH}\Delta T + S_T\Delta RH \tag{2.5}$$

S_{RH} and S_T are the relative humidity sensitivity and the temperature sensitivity, respectively, of the coated FBG, defined as:

$$S_{RH} = \left.\frac{\partial\lambda_B}{\partial RH}\right|_{constant T} \tag{2.6}$$

$$S_T = \left.\frac{\partial\lambda_B}{\partial T}\right|_{constant RH} \tag{2.7}$$

In the most general case, S_{RH} and S_T are functions of both temperature and relative humidity. [47, 48]

It should be noticed that even in the case of coated FBG-based sensors, as already mentioned for strain FBG-based sensors, there is a humidity-temperature cross sensitivity which has to be taken in account. Therefore in real sensing applications, in presence of both temperature and humidity variations, one should contemplate the application of temperature compensation techniques. A precise deconvolution of the temperature and humidity effects from the sensor signal requires therefore an independent temperature reading as close as possible to the humidity sensor position. [9]

In addition, in order to protect the FBG sensor and to avoid unwanted additional stress (not due to humidity variations), appropriate holders needs to be used to package the optical gratings and keep them in a tension-free state.

2.6 STATE OF ART OF RELATIVE HUMIDITY SENSORS BASED ON FBG TECHNOLOGY

The concept of FBG grating-based devices for humidity sensing is still fairly new and there have only been a few contributions in literature on this subject, the earliest of which dates back to 2001. [50]

As a matter of fact, the first example of the utilization of the strain effect to realize a relative humidity sensor based on FBG technology is the work proposed by Kronenberg et al. [46] who suggested the use of polyimide (Pyralin) as sensitive coating for the grating.

To quantify the influence of the coating thickness on the sensor sensitivity, seven gratings, organized in a multi point array, with average coating thickness between 3.6 µm (FBG 2) and 29.3 µm (FBG 8) were installed in the measurement system, together with a bare grating (FBG 1). A schematic of the set-up used for the FBG-based characterization is given in Fig. 2.7. The sensors were analyzed in terms of their operation in the range $10-90$ %RH at five different temper-

9 This is in any case required in order to evaluate the local water vapor content, the information which is often of primary importance for engineering applications, starting from the locally recorded value of the relative humidity. The temperature information needed for the signal deconvolution can be simply obtained through a temperature sensor placed on an independent fiber nearby the humidity sensor. However, a more compact and elegant solution might be envisaged by combining two FBG into a multi-sensing element on the same fiber, as also reported by Frazão et al. in [49], to produce a FBG-based thermo-hygrometer.

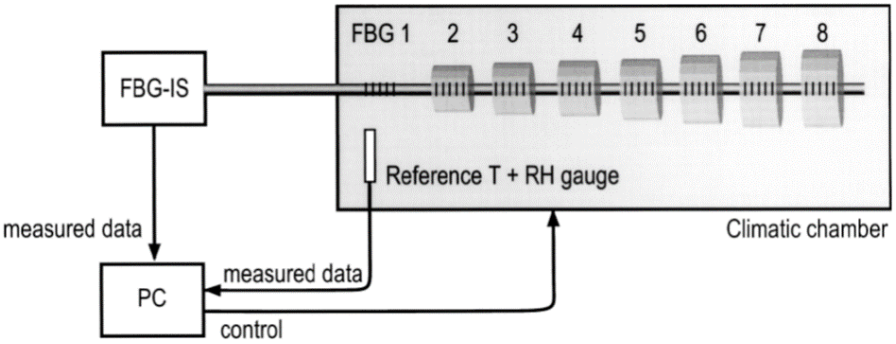

Figure 2.7: Schematic of the set-up used for the FBG-based characterization reported by Kronenberg et al. in [46]

atures ranging from 13 to 60 °C, in both ascending and descending direction. Reported experimental data, shown in Fig. 2.8 and referring to the sensor with a coating thickness of 29.3 µm, were found to vary linearly with changes in temperature and relative humidity, confirming a linear relationship between RH and polyimide expansion at each considered temperature. Investigations concerning the dependency of temperature and relative humidity sensitivities on the coating thickness were also carried on, as summarized in Fig. 2.9, from which it was concluded that there exists a linear dependence, with the sensor becoming more sensitive with increasing coating cross-section area. Due to the inherent sensitivity of the grating to the temperature, with the coated-FBG T sensitivity much higher than its RH sensitivity, a temperature compensation scheme was found to be required to extract humidity measurements from the sensor reading. [50]

A further example in literature of utilizing a PI-coated FBG is in the work published by Yeo et al. [51] where a detailed study of the proposed sensor in terms of its relative humidity sensitivity as well as time response and hysteresis effect is presented. As a matter of fact, 6 FBGs, with coating thicknesses between 10 and 42 µm were fabricated and investigated by exposing them sequentially to different humidity conditions, controlled by different chemical salt solutions, in the range from 23 to 97 %RH at constant room temperature. Obtained results, reported in Fig. 2.10, confirmed the linearity of the sensor response and the dependence of the magnitude of the strain induced on the grating due to relative humidity change on the coating thickness of the polymer. The time response characteristic was also investigated by subjecting the sensors to a step humidity change at 23 °C and a time response of approximatively 45 and 18 min was observed for the sensors with the thickest and the thinnest coating,

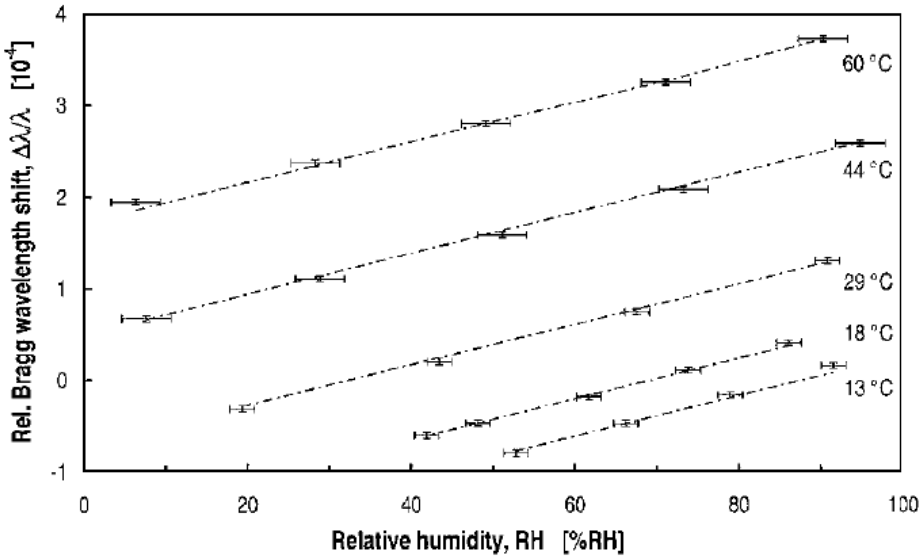

Figure 2.8: Bragg wavelength shift for several values of temperatures reported by Kronenberg et al. in [46]

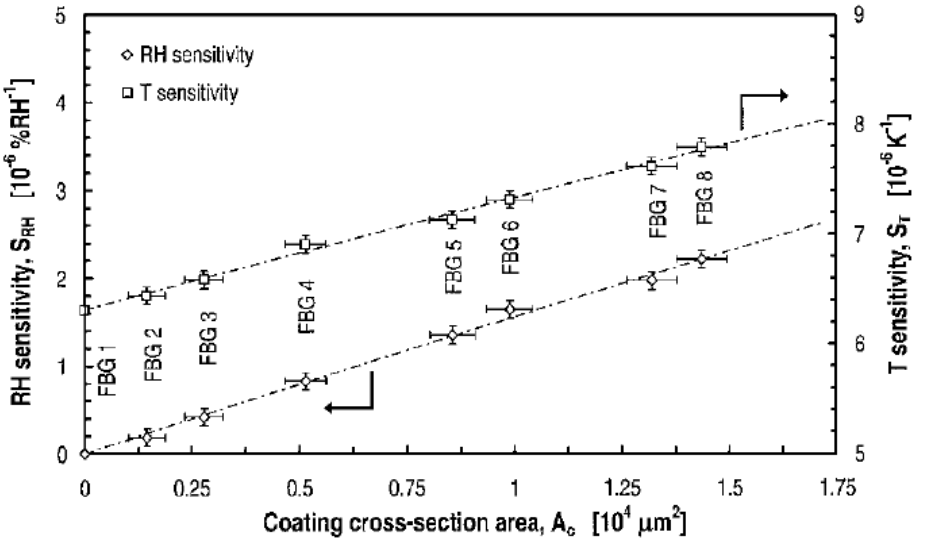

Figure 2.9: T an RH FBGs sensitivities in function of different polyimide coating thicknesses reported by Kronenberg et al. in [46]

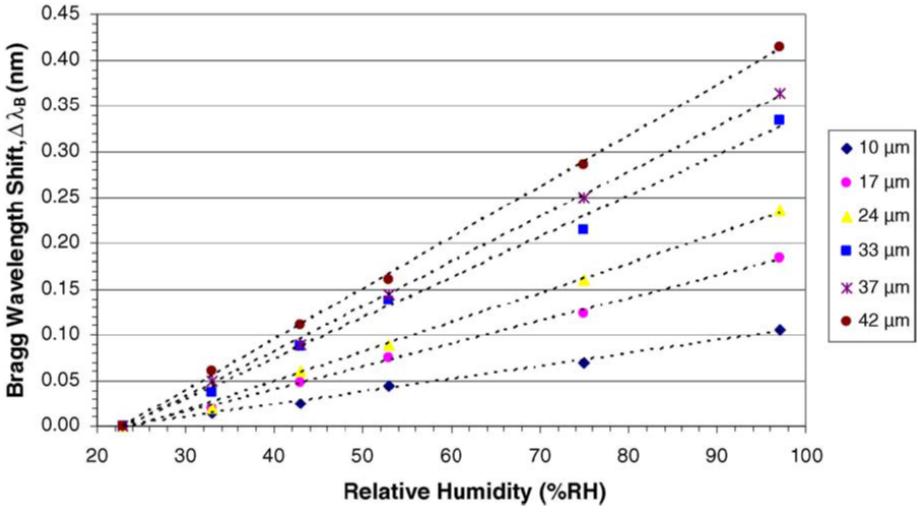

Figure 2.10: RH response of FBG-based sensors with different coating thicknesses at 23 °C reported by Yeo et al. in [51]

Table 2.1: Polymer coated FBG-based sensors for relative humidity monitoring proposed in literature between 2001 and 2011

Year	Coating	Thickness µm	S_{RH} $pm/\%RH$	RH %	T °C	Ref.
2001	PI	18.5	4.36	10 −90	23 −50	[50]
2002	Pyralin	29.3	2.21	10 −90	13 −60	[46]
2005	*PI*2525	33	4.5	22 −97	Room	[51, 52]
2009	PI	–	6.8	30 −90	10 −50	[53]
2010	PI	–	1.67	30 −80	25 −45	[54]

respectively, as shown in Fig. 2.11. A small and acceptable degree of hysteresis (< 5 %RH) was also observed, as reported in Fig. 2.12.

The same sensing scheme proposed by Kronenberg and Yeo for humidity sensing was further explored over the years for several interesting applications, as the soil moisture monitoring, demonstrated by Kunzler et al. in 2003 [55], or moisture sensing in concrete environment, showing the versatility of such devices even as a promising diagnostic tools in structural health monitoring [56].

In order to facilitate a cross comparison between the published data, Tab. 2.1 provides an overview of the main results reported in literature between 2001 and 2011 [10] concerning the development and testing of polymer coated FBG-based sensors for relative humidity monitoring. [11] As evidenced in the table, the investigations reported

10 In 2011, we started the research concerning this topic.
11 In some cases data are not available and therefore there are blanks in the table.

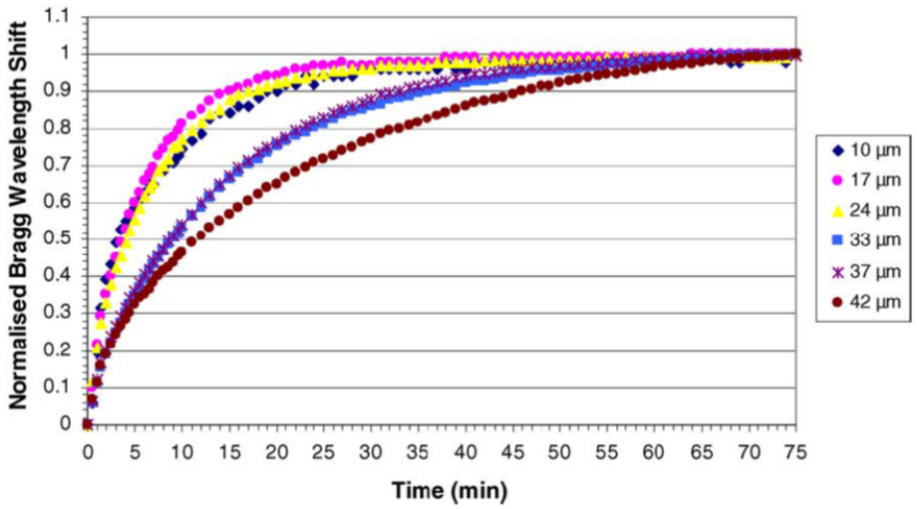

Figure 2.11: Response time of FBG-coated relative humidity sensors reported by Yeo in [51]

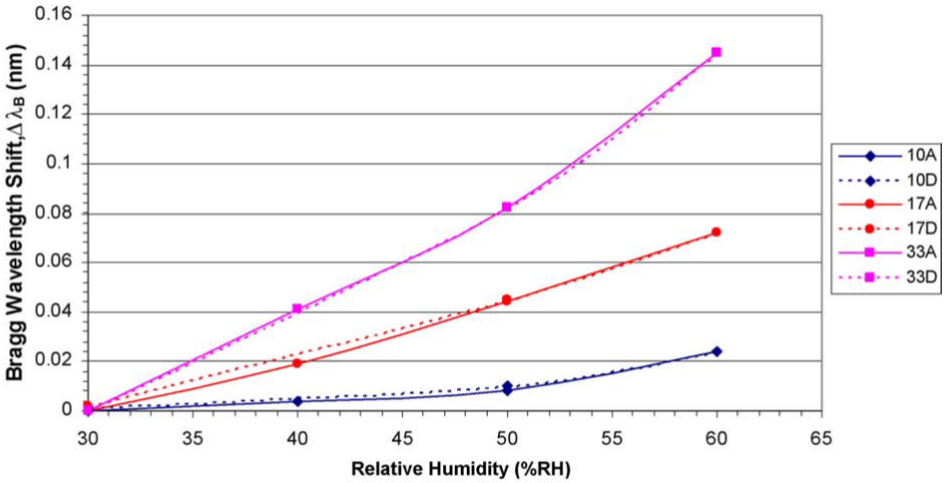

Figure 2.12: Hysteresis plot concerning three polyimide-coated FBGs subjected to a humidity change from 30 %RH to 60 %RH, in both ascending (A) and descending order (D) (yeo in [51])

in literature do not cover a wide range of both temperature and relative humidity. As a matter of fact no demonstration of the correct operation of coated Fiber Bragg Gratings is given below 10 °C and in the low relative humidity range.

2.7 RADIATION EFFECTS ON OPTICAL FIBERS AND FIBER OPTIC SENSORS

Nuclear radiation effects on optical fibers and photonic devices have been studied since several decades. In the early days one of the main concerns of the research on this topic was to determine whether such advanced technologies could withstand military and tactical environments such as surveillance satellite missions and nuclear weapon explosions.

As well known, radiations may interact with the materials altering their characteristics and this most often modifies the performance and affects the reliability of the devices, with dramatic consequences on safety carrying significant financial repercussions. For all these reasons careful investigations concerning how the radiation affects the operation of photonic components intended for use in these harsh environments have been carried out over the years. Moreover it is important to take in account is that human intervention to replace components or to repair systems in radiation environments is often impossible and this is due to the radioactivity levels involved or for accessibility reasons. It is indeed almost impossible to repair equipment once a satellite has been put into orbit or when an high radiation experiment has started running.

Generally speaking, ionizing radiation may have a profound and variable impact on optical fiber performance, as well documented in literature [40, 57]. Highly energetic radiation brings to an increase of the so-called radiation induced attenuation, which is primarily due to the creations of point defects, the so-called "color centers", and to the trapping of radiolytic electrons at defect sites in the fiber silica. These color centers can be made disappear through thermal or optical processes, which cause a decrease of the RIA. Depending on the number, nature and time dependent evolution of these defects, radiation induced attenuation may make certain fiber types and operational wavelengths totally unsuitable for specific high radiation environments.

The impact of radiation on optical fiber performance is a function of variables such as fiber type and composition, doping of core/cladding, operation wavelength and light power, annealing, as well as operation temperature and irradiation history. Total radiation dose and dose rate as well may have a large impact for the total damage to optical fibers. For example, specially for optical fibers, a high radiation dose over a short time can be more damaging than a similar dose experienced over an entire cable lifetime. It is therefore of critical importance to match the fiber type for a given cable design to the application environment within the high radiation environment.

Today, modern fiber fabrication technologies allow obtaining radiation tolerant fibers, depending on the wavelength range [40]. Indeed standard telecom fibers have proven their radiation resistance, even when exposed to high gamma dose rates and high level cumulated doses. For example the commonly used Corning SMF-28 optical fibers were found to exhibit typical RIA level of the order of around 10 dB/km measured at 1550 nm for total doses of 10 kGy and even above. [40, 58] Even at CERN, specific investigations have been conducted in order to assess the radiation resistance of optical fibers and today dense network of SMF-28 optical fibers is used in CMS experiment for data transfer. [12] [59]

For what concerns Fiber Bragg Gratings, it was demonstrated in literature that they are radiation resistant, which means that they survive at high radiation doses exposures, but they are not completely insensitive to radiations. As a matter of fact, radiation can influence the "normal" response of a FBG-based sensor via a change of Λ as well as n_{eff}. [60]

Experimental studies showed that the amplitude of the radiation-induced shift of λ_B, which results from the radiation-induced modification of both Λ and n_{eff}, can be affected by different parameters.

In [61, 60], the influence of the fiber composition and the grating fabrication on the radiation sensitivity of FBGs was studied. Twelve fibers with Ge-contents between 0 and 30 % and different kind of dopants and codopants materials (Boron, Fluorine, Aluminum, Phosphorus, Cerium) were investigated up to a dose of 100 kGy at room temperature. Despite differences in the RIA of several orders of magnitude between the twelve fibers under investigation, only moderate

12 For all these reasons, today many other applications associated with presence of highly energetic radiation, including for example space, healthcare, civil nuclear industry and high energy physics experiments, can benefit from the enhanced functionalities offered by photonic technologies for communication and sensing.

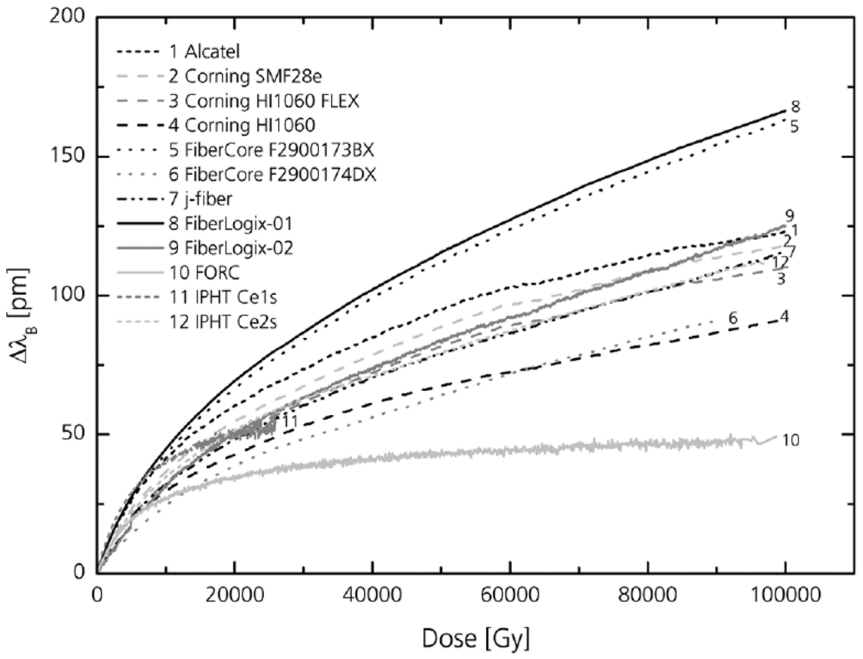

Figure 2.13: Influence of fiber composition on the FBG response under irradiation reported by Henschel et al. in [61, 60]

Bragg wavelength shift were observed, as shown in Fig. 2.13. The highest value, of about 160 pm, was obtained with the two fibers Fibercore Jena (numbers 5 and 8 in Fig. 2.13), with about 21 and 10 mol% GeO_2. [13] On the other hand, the lowest Bragg wavelength shift was found with the Ge-free fiber (number 10).

The hydrogen loading, which is a typical solution used to increase the sensitivity of the optical fiber to the UV- laser light, may also affect the FBG response to irradiation. As a matter of fact it was found by Gusarov et al. that the soaking of the fibers with hydrogen before the grating inscription dramatically reduces the radiation tolerance characteristic of FBGs [60], as shown in Fig. 2.14 (the black curve corresponds to a FBG without hydrogen loading), thus making this kind of fibers more suitable for dosimetry applications.

All these considerations turn to the fact that it is possible to expect that the sensitivity to radiation of a Fiber Bragg Grating can be optimized by a proper choice of the gratings parameters as well as the correct selection of the fiber chemical composition.

13 This result suggested that gratings made of fiber n. 8 could be well suited for radiation dosimetry.

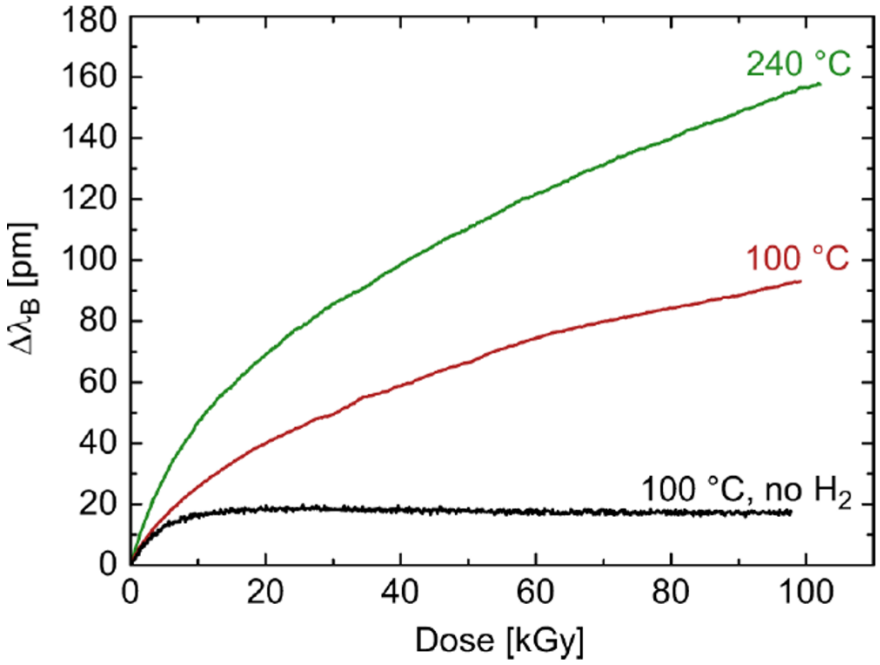

Figure 2.14: Influence of fiber hydrogen loading on the FBG response under irradiation reported by Gusarov et al. in [60]

2.8 CONCLUSIONS

With the advent of optical fiber technology, a considerable level of research has been focused on fiber optic-based techniques for humidity sensing. Although many different approaches to humidity measurement through optical fibers have been reported in literature, no commercial optical sensor has appeared on the market, and only a few approaches have proved really conclusive performances for a practical application out of the environment of a laboratory.

In the wide family of fiber optic devices, we decided to focus our attention on the Fiber Bragg Grating technology, which is playing the important role in wide range of measurement fields, offering the potentials of multiple-parameter sensing, embedding into other structures and multiplexing in a single mode fiber to form an all-fiber sensor network of which the counterpart electronic sensors lack.

In particular, in literature we found the first implementations of relative humidity sensors based on FBG technology, obtained by coating the grating with a sensitive polymeric material. However, the measurements were limited to the temperature range from 10 to 60 °C and between 10 and 90 %RH. Moreover, even if the radiation resistance of Fiber Bragg Gratings is well documented in literature, we

found that the effect of radiations on coated gratings was completely unexplored.

This fixed the aims of our research concerning the development of hygrometers for high radiation experiments at CERN: for a possible application of this technology in the CMS detector we had to demonstrate the correct operation of the sensors below 0 °C , even in the low humidity range, as well as their resistance to radiations.

The results of our deep investigations at CERN in collaboration with University of Sannio are presented in the next chapter.

3 DESIGN AND DEVELOPMENT OF FBG-BASED RELATIVE HUMIDITY SENSORS FOR HIGH RADIATIONS ENVIRONMENTS

The aim of the chapter is to present the work carried out at CERN in collaboration with the Optoelectronic group of University of Sannio concerning the development of relative humidity sensors based on Fiber Bragg Grating technology and their feasible application in high energy physics environments.

Results collected from 2011 during thorough campaigns of characterization of several samples based on this technology, both custom - that is to say fabricated in-house at the Institute for Polymers Composite and Biomaterials in Naples- and commercial ones, are reported. The performance of the sensors in terms of relative humidity and temperature sensitivities, repeatability, hysteresis and time response are presented, before and after high γ-ionizing radiation doses exposure.

3.1 CHOICE OF THE SENSITIVE MATERIAL

As already explained in the previous chapter, the sensing principle of the proposed humidity sensors based on Fiber Bragg Grating technology is based on the strain effect induced onto the grating through the swelling of the polymer coating for the effect of the absorption or desorption of moisture. The humidity response of the optical sensors monitored in terms of Bragg wavelength shift is dependent on how effectively the swelling of the material stretches the fiber. As a consequence, the adhesion of the coating onto the grating may affect the sensor performances.

As different materials possess different moisture swelling properties, the choice of the optimum polymeric material plays a crucial role in the performances of the FBG-based relative humidity sensor. Some materials give a linear response in terms of Bragg wavelength shift while some others may not. On the other hand, it is desirable to use a material that has a high moisture swelling property, but the strength of the hydrated material may be too weak to induce a de-

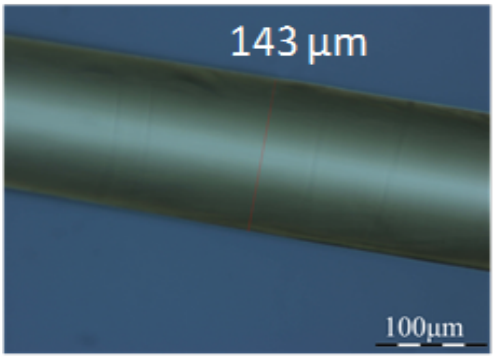

(a)

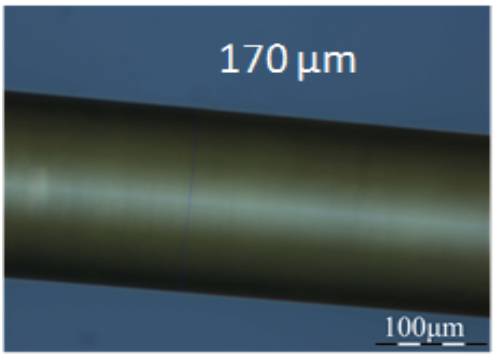

(b)

Figure 3.1: (a) Optical microscope images of the PI-coated samples *FBGcoated*1 and (b) *FBGcoated*2 under investigation

tectable strain on the fiber. Therefore, there should be a trade-off between these factors when selecting a suitable material for an optimized FBG-based relative humidity sensor.

Due to its excellent properties, that include high thermal and chemical stability, we decided to use polyimide as sensitive material. Even if the water absorption properties of polyimide are limited when compared to other moisture sensitive polymers, it seems to be the best choice as the volume expansion of this material, when exposed to humidity change, is linear and FBG sensors coated with polyimide exhibit a linear and a reversible response with the humidity change. [46, 51]

3.2 SENSORS SELECTION AND FABRICATION

Different samples of polyimide-coated FBG-based sensors were successfully produced in house by the colleagues from the Optoelectronic Group of University of Sannio, in collaboration with IPCB.

As to the sensors fabrication, the dip coating procedure was exploited, with the Fiber Bragg Gratings being submerged in a solution of commercial polyimide [1] using a stepper motor to control the speed of the dip-coating process. In particular, a slow coating speed of around 5 mm/min was used to allow a smooth coating layer to form on the fiber surface.

Before the deposition of the polymer, the gratings had been cleaved at one end and cleaned to facilitate the application of the dip coating technique. The gratings were also treated with an organosilane coupling agent [2] in order to improve the adhesion at the silica/polymer interface [3].

To achieve a polyimide coating layer of the desired thickness, a repetition of the dip coating procedure was performed and a short thermal treatment of approximately 5 min at 150 °C was carried out after each layer deposition.

Once reached the desired coating thickness, the process of fabrication was completed by applying a final curing at 150 °C overnight.

The final thickness of the coating deposited on the FBG sensors was measured by using an optical microscope [4] using a reflected setup, that was exploited to measure the diameter of the entire fiber, with and without the polyimide overlay.

The obtained measurements have an uncertainty of $\pm$ 3 µm.

Here we focus our attention on the samples named *FBGcoated*1 and *FBGcoated*2, characterized by a coating thickness of around 9 µm (with the whole fiber diameter of around 143 µm) and 22.5 µm (with the whole fiber diameter of around 170 µm), respectively. [5]

The optical microscope images of the gratings after the sensitive coating deposition are shown in Fig. 3.1a and Fig. 3.1b.

1 The selected polyimide solution was *PyralinPI*2525 from HD Microsystem
2 0.1 % *w*/*w* of HD Microsystem, *PyralinVM*651 solution
3 This treatment ensures an effective strain transfer to the gratings as a result of the polymer swelling.
4 The optical microscope used for the observations of the fabricated sensors is an Olympus *BX*51
5 The choice of such diameters was made with the aim of obtaining two relative humidity fiber optic probes with significantly different coating thicknesses and verify the thickness impact on the sensing performances as well as on their radiation resistance characteristic. To this aim, 140 µm and 170 µm were fixed as the nominal thickness values while the real values take into account the actual deposition capability in terms of accurate control of the deposition process (actually limited to few microns). For the fabrication of the probes *FBGcoated*1 and *FBGcoated*2, three and eight dipping steps were performed, thus meaning that each dip step resulted in the deposition of around 3 µm of polyimide layer onto the grating.

Their optical spectra at a constant temperature of 20 °C reveal a central Bragg wavelength of around 1530.1 nm and 1569.7 nm, for *FBGcoated*1 (Fig. 3.2b) and *FBGcoated*2 (Fig. 3.2a), respectively.

3.3 EXPERIMENTAL SETUP FOR TEMPERATURE AND HUMIDITY CHARACTERIZATIONS

In order to analyze the performances of the fabricated fiber optic hygrometers a precise control of the environment surrounding the sensors was strictly required. To this aim, a suited full-metal climatic chamber, placed in an airtight polystyrene box, was especially designed for humidity sensing applications and fabricated at CERN in stainless steel. Pictures of the vessel used for the humidity tests in the CERN lab are shown in Fig. 3.4.

The test facility is provided with a thermo-regulation circuit for temperature control in the range from −20 to 30 °C and stabilization, while a system of manual valves enables the creation of controlled levels of humidity up to 90 %RH, mixing different quantities of dry air and wet air which are sent directly to the chamber.

The compressed air belonging to the general circuit of compressed air available at CERN passes through a dryer [6], providing dry air flow, while wet air is obtained thanks to an air flow being saturated in water using an appropriate bubbler.

The details of the pipes connections used in the test stand as well as the precise position of the valves and the bubbler is sketched in Fig. 3.3.

A high performance chilled mirror dew point hygrometer (Dew Prime I from Edge Tech [62]) was exploited in order to obtain the reference humidity values during the experimental tests, as it is able to guarantee stable and precise humidity measurements, together with three miniaturized commercial electronic hygrometers (Honeywell $HIH-4000$ Series [63]). The latter were used to monitor the uniformity of the relative humidity values in the chamber and to benchmark the dynamic response to RH changes of the FBG-based sensors.

6 The dryer unit in use in the PH-DT laboratory at CERN is Ecodry K-MT, distributed by Parker Zander.

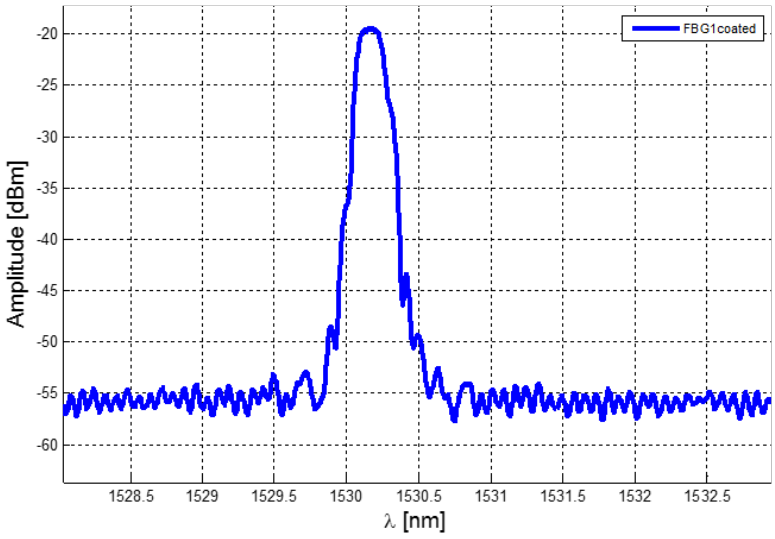

(a)

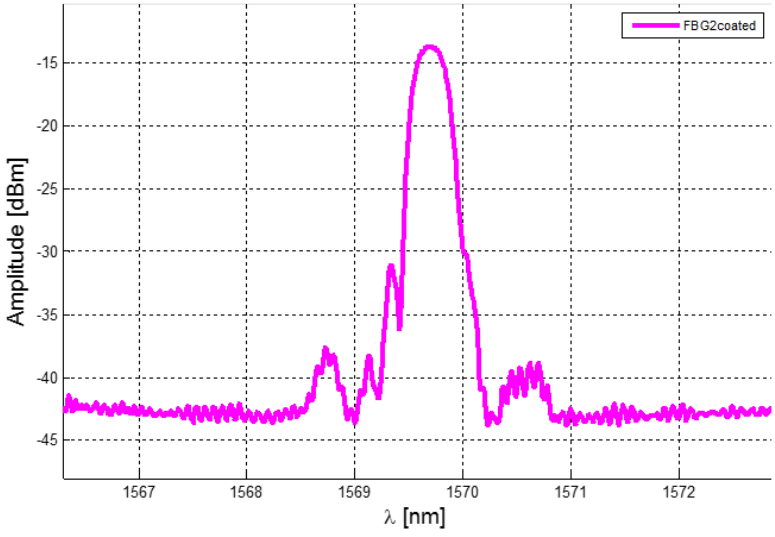

(b)

Figure 3.2: (b) Spectral response of the PI-coated samples *FBGcoated*1 and (a) *FBGcoated*2 under investigation

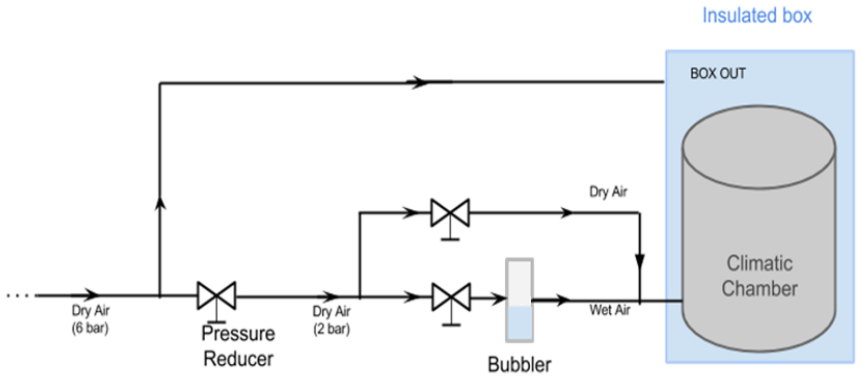

Figure 3.3: Pipes connections and valves position in the experimental setup available at CERN for humidity tests

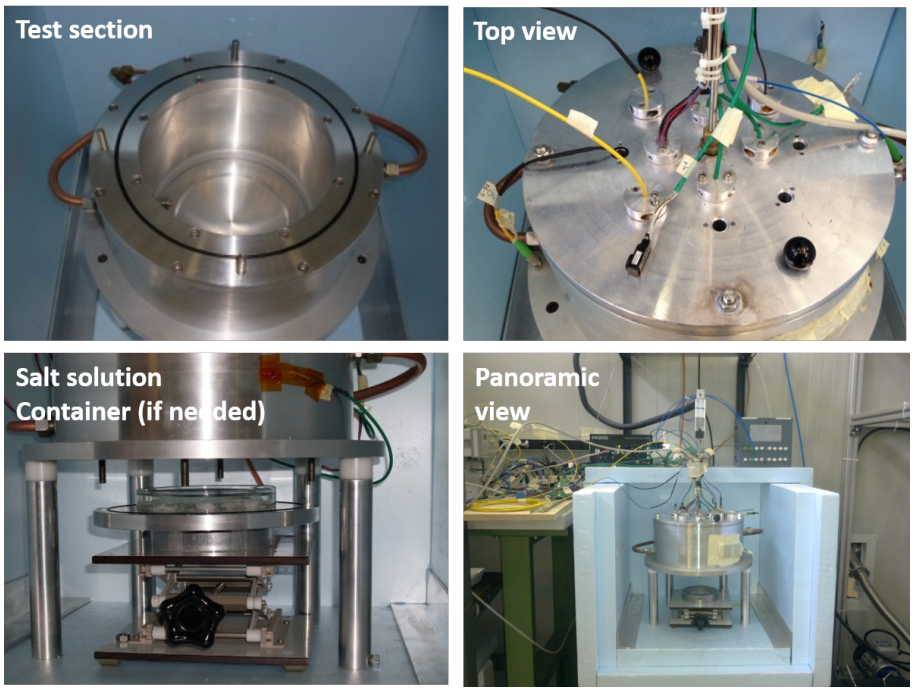

Figure 3.4: Full-metal climatic chamber, placed in an airtight polystyrene box, designed ad hoc for humidity sensing applications and available in PH-DT lab

Table 3.1: Optical properties of Micron Optics $sm125-500$ interrogator

Parameter	Value
Number of channels	4 (up to 16)
Scan frequency	2 Hz
Wavelength range	1510-1590 nm
Wavelength range	1 pm
Wavelength repeatability	0.5 pm at 1 Hz

The chamber was also equipped with three resistance temperature detectors ($PT-100$) to monitor the thermal variations during the tests as well as the temperature distribution inside the chamber itself.

In case of PI-coated FBGs (such as $FBGcoated1$ and $FBGcoated2$) fabricated through the deposition of the sensitive layer on the grating placed at the tip of the grating, the sensors were inserted inside the climatic chamber by using ad hoc designed and realized metal feedtroughs.

The fiber optic sensors were interrogated by means of a compact, field proven and accurate optoelectronic interrogator ($sm125-500$ from Micron Optics [64]), characterized by a resolution of 1 pm and operating in the wavelength range from 1510 to 1590 nm. The most relevant features of this instrument are reported in Tab. 3.1.

A schematic illustration of the final experimental setup exploited for the temperature and humidity measurements with fiber optic sensors is given in Fig. 3.5 [7].

3.4 CHARACTERIZATION OF FBG-BASED DEVICES FOR RELATIVE HUMIDITY DETECTION

In this section, the general methodology applied for the characterization of FBG-based hygrometers at CERN is described.

For tests related to the relative humidity characterization and calibration of the optical sensors, we followed the typical approach described in literature [46, 51], consisting in maintaining the climatic chamber at constant temperature and performing incremental or decremental relative humidity changes.

7 The experimental setup for optical fiber-based sensors interrogation is available in the PH-DT laboratory at CERN.

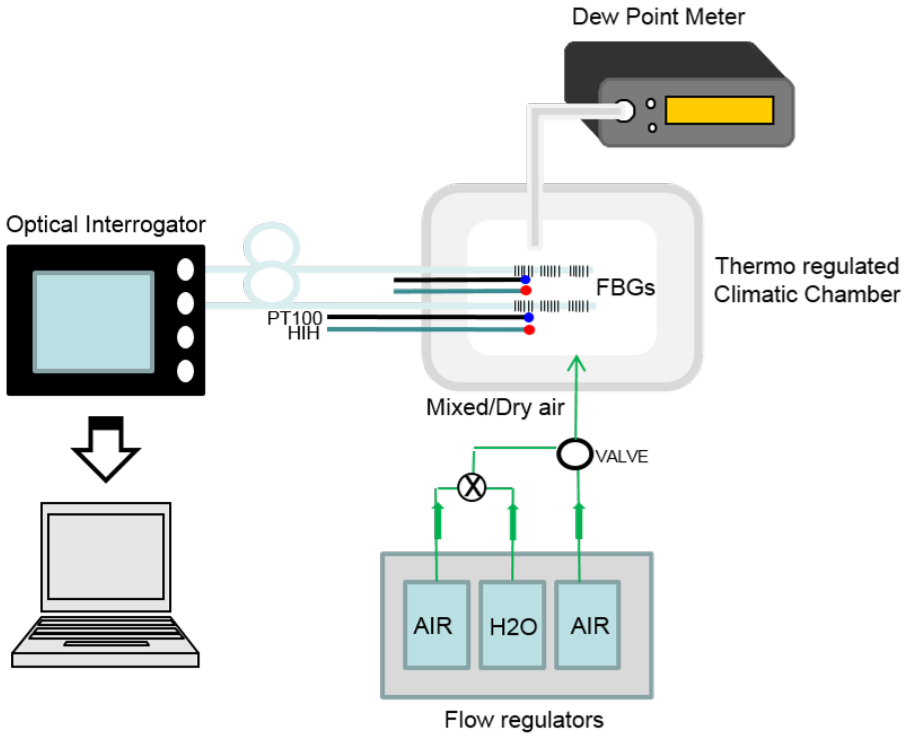

Figure 3.5: Schematic illustration of the experimental setup available at CERN for FBG-based sensors characterization

In our investigations the relative humidity was typically raised incrementally from 0 to 75 %RH and then lowered back at three different temperature values, such as 20 , 0 and -15 °C.

For each temperature and relative humidity combination, we made measurements around every two hours, to make sure that the water content within the polyimide reached an equilibrium state.

In this section we report the very first results collected from 2011 during a wide experimental testing campaign of the two samples already introduced in section 3.2, carried out in the laboratory at CERN. [47, 48]

Fig. 3.6a and Fig. 3.6b show the typical Bragg wavelength variations of the two investigated probes during a humidity test at 20 °C, with relative humidity increased up to 50 %RH. For comparison, the response provided by the reference humidity sensor during the same test is also reported (black curve).

As theoretically expected, increasing the humidity content inside the test chamber causes a red shift of the Bragg wavelength (i.e. a shift towards longer wavelengths). This is due to an increase of the mechanical strain induced on the grating by the polyimide layer, as

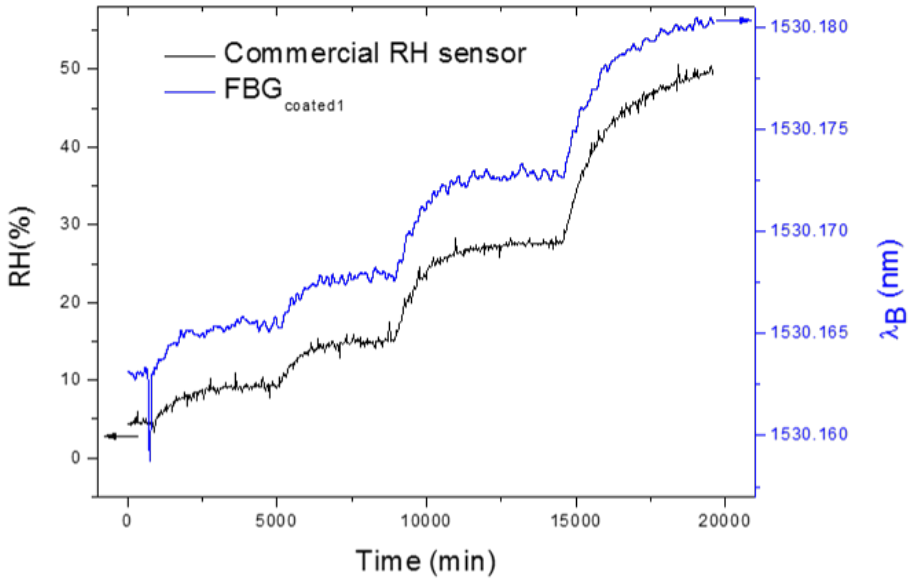

(a)

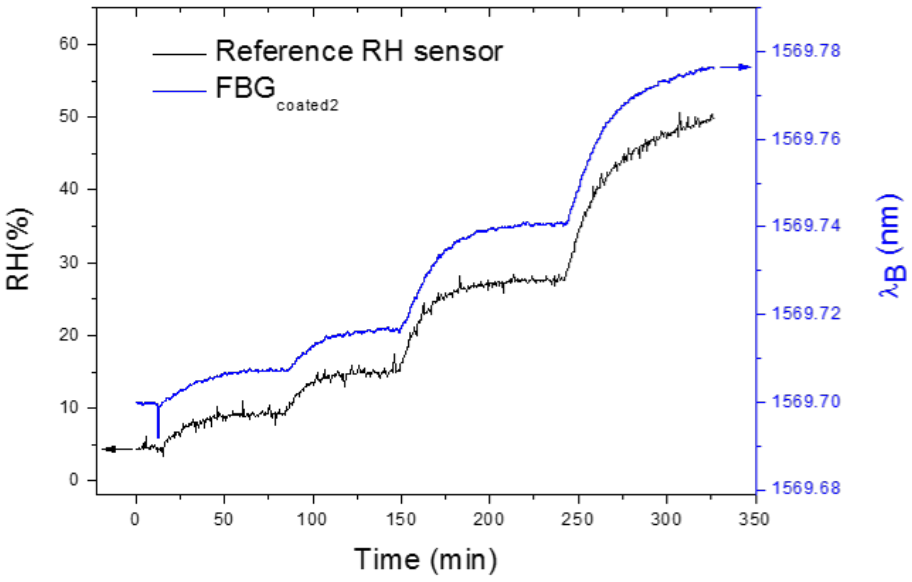

(b)

Figure 3.6: (a) Typical Bragg wavelength variation for the sensors *FBGcoated*1 and (b) *FBGcoated*2 (blue curves) during a humidity characterization test at 20 °C (for comparison the response of the commercial reference sensor is reported in black)

consequence of the higher amount of the water absorbed by the sensitive coating itself.

This behavior is also evident in Fig. 3.7b and Fig. 3.7a where the spectral responses of the two considered sensors at each humidity level is reported during the same characterization test at 20 °C.

Similar results were also obtained during the humidity tests performed at −15 °C and 0 °C, showing the capability of the PI-coated sensors to work correctly also at low temperature values in the relative humidity range of interest.

In particular the Bragg wavelength variations as a function of relative humidity at the three considered temperatures (steady state average values) are shown in Fig. 3.8a for *FBGcoated*1 and in Fig. 3.8b for *FBGcoated*2.

It can be clearly noticed that, in agreement with the standard operation of the fiber optic sensor based on Fiber Bragg Grating technology, a blue shift of the Bragg wavelength (i.e. a shift towards shorter wavelengths) was observed for both the optical devices as a consequence of the reduction in the ambient temperature.

In addition, the response towards the relative humidity changes was found to be linear, even at −15 °C and 0 °C, as emphasized by the linear fit made to all data sets in the plot. This confirmed the observations by Kronenberg et al. in [46] concerning the linear variation of the volume expansion of polyimide film with relative humidity [8].

3.4.1 Relative humidity sensitivity and temperature sensitivity

From the characteristic curves of the two investigated samples reported in Fig. 3.8a and Fig. 3.8a, it was possible to evaluate both the sensitivity terms S_{RH} and S_T as well as their variation with the temperature and relative humidity.

In particular, working at constant temperature, the relative humidity sensitivities at 20 , 0 and −15 °C can be derived, as the slopes of the linear curves resulting from the fitting procedure.

The results are shown in Fig. 3.9, where the S_{RH} values of the sensors *FBGcoated*1 and *FBGcoated*2 at the three tested temperatures are reported.

A slight dependence of S_{RH} on temperature can be clearly appreciated; in particular a small increase occurs when temperature decreases.

8 The temperature range in Kronenberg investigations was from 13 to 60 °C.

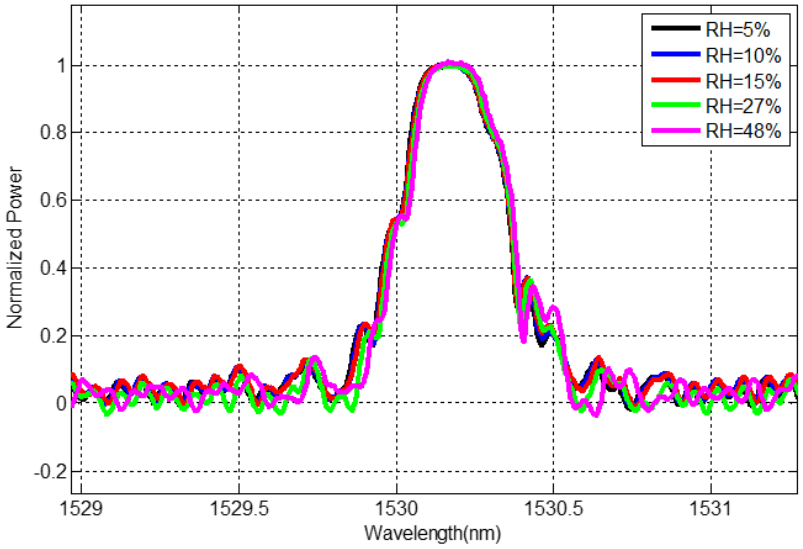

(a)

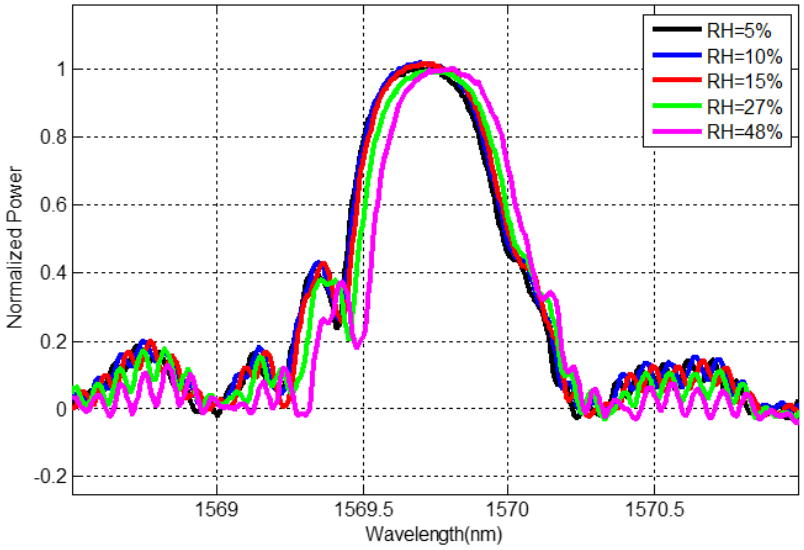

(b)

Figure 3.7: (a) Reflection spectral variations at different humidity levels at 20 °C for the sensors *FBGcoated*1 and (b) *FBGcoated*2

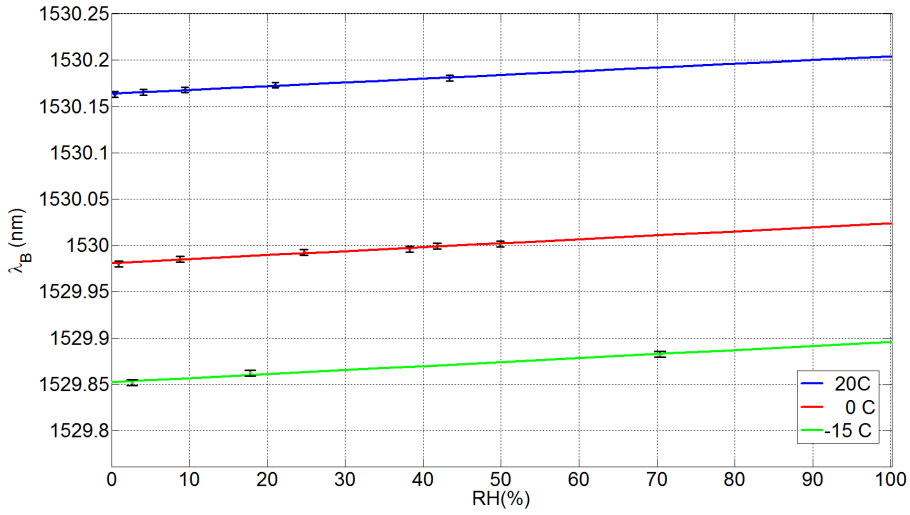

(a)

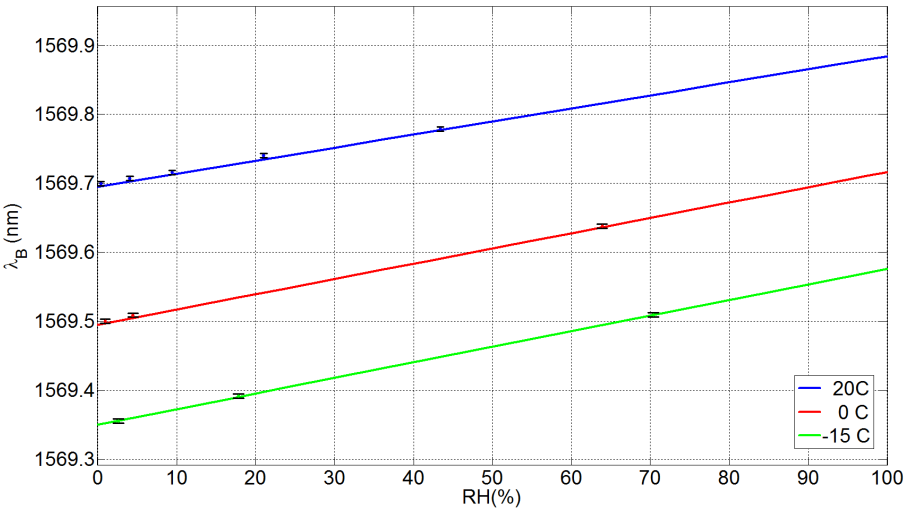

(b)

Figure 3.8: (a) Characteristic curves of sensor *FBGcoated*1 and (b) *FBGcoated*2 at the three considered temperatures of investigation

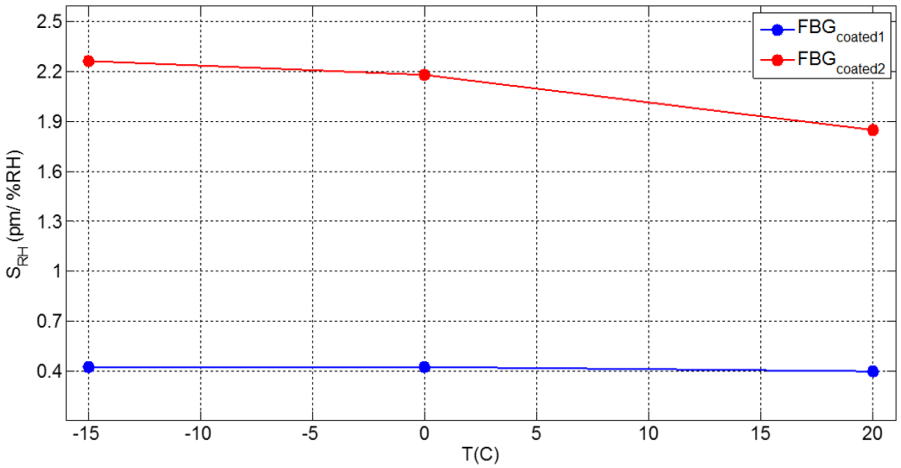

Figure 3.9: Relative humidity sensitivity dependence on temperature of samples *FBGcoated*1 (blue circles) and *FBGcoated*2 (red circles)

However, mean S_{RH} values of about 0.4 pm/%RH (with a standard deviation of $\pm$ 0.02 pm/%RH in the whole considered T range) and 2.1 pm/%RH (with a standard deviation of $\pm$ 0.2 pm/%RH in the whole considered T range) were estimated for the sensors *FBGcoated*1 and *FBGcoated*2, respectively.

It is noteworthy that the difference in the S_{RH} between the two considered sensors is due to their different coating thickness [46, 51], that is to say 9 µm for *FBGcoated*1 and 22.5 µm for the sample *FBGcoated*2.

We want also to focus the attention on the fact that, considering the minimum shift in the Bragg wavelength that can be detected by the setup presented in section 3.3, corresponding to 1 pm, relative humidity resolutions [9] as low as 2.5 %RH and 0.5 %RH can be obtained for the sensors *FBGcoated*1 and *FBGcoated*2, respectively.

From Fig. 3.8a and Fig. 3.8b, working at constant humidity, the temperature sensitivity of both the considered sensors was evaluated by deriving the λ_B versus T curves, obtained extrapolating the values of λ_B for each temperature from the linear fittings.

The results of this procedure, for three different RH values such as 0, 50 and 100 %RH, are shown in Fig. 3.10, where the blue points refer to sensor *FBGcoated*1 and the red points refer to sensor *FBGcoated*2.

It can be clearly observed that the temperature sensitivity is not constant with the relative humidity but slightly decreases with it. However, mean S_T values of about 9.5 pm/°C (with a standard deviation

9 The sensor resolution is defined as the smallest detectable incremental change of input parameter that can be detected in the output signal. In our case it was evaluated as the ratio between the minimum resolution of the optoelectronic interrogator and the relative sensitivity of the optical sensors.

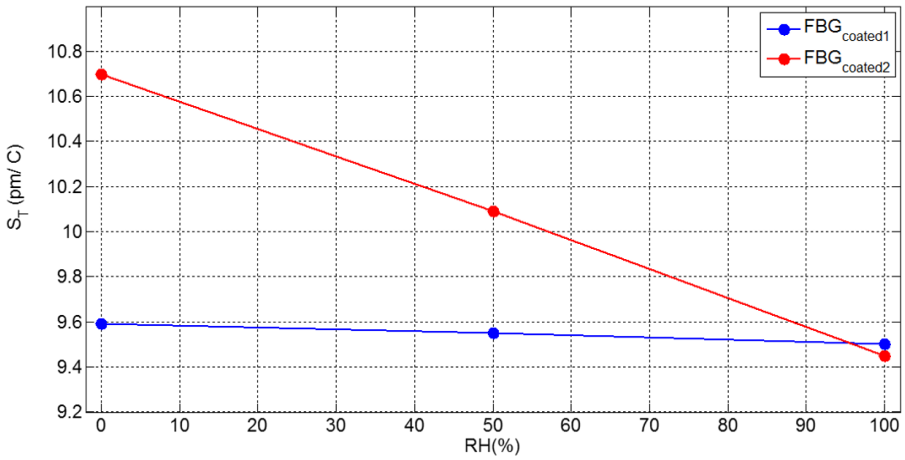

Figure 3.10: Temperature sensitivity dependence on relative humidity of samples *FBGcoated*1 (blue circles) and *FBGcoated*2 (red circles)

of $\pm$ 0.04 pm/°C in the whole considered RH range) and 10.1 pm/°C (with a standard deviation of $\pm$ 0.60 pm/°C in the whole considered RH range) were evaluated respectively for sensors *FBGcoated*1 and *FBGcoated*2. Also in this case, the increased sensitivity of the sample *FBGcoated*2 with respect to *FBGcoated*1 can be attributed to the higher thickness of the polyimide coating. [51]

Taking into account the reported results, since it was found that S_T is typically one order of magnitude higher than S_{RH} (Fig. 3.9 and Fig. 3.10), it is confirmed the extreme importance of the application of thermal compensation for the application of this technology in real environments characterized by simultaneously changes of temperature and humidity.

For this reason, our final proposal is actually a FBG-based thermo-hygrometer consisting of two gratings mounted in appropriate strain-free package and coupled side by side: one coated with polyimide, sensitive to temperature and humidity, plus an uncoated one, working as pure thermometer, located as close as possible to the first one [65]. Clearly, in order to avoid large errors induced on the relative humidity measurements, the thermometer coupled to the PI-coated FBG should be able to provide high precision temperature measurements. For example, a temperature reading error of $\pm$ 1 °C would induce an error of around $\pm$ 23 %RH in case of *FBGcoated*1 and of almost $\pm$ 5 %RH in case of *FBGcoated*2.

The sketch of the final proposed solution is reported in Fig. 3.11.

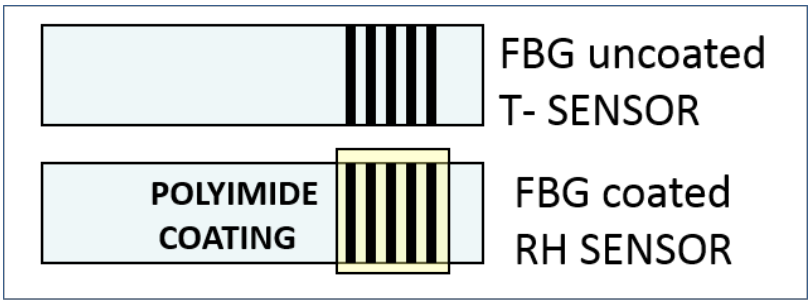

Figure 3.11: The proposed fiber optic thermo-hygrometer based on FBG technology

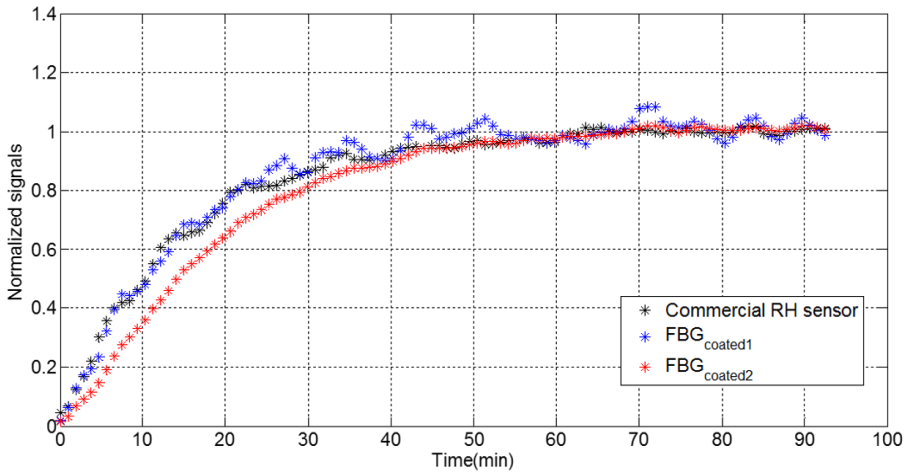

Figure 3.12: Response time of the samples *FBGcoated*1 (blue data points) and *FBGcoated*2 (red data points) when subjected to a step humidity change from 15 %RH to 28 %RH at constant temperature (for comparison, the response provided by the reference humidity sensor during the same humidity change is reported in black)

3.4.2 Time response and hysteresis

The response time characteristic of the two polyimide coated FBGs was also investigated exposing the sensors to a step of humidity change from 15 %RH to 28 %RH at a constant temperature of 20 °C. The response time of *FBGcoated*1 and *FBGcoated*2, which represents the time taken by the sensors to reach 90 % of their final value, were determined from the data curves plotted in Fig. 3.12.

Considering the time response of the reference commercial sensor, which takes also in account the time response and the dynamics of the climatic chamber, a response time of a few seconds, basically coincident with the one of the capacitive sensor, was observed for the grating coated with thinnest layer of sensitive coating, while for the thickest one it was found be around 3 min.

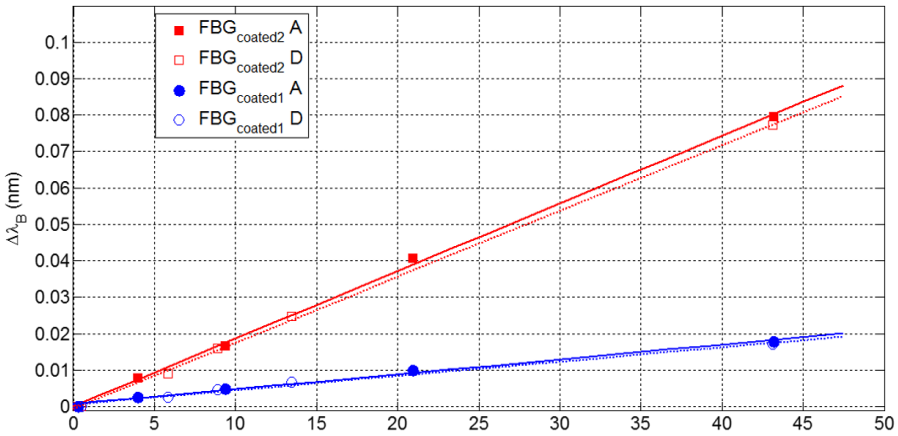

Figure 3.13: Hysteresis plots of the sensors *FBGcoated*1 (in blue) and *FBGcoated*2 (in red), subjected to humidity changes in the range 0 −45 %RH in both ascending (A) and descending (D) order

These results confirmed the existing relation between the coating thickness and the time response of the sensor, with higher time response requested in case of thicker overlays, due to an increase diffusion time of the water molecules inside the layer itself [46, 51]

In Fig. 3.13 we also report the hysteresis curves obtained for both the fabricated sensors at 20 °C. In particular, the humidity level inside the chamber was varied from 0 to 45 %RH in both the ascending and descending order. [51] Sufficient time of around two hours was given at each humidity level before the stabilized readings were recorded. The obtained results evidenced that a very small and acceptable degree of hysteresis, calculated as the maximum relative humidity difference between the linear fitting curves in the investigated humidity range, was observed. As a matter of fact, for the sensor *FBGcoated*1 a hysteresis value of around 2 %RH was measured, while for the sample *FBGcoated*2 it was found to be close to 1.6 %RH. On the other side, the observed hysteresis of the commercial reference sensor, evaluated in the same way as described for the optical devices, was found to be around 1.3 %RH, as shown in Fig. 3.14.

3.4.3 Sensors repeatability

The humidity tests at the three considered temperatures were repeated several times in order to investigate the measurements repeatability. In Fig. 3.15, the results of three tests of the samples *FBGcoated*1 at 20 °C subjected to gradual humidity variations from 0 to 60 %RH

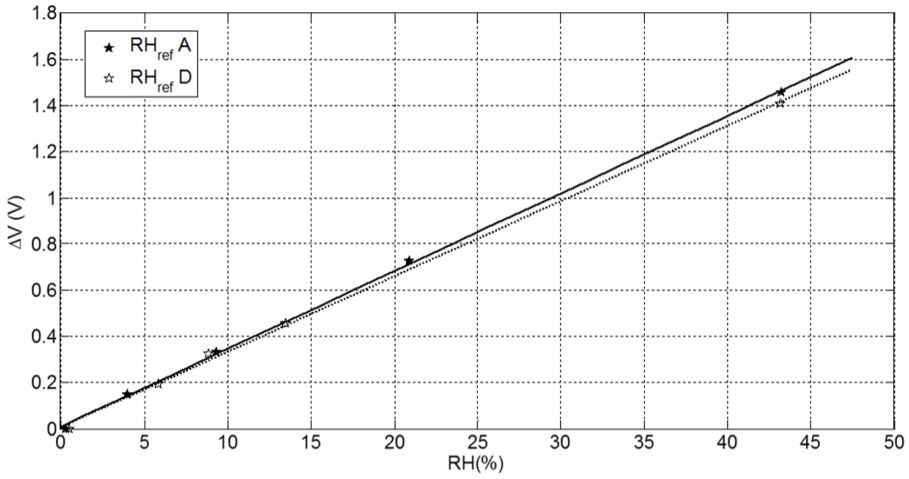

Figure 3.14: Hysteresis plot of the commercial reference relative humidity sensor subjected to humidity changes in the range $0 - 45$ %RH in both ascending (A) and descending (D) order

are reported, showing a good repeatability of the measurements from the fiber optic sensor. As a matter of fact the Bragg wavelength variations at each humidity value are inside the measurement error and for this reason can be considered negligible.

Same considerations can be done for the other investigated sample.

3.5 RADIATION TOLERANCE CHARACTERISTIC OF FBG-BASED THERMO-HYGROMETERS

Once demonstrated the performances of FBG-based relative humidity sensors at low temperatures and in the whole range of interest of relative humidity, to assess the possibility to use this technology in high radiation environments, it is still needed to evaluate their behavior in presence of radiations.

In particular, as our final design of fiber optic-based relative humidity sensor actually consisted of two gratings, one coated (sensitive to temperature and humidity) and one uncoated (sensitive only to temperature), the radiation tolerance characteristics of both the gratings had to be investigated. For this reason incremental irradiation campaigns were performed on samples of commercial humidity and temperature sensors based on Fiber Bragg Grating technology.

The irradiation processes were performed in an external company using Cobalt-60 radioactive source and after each campaigns, the sen-

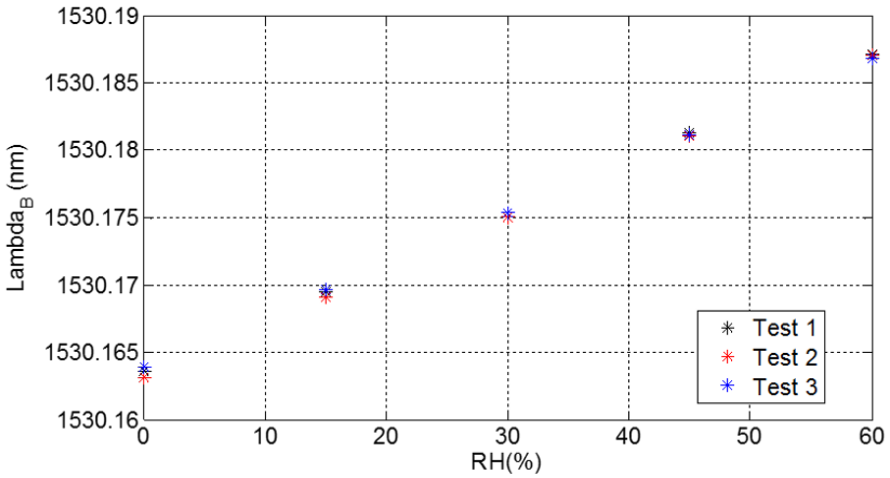

Figure 3.15: Repeatability of the sensors *FBGcoated*1 at 20 °C in the range 0 – 60 %RH

sors were tested in the climatic chamber available in the CERN laboratory.

Results of these investigations are presented in the next sections.

3.5.1 FBG-based temperature sensors irradiation campaigns

Four samples of commercial temperature FBG sensors (*os*4300 from Micron Optics [66] with an accuracy declared on the data sheet of 0.1 °C) belonging to two different batches were irradiated.

Six irradiation campaigns were performed, providing to the sensors a total adsorbed γ-ionizing radiation dose of 10 , 20 , 50 , 90 , 150 and 210 kGy at each intermediate step.

The temperature FBG-based sensors were fully characterized at CERN before and after each campaign during specific tests at low humidity, changing temperature typically in the range from 0 to 20 °C, using the same steps and methodology described in section 3.4.

The sensing characteristic of the sensors were investigated after each radiation exposure as well as the saturation properties of their radiation-induced wavelength shift.

In Fig. 3.16 results of the campaigns are summarized, for one of the four tested sensors as an example.

Interestingly, all the FBG-based temperature sensors under analysis did not change their sensing characteristic even after the absorption oh high radiation doses and still exhibited a linear behavior after each irradiation step. This means that the sensitivity to temperature values, evaluated as the slope of the fitting curves in at each irradiation level,

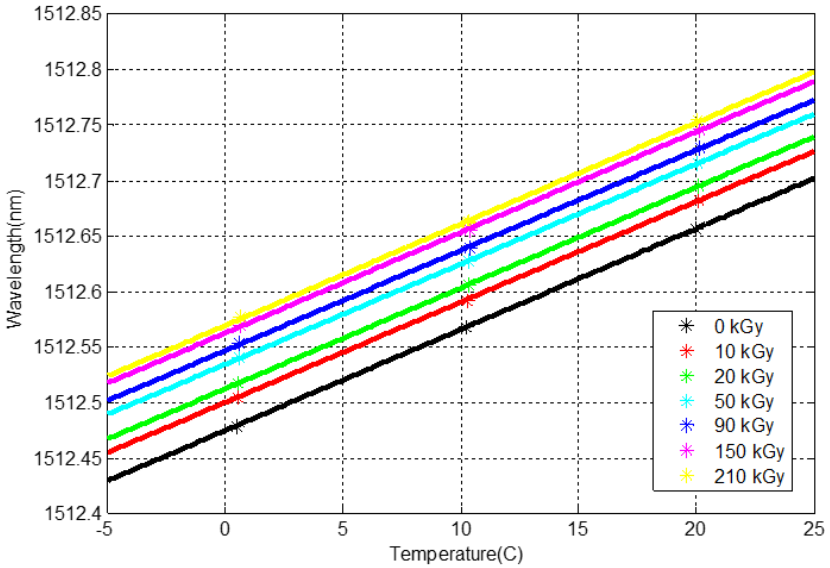

Figure 3.16: Radiation-induced wavelength shift after the exposure to incremental γ-ionizing radiation doses for one temperature FBG-based sensor

were found to be almost unchanged all over the six campaigns. For example, for the sensor considered in Fig. 3.16, the mean temperature sensitivity S_{Tmean} was found to be around 9.1 pm/°C with a standard deviation of $\pm$ 0.04 pm/°C in the range of radiation exposure from 0 kGy to 210 kGy. Clearly, these variations of the temperature sensitivity can be considered negligible as they are inside the measurement error.

A radiation-induced red shift, also evident from the spectral response of the same sample after each absorbed dose in Fig. 3.17, was observed at each irradiation step [10], confirming the observations found in literature [67].

The same characterization was conducted for the other three samples [11] and same conclusions in terms of invariant temperature sensitivity to radiations as well as wavelength shift induced by radiations can be derived (as evidenced in Fig. 3.18a and Fig. 3.18b).

3.5.2 FBG-based relative humidity sensors irradiation campaigns

The response to ionizing radiations of FBG-based relative humidity sensors was also investigated. Indeed, as these sensors are fabricated

10 The spectral response after the exposure of the considered sensor to the dose of 90 kGy was not acquired.

11 *Sample* 1 and *Sample* 2 belong to the same batch while *Sample* 3 and *Sample* 4 are linked to a different one.

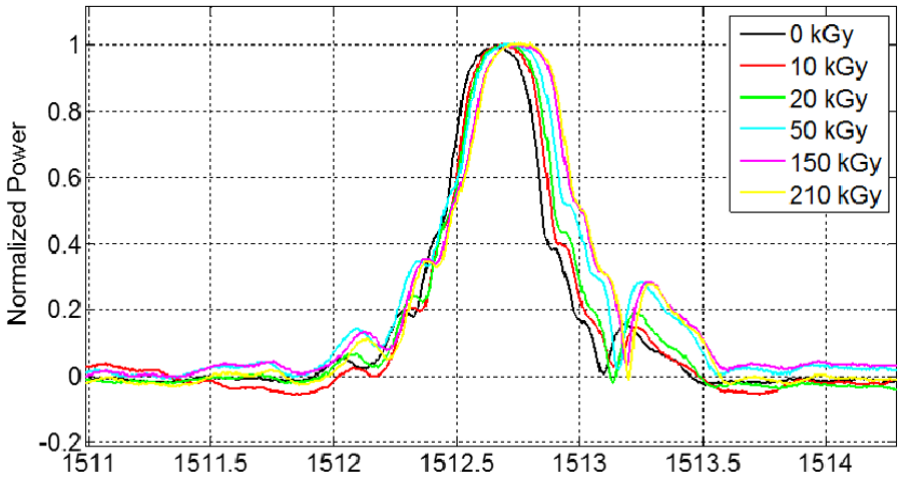

Figure 3.17: Spectral response of the same temperature FBG-based sensor shown in Fig. 3.16, after the exposure to incremental γ-ionizing radiation doses

by coating the grating with a layer of polyimide, their behavior may be different from the one shown by the uncoated gratings, depending on the effect of the radiations on the sensitive material itself.

For these tests, it was decided to outsource the production of the sensors to an external company (Welltech Instrument CO.)

Four samples of PI-coated FBGs belonging to same batch were irradiated at incremental doses of γ-ionizing radiations. In particular, five campaigns were performed, providing to the sensors a total adsorbed dose of 10 , 50 , 90 , 150 and 210 kGy at each intermediate step.

The sensors were fully characterized at CERN after each radiations exposure, performing humidity tests at different constant temperature values, changing the relative humidity from 0 to 45 %RH.

The humidity response at 20 °C of one of the investigated FBG-based relative humidity sensors for different to radiation exposures is shown in Fig. 3.19a and Fig. 3.19b. The sensor still exhibited a linear behavior after each irradiation step and the mean relative humidity sensitivity S_{RH} was found to be 1.34 pm/%RH with a standard deviation of $\pm$ 0.02 pm/%RH in the range of radiation exposure from 0 kGy to 210 kGy. The RH sensitivity variations are inside the measurement error and for this reason can be considered negligible.

Similar results were obtained at lower temperatures, such as 10 °C and 0 °C, in the same humidity range, even with the other three investigated samples [65].

For comparison, the irradiation process was also performed on one of the HIH capacitive sensors available in the climatic test chamber at CERN. However, the capacitive sensor resulted definitely damaged

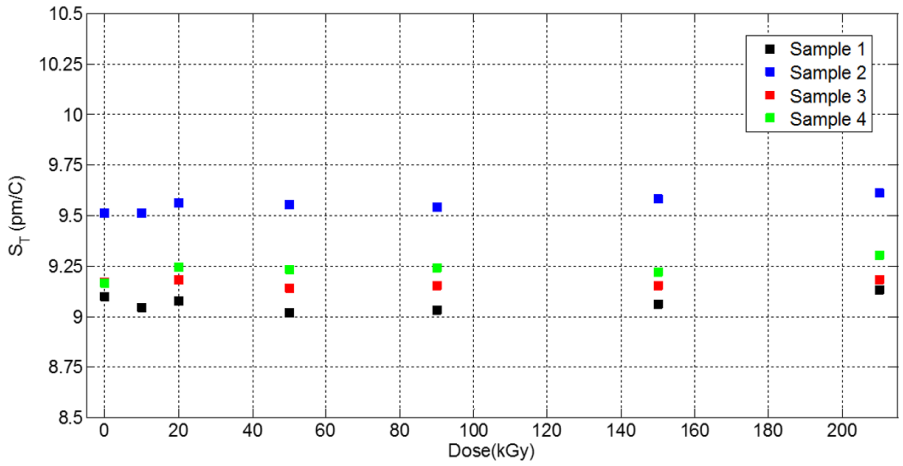

(a)

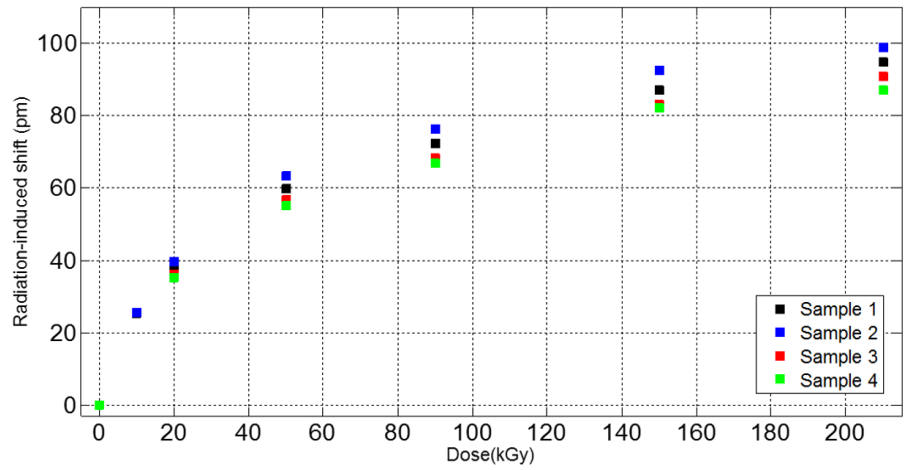

(b)

Figure 3.18: (a) Invariance of the temperature sensitivity on radiation doses and (b) radiation-induced wavelength shifts for the four tested FBG-based temperature sensors

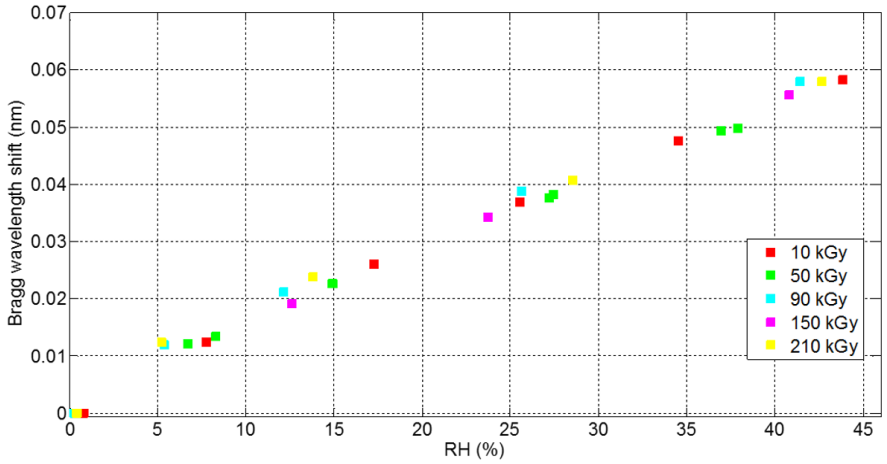

(a)

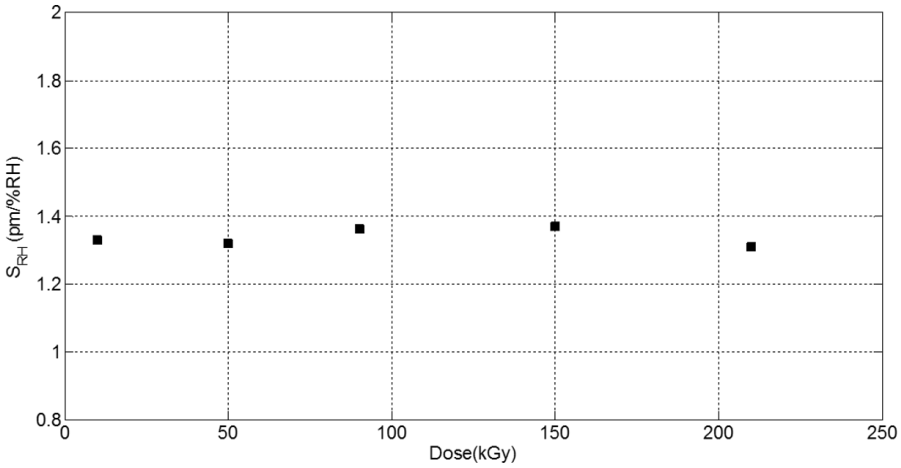

(b)

Figure 3.19: (a) Response of the selected FBG-based RH sensor to high ionizing radiations dose at 20 °C; (b) invariance of relative humidity sensitivity on radiations

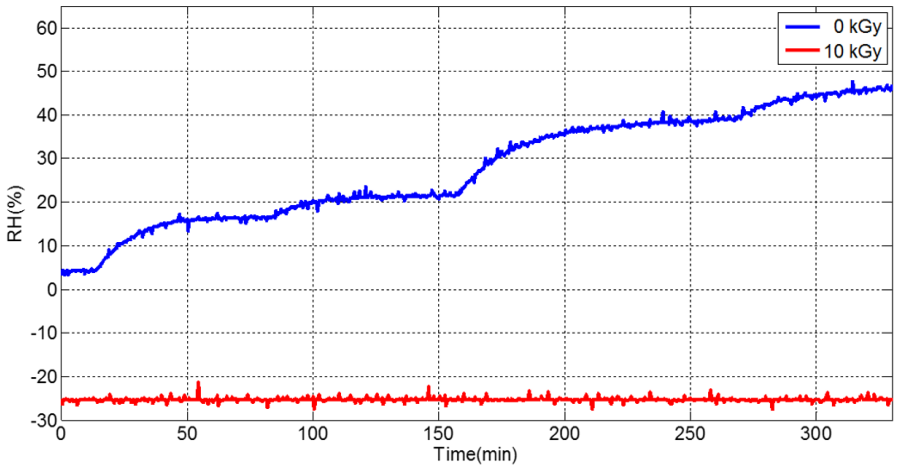

Figure 3.20: HIH relative humidity sensor before and after a γ-ionizing radiation dose of 10 kGy

after the exposure to a ionizing radiation dose of 10 kGy [12], as shown in Fig. 3.20. This confirmed that they have a poor resistance to radiations and cannot be used in high radiations environments [48].

On the other hand, with our investigations we demonstrated for the first time that polyimide-coated Fiber Bragg Gratings have good radiations resistance characteristics and that, apart a radiation-induced shift already mentioned also in case of the FBG-based thermometers, the sensing performance of these devices are not affected by the radiations exposure. This suggested that, providing a method thanks to which it is possible to take into account the shift of the observed Bragg wavelength due to irradiation process, thermo-hygrometers based on FBG technology can be a very interesting solution to the problem of humidity monitoring in the CMS experiment as well as in other high radiations environments.

3.6 POSSIBLE OPERATION IN HIGH RADIATIONS ENVIRONMENTS

In order to asses the possibility to exploit the thermo-hygrometers based on Fiber Bragg Grating technology in high radiations environments, we need to understand how it is possible to take into account the Bragg wavelength shift induced by exposing the sensors to radiations.[65, 68]

12 10 kGy is the absorbed dose expected after two years of LHC activity (considering a luminosity of 100 fb^{-1}) for sensors installed at 40 cm distance from the beam pipe.

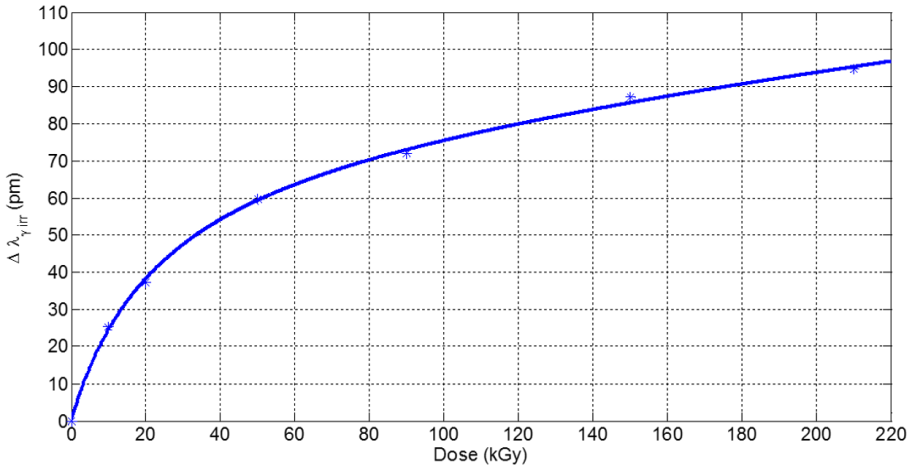

Figure 3.21: Radiation-induced wavelength shift of the considered FBG-based sensor in function of the γ-ionizing radiation dose

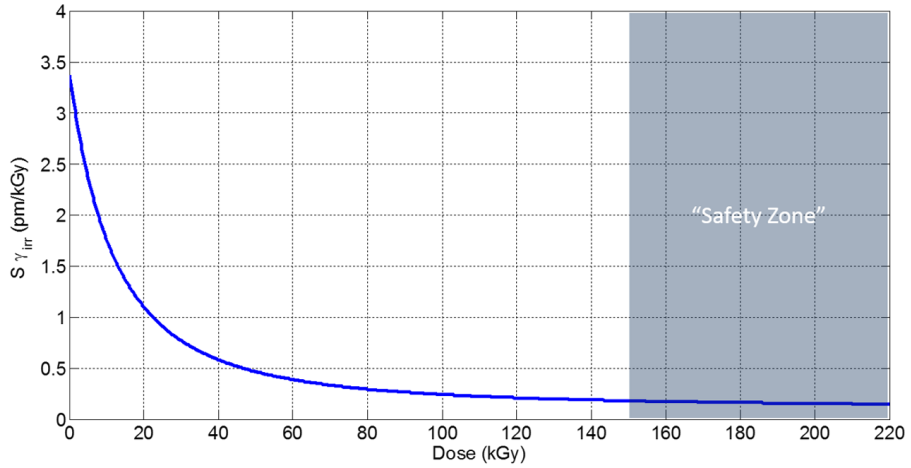

Figure 3.22: Sensitivity of the considered FBG-based sensor to further γ-ionizing radiations in function of the dose

As a matter of fact, we found that it is possible to find a general correlation between the radiation-induced wavelength shift $\Delta\lambda_{\gamma\text{-rad}}$ and the total adsorbed dose as shown in Fig. 3.21.

As an example, we will refer here to the same FBG-based temperature sensor considered for the plots in Fig. 3.16 and Fig. 3.17.

The observed wavelength shift of the FBG is not saturated up to 210 kGy. However, above a 100 kGy total adsorbed dose, the shift shows an almost linear and relatively small increase with the dose.

Fig. 3.22 shows the values of the derivative of the radiation-induced wavelength shift, which corresponds to the sensitivity of the sensor to further γ-ionizing radiation doses exposure ($S_{\gamma\text{-irr}}$).

It can be observed that after an adsorbed dose of 150 kGy, $S_{\gamma\text{-irr}}$ is below 0.15 pm/kGy. A sensor pre-irradiated at doses $\geq$ 150 kGy will therefore exhibit a radiation-induced shift lower than 0.15 pm per any additional kGy absorbed.

In CMS, considering an integrated luminosity up to 150 fb^{-1}, the maximum absorbed dose can be estimated to 12 kGy for any sensor placed at a radial distance $\geq$ 400 mm from the beam line. Such a maximum dose corresponds, for a correctly pre-irradiated sensor, to a wavelength shift of 1.8 pm. This corresponds to a radiation-induced error on the temperature reading of the order of 0.18 °C, comparable to the temperature measurement accuracy of the sensor.

Very similar considerations can be applied to all the other sensors examined, even in case of coated FBGs. [65, 68]

This means that we can use optical thermo-hygrometers based on FBG technology in high radiation environments, just performing a pre-irradiation step of both the coated and uncoated sensors at a dose higher than 150 kGy in order to bring them in the "safety-zone", characterized by a very low sensitivity to additional γ-ionizing radiation doses.[65, 68]

Such pre-irradiated sensors will not necessitate any recalibration, if placed at a distance $\geq$ 400 mm from the beam line, up to an integrated luminosity of 150 fb^{-1}. Pre-irradiated sensors placed at smaller radial positions can in any case be considered, introducing a simple on-line correction to their reading, based on an estimate of the effectively absorbed dose.

3.7 CONCLUSIONS

The presented results gave the first demonstration of the real feasibility of coated FBG-based sensors for applications of relative humidity monitoring in high radiation environments.

As a matter of fact, with our research, we actually filled the gap in the state of art of relative humidity sensors based on FBG technology (summarized in Tab. 2.1), as we demonstrated for the first time to our knowledge that PI-coated Fiber Bragg Gratings can correctly work at temperature below 0 °C, giving reasonable and repeatable measurements in the whole relative humidity range of interest, even at low humidity values.

Moreover, we provided a clear proof of the tolerance to radiations of these sensors. Indeed we found that the sensing performance of

these devices are not affected by radiations and that they can be applied in high radiation environments just performing, before their installation, a pre-irradiation step, in order reduce the cross-sensitivity due to radiations.

These exclusive features of the proposed technology made the developed sensors very attractive for the CMS experiment which has financed in 2012 the purchasing of 80 thermo-hygrometers based on Fiber Bragg Grating technology for the thermo-hygrometric control of the air in front of the tracker volume.

4 FBG-BASED THERMO-HYGROMETERS FOR CMS TRACKER

Following the very promising results collected within our investigations about fiber optic sensors for relative humidity sensing, the CMS Tracker financed in 2012 the purchasing of 80 optical thermo-hygrometers based on Fiber Bragg Grating technology with aim to have a complete mapping of temperature, humidity and dew point temperature in front of the Tracker volume of the experiment.

The standard telecommunication silica fiber SMF28, already in use for the optical read-out of the particle signals from the Tracker, was selected. Therefore, silica fibers were also selected for the fabrication of the FBG gratings.

The installation of the network of FBG-based thermo-hygrometers in CMS, which started in December 2013, represents the very first application of this technology outside of a laboratory environment.

In this chapter some examples of the first operation of the optical thermo-hygrometers installed inside the detector are provided. The limits and the benefits of this technology are also underlined at the end of the chapter.

4.1 FINAL DESIGN OF THERMO–HYGROMETERS BASED ON FBG TECHNOLOGY FOR CMS

In order to fulfill the demand from CMS concerning the installation of a network of about 80 thermo-hygrometers around the cold services in front of the Tracker volume of the experiment in the requested time, it was decided to select a commercial partner.

The order was placed with OptoSmart, a spin-off company of University of Sannio and CNR, who was responsible for the procurement of both the coated and uncoated FBGs, and for the assembly of the FBGs arrays.

As to the thermometers, the choice was oriented towards reliable and very stable FBGs, mounted in a strain-free ceramic package, developed and produced by Micron Optics.

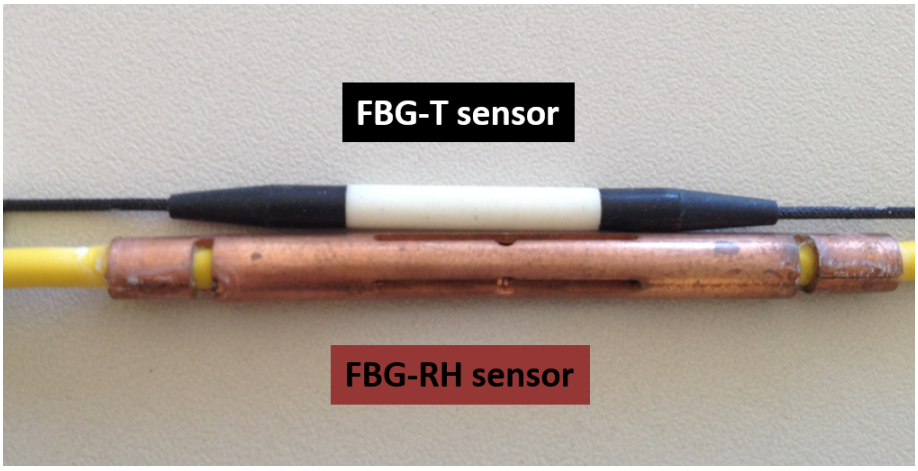

Figure 4.1: Picture of a FBG-based thermo-hygrometers for the installation in the CMS experiment

For the polyimide-coated sensors, gratings provided by the company Welltech, with a requested nominal thickness of the sensitive layer of 10 µm ± 2 µm, were finally selected. For the installation of FBG-based relative humidity sensors in harsh environment such as the CMS detector, a special copper packaging was designed, in order to protect the gratings and keep them in a strain-free condition.

The final configuration of the proposed thermo-hygrometer developed for the CMS experiment is shown in Fig. 4.1. As already mentioned, it consists of two FBG-based sensors, one sensing temperature and relative humidity variations (coated grating) and one sensitive only to temperature (uncoated grating), needed for temperature compensation purposes.

The different FBG-based arrays were assembled by OptoSmart, following the specifications agreed with the CMS experiment, in terms of distance between two consecutive gratings and total length of the fibers. This activity will be fully detailed in the next section.

As to coated gratings, during the quality check performed by OptoSmart, measurements of the thickness of the polyimide coating were performed over a sample of 17 gratings [1], i.e. $\sim$ 20 % of the procured gratings. Results of the measurements are shown in Fig. 4.2 and demonstrate the non-homogeneity of the polyimide coating thickness deposited onto the gratings (with even 5 microns of difference respect to the nominal requested thickness, as in the case of sample 4).

1 In particular, for each sample, three measurements of the thickness of the polyimide layer were conducted and the values reported in the histogram in Fig. 4.2 represent the mean thickness value.

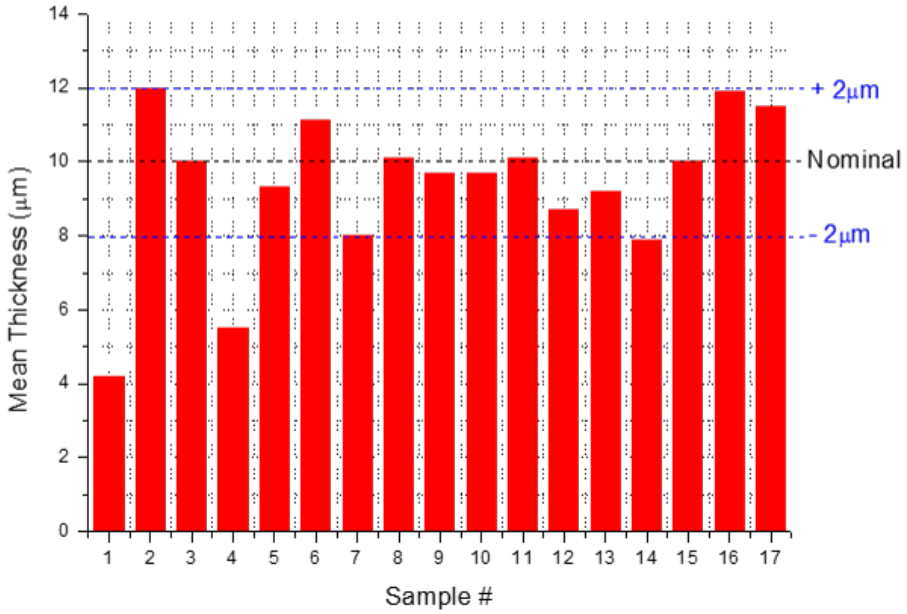

Figure 4.2: Measurements of the thickness of the polyimide coating of a sample of 17 coated FBGs for CMS performed by OptoSmart

Due to the strict timing of the preparation process in order to match the installation window, this non conformity was accepted, thus predicting differences in the response of the sensors in terms of sensitivity to relative humidity changes. [46]

Once organized in arrays, the thermo-hygrometers were delivered at CERN for their full characterization in respect to temperature and relative humidity variations, following the general methodology described in Section 3.4. This allowed us to apply a kind of second quality control of the sensors, discarding eventually the ones which we labeled as "flawed", in case they were not providing very good performance in terms of linearity and sensitivity in comparison to all the others.

Prior to the installation in CMS, the selected sensors were irradiated in an external company at 210 kGy, in order to bring them in the "safety-zone", characterized by a very low sensitivity to additional γ-ionizing radiation doses, as explained in Section 3.6.

For each temperature and relative humidity sensors, we evaluated the wavelength shift due to irradiation comparing the data acquired in the experiment in stationary conditions with the data accumulated in the laboratory. We finally implemented a mathematical model to translate the wavelength readings provided by the optical thermo-

hygrometers in temperature and relative humidity, taking into account the measured radiation-induced shifts.

4.2 INSTALLATION OF FBG-BASED THERMO-HYGROMETERS IN CMS EXPERIMENT

The final designed monitoring system in the CMS detector consisted of a total number of 144 FBG-based sensors, 72 providing the humidity measurements plus other 72, providing the temperature readings. The original plan consisted in using 4 arrays of 28 FBG-based sensors each (two arrays for T-FBGs and two arrays for RH-FBGs) in order to cover the inner side of the Tracker Bulkhead of the CMS experiment plus 2 arrays of 8 FBG-based sensors (one for T-FBGs and one for RH-FBGs) for the monitoring on the outer side.

Nevertheless, as we found that for the "long" arrays (i.e. made of 28 gratings), an attenuation of the peaks amplitude took place due to power losses along the fiber (with a difference of tens of dBm between the amplitude of the first and the last peaks present on the same fiber), we finally decided to change the final configuration of the arrays for CMS, by choosing to have a maximum number of 12 gratings in the same array. [2]

The assembly of the final arrays, conducted by the colleagues of OptoSmart, consisted in performing a series of junctions FBG-SMF28 with a fusion splicer.

The fibers prepared for the installation in the CMS experiment were finally organized as follows:

Bulkhead (inside) on the Positive side:

- 3 fibers with 28 RH-FBGs (12+12+4)
- 3 fibers with 28 T-FBGs (12+12+4)

Bulkhead (inside) on the Negative side:

- 3 fibers with 28 RH-FBGs (12+12+4)
- 3 fibers with 28 T-FBGs (12+12+4)

2 We decided to assure a minimum peak amplitude of 15 dBm, in order to avoid troubles with the application of the peak detection algorithm. In this regard, a number of 12 gratings per fiber seemed to be a reasonable compromise, well matching the planned sensor pattern.

Bulkhead (outside) on the Positive side:

- 1 fiber with 8 RH-FBGs
- 1 fiber with 8 T-FBGs

Bulkhead (outside) on the Negative side:

- 1 fiber with 8 RH-FBGs
- 1 fiber with 8 T-FBGs

To determine the minimum spectral spacing between each FBG sensor, it was needed to take into account the spectral range of variation of the central wavelength of the grating due to temperature variations (as the T sensitivity of a Fiber Bragg Grating is typically one order of magnitude higher than its sensitivity to relative humidity changes).

The distance between each adjacent sensor was decided taking into account the positions that the sensors themselves should have reached in the experiment, according to the CMS specifications.

The routing of the fibers installed in the inner face of the Tracker Bulkhead [3] on both Positive and Negative sides of the detector as well as the positions of each FBG-based thermo-hygrometers on the volume are reported in Fig. 4.3a and Fig. 4.3b, respectively.

The fibers with temperature and humidity sensors follow exactly the same pattern. For simplicity, the routing of the two long fibers with 12 sensors each is reported in the pictures using one single color.

In Fig. 4.4a and Fig. 4.5a the routing of the fibers and the position of the FBGs on the outer face of the Tracker Bulkhead on both sides of the detector are specified. Pictures made after the installation of these arrays are provided in Fig. 4.4b and Fig. 4.5b. The red and yellow circles evidence the different positions of the installed sensors in the volume.

We started the installation of the first 56 thermo-hygrometers based on FBG technology (56 RH-FBGs and 56 T-FBGs) on the inner face of the Tracker Bulkhead in December 2013 and it took around ten working days to complete it on both sides of the detector.

On the other hand, the installation of the remaining 16 thermo-hygrometers (16 RH-FBGs and 16 T-FBGs) on the outer face of the

3 The CMS tracker Bulkheads are the end flanges closing the Tracker volume and separating its cold volume from the external environment at room temperature. On the Bulkheads, hundreds of electrical connectors are housed and thousands of services, including many cold pipes, cross the volumes through them. A constant monitoring of the dew point is vital in this region to avoid dangerous phenomena of condensation.

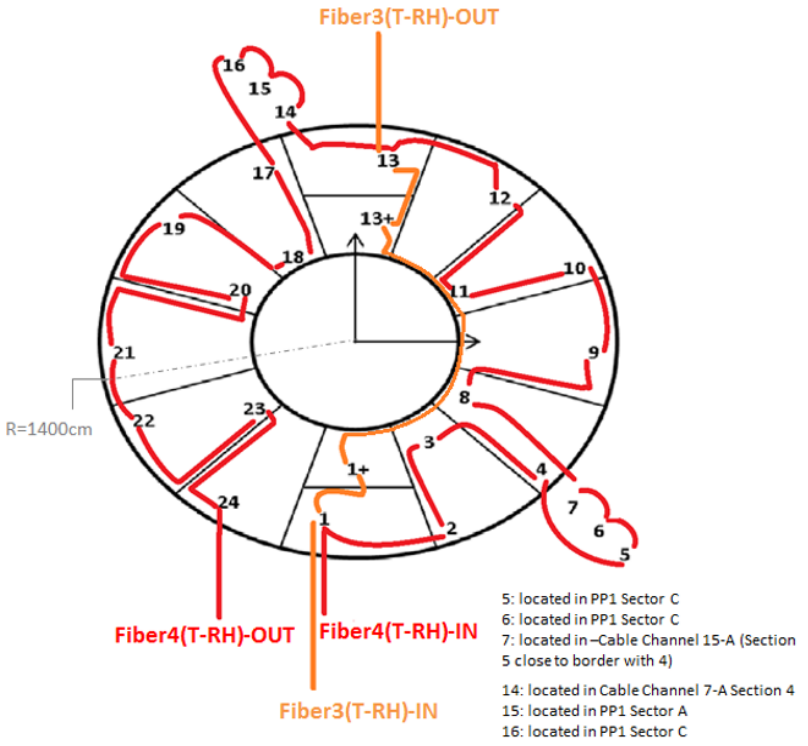

(a)

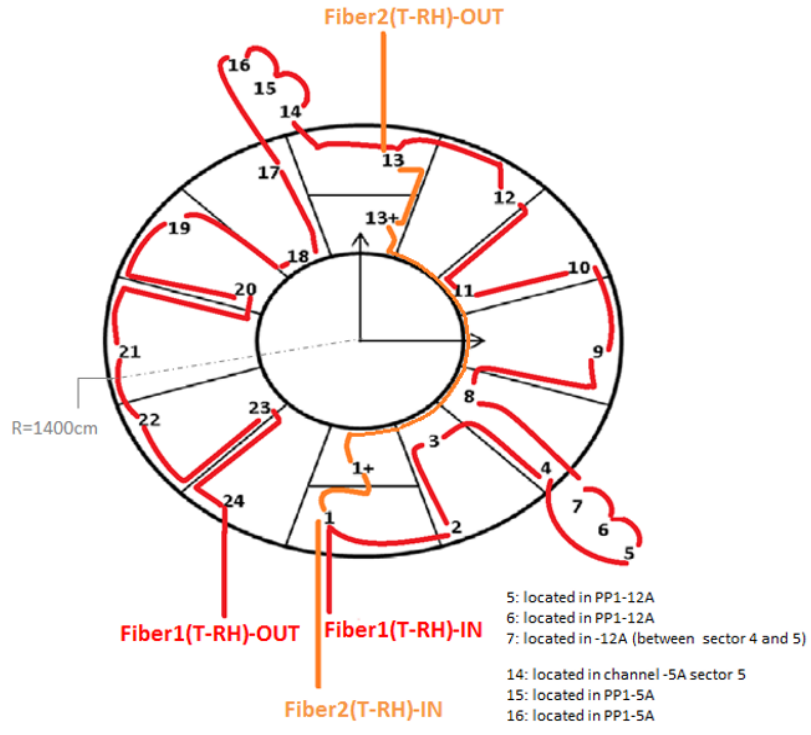

(b)

Figure 4.3: (b) Schematic of the FBG-based thermo-hygrometers installed on the inner face of the Tracker Bulkhead on the Positive and (a) Negative sides of the CMS experiment

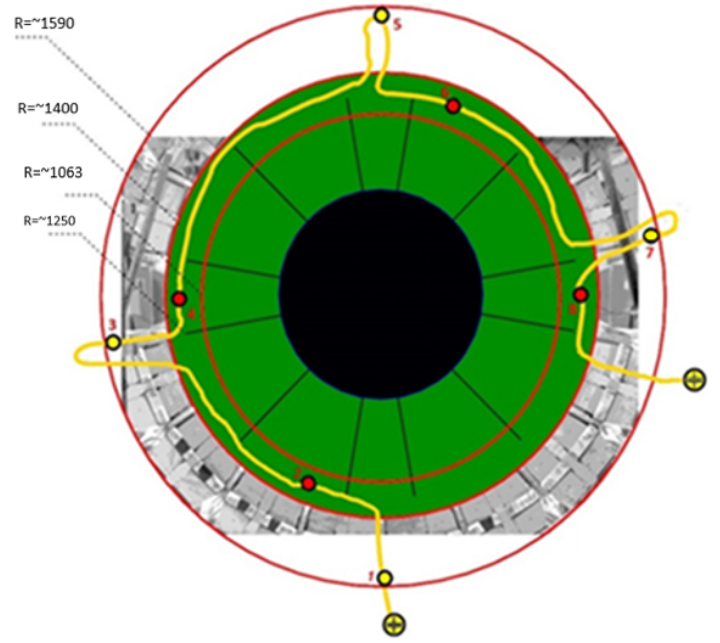

(a)

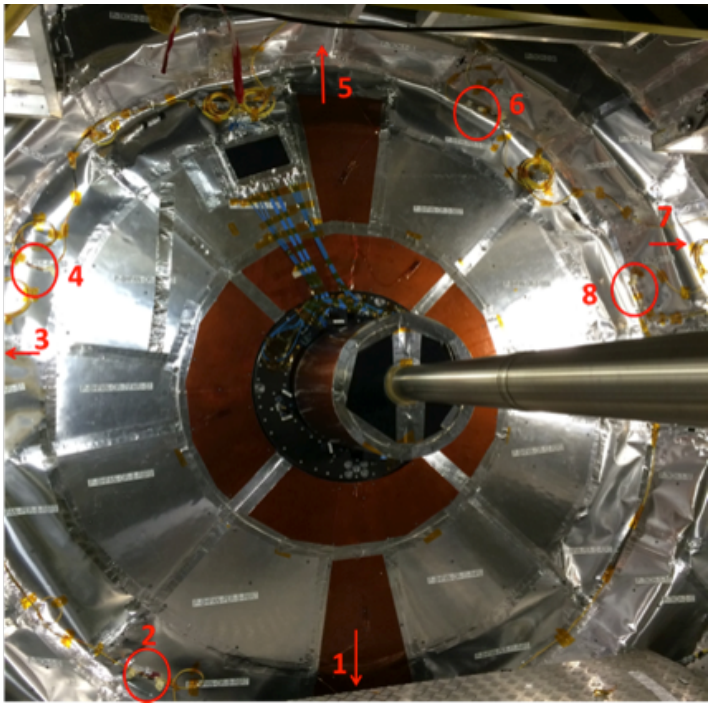

(b)

Figure 4.4: (a) Schematic of the FBG-based thermo-hygrometers installed on the outer face of the Tracker Bulkhead on the Positive side of the CMS experiment. (b) Pictures of outer face of the Tracker Bulkhead on the Positive side where the FBGs were installed (red circles evidence the position of the FBGs)

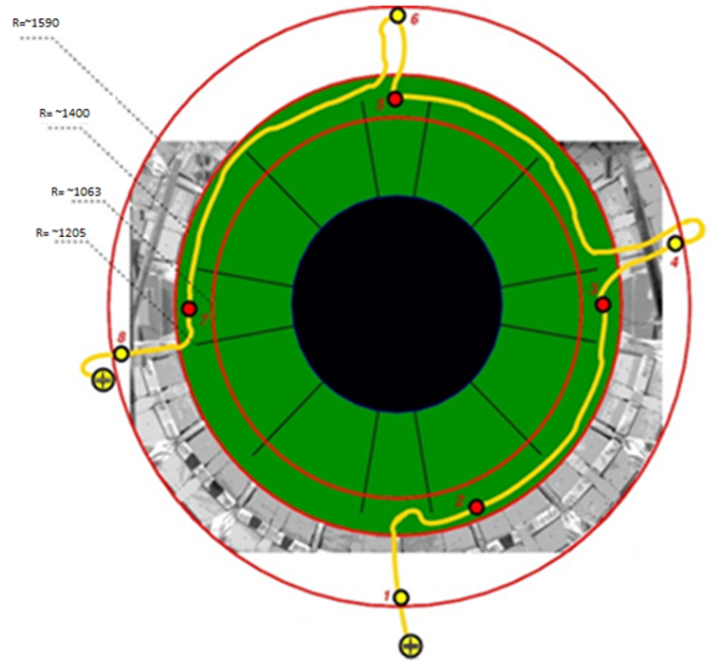

(a)

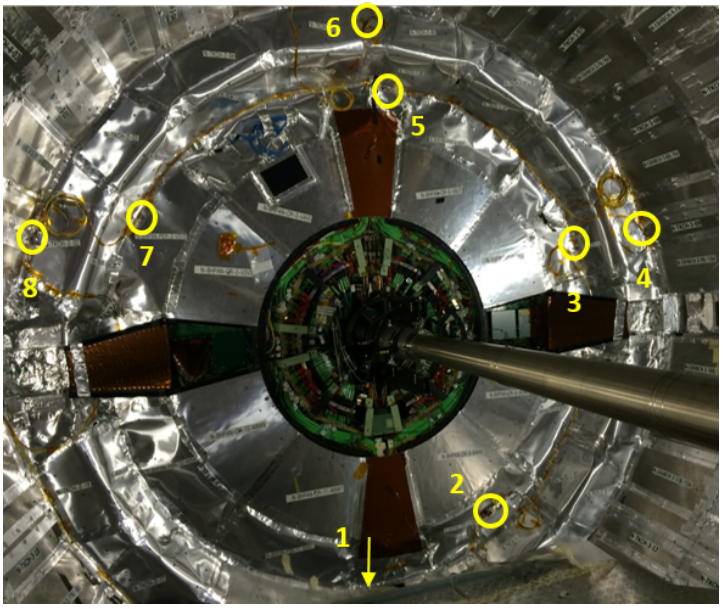

(b)

Figure 4.5: (a) Schematic of the FBG-based thermo-hygrometers installed on the outer face of the Tracker Bulkhead on the Negative side of the CMS experiment. (b) Pictures of outer face of the Tracker Bulkhead on the Negative side where the FBGs were installed (yellow circles evidence the position of the FBGs)

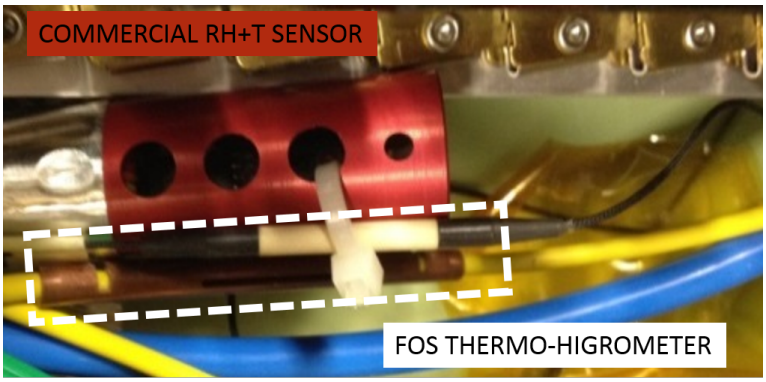

Figure 4.6: FBG-based thermo-hygrometer installed in the CMS Tracker (coupled to standard T+RH sensors placed in an appropriate casing)

Bulkhead took place at the end of January 2015, immediately before the end of the LS1 period, in respect of CMS long shutdown activity schedule.

In the inner face of the Tracker Bulkhead, during the installation, we coupled, wherever possible, our sensors to a standard hygrometer (Honeywell $HIH-4030$ capacitive sensor plus Dallas $DS2438$ digital semiconductor thermometer for humidity and temperature measurements, respectively), read out with Arduino microcontrollers, as shown in Fig. 4.6. These sensors have been introduced in CMS during the Long Shutdown 1 period to get a more fine-grained understanding of the humidity situation in the various volumes of the experiment during the maintenance time window. As already discussed in the first chapter, they are not expected to be radiation hard and probably will not survive for a long time to the radiations due to the particles collisions. However their presence in the same installation points as our FBG-based thermo-hygrometers gave us the possibility to prove the performance of our optoelectronic monitoring system. Indeed, as they provide temperature, humidity and dew point measurements, we used them to benchmark the optical sensors performance.

Only in a few points of the inner part of the Tracker volume, sniffers are also available for comparisons. These correspond to the positions 1 and 13 on both Positive side and Negative side, shown in Fig. 4.3a and Fig. 4.3b. In all these cases, we coupled the optical sensors to both the T+RH sensors and sniffing pipe, as shown in Fig. 4.7

On the outer face of the Tracker Bulkhead, there is only one point per side where both T+RH standard sensors and sniffer are available for comparison, in the same position as the optical sensors. This corresponds to the position 2 in both Fig. 4.4a and Fig. 4.5a. Apart

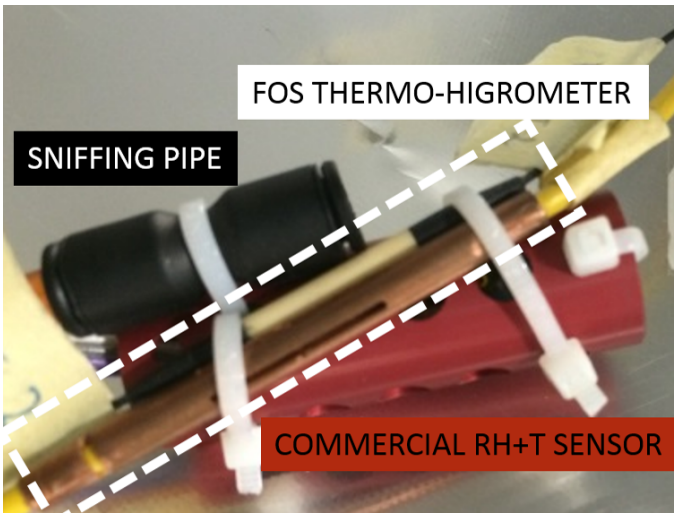

Figure 4.7: FBG-based thermo-hygrometer installed in the CMS Tracker (coupled to standard T+RH sensors and sniffer pipe available in the same position)

from these two installation points, on the outer face of the Tracker Bulkhead of the experiment, the optical fiber sensors are the only devices available which provide the temperature and humidity measurements.

4.3 FOS ACQUISITION SYSTEM AT CMS

The optical fibers installed on both sides of the CMS Tracker have been directed to the so-called Underground Service Cavern, about 100 meters far from the sensors, in order to reach the optical interrogator.

USC is one of the twin caverns of the CMS experiment and it is isolated by means of thick concrete walls from the experimental one that houses the detector itself. Being radiation safe, this cavern is always accessible, even during the operations of the accelerator.

The optical fiber sensors are read out by a Micron Optics *sm*125 optical interrogator system (already presented in 3.3) that is equipped with an Ethernet interface and can be accessed through a proprietary TCP/IP protocol. In order to reduce network traffic on the interrogator, it is connected to a mini private network created by the readout computer. This computer has another network interface installed as well, that allows the integration and sharing of the FOS system data with the CMS Detector Control System.

Moreover the read out software, which communicates directly with the Micron Optics interrogator, has been written in Java language by

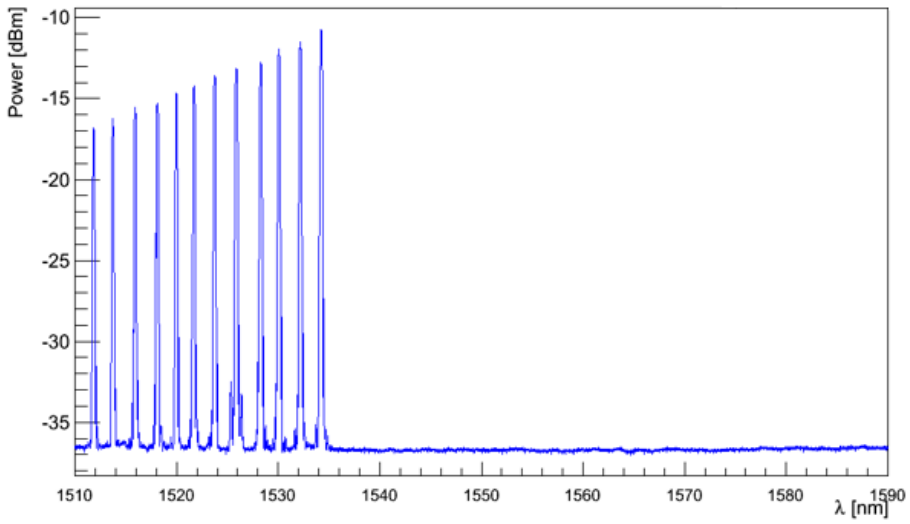

Figure 4.8: Reflected spectrum of one of the fibers installed in the CMS Tracker: the 12 peaks correspond to the 12 FBG-based sensors, inscribed on the same fiber

our group. It downloads peak definition parameters and reads out both peak information and the spectrum of each optical fiber.

More details about the acquisition system are provided in [69].

In Fig. 4.8, the reflected spectrum of one of the fibers installed in the CMS experiment is shown. The 12 peaks correspond to the 12 FBGs inscribed on the same optical fiber. This is also a good example of wavelength division multiplexing applied in practical applications.

4.4 FBG-BASED THERMO-HYGROMETERS IN OPERATION IN CMS

In this section results of some FBG-based thermo-hygrometers in operation in the CMS experiment are provided.

In order to facilitate the dissertation and to evaluate the performance of the proposed sensors, it is convenient to present their temperature, humidity and dew point temperature reconstructions in different subsections, each referring to the following situations:

- Optical thermo-hygrometers coupled only to T+RH standard sensors, installed in the inner face of the Tracker Bulkhead
- Optical thermo-hygrometers coupled to both T+RH standard sensors and sniffing pipe installed in the inner face of the Tracker Bulkhead

- Optical thermo-hygrometers installed in the outer face of the Tracker Bulkhead

Example of FBG-based thermo-hygrometer coupled only to T+RH standard sensors

Fig. 4.9a, Fig. 4.9b and Fig. 4.9c report, respectively, the temperature, relative humidity and dew point temperature reconstructions of one of the FBG-based thermo-hygrometers installed in the inner face of the Tracker Bulkhead, on the Positive side of the experiment.

In particular the plots refer to the sensor installed in position 15 of the schematic in Fig. 4.3a . In the same installation point, in addition to the optical thermo-hygrometer, a standard thermo-hygrometer is placed for comparison.

Reported data are related to ten months of operation of the considered sensor in CMS - from September 2014 to July 2015. [4]

Comparing the FOS reconstructions (blue line) with the signals provided by the standard sensors (red line), good correlation is found between the two data sets, therefore validating the FBG-based technology. As a matter of fact, considering Fig. 4.9a, the difference between the optical measured values and those from the reference is below $\pm$ 0.2 °C while considering the RH reconstructions in Fig. 4.9b, this difference is around $\pm$ 3 %RH, fully within the declared accuracy of the HIH sensor and the requirements set from the CMS experiment for FBG-based humidity sensors, as mentioned in Section 1.3.

Moreover, a small deviation in the relative humidity measurements between the FOS and the standard sensors has a direct effect on the dew point reconstructions, as shown in Fig. 4.9c, mostly when dry conditions of the air are detected in the volume.

For a better understanding of this phenomenon, it is convenient to refer to a particular moment of the data acquisition, when both the optical and standard sensors under analysis measure low relative humidity values. For example, plots reported in Fig. 4.10 corresponds to a stationary condition reached by the sensors on the 7^{th} of January 2015: the operation temperature is around 19 °C and the hygrometers are working in the low humidity sensing range, where their measurement error is expected to be very high (i.e. even higher than the 100 % of the measured value). Even if the relative humidity values measured by the two sensors are very similar, with a mean deviation of around 0.2 %RH between each other and, probably, with the optical

4 Data reported in this work of thesis are updated to the first days of July 2015.

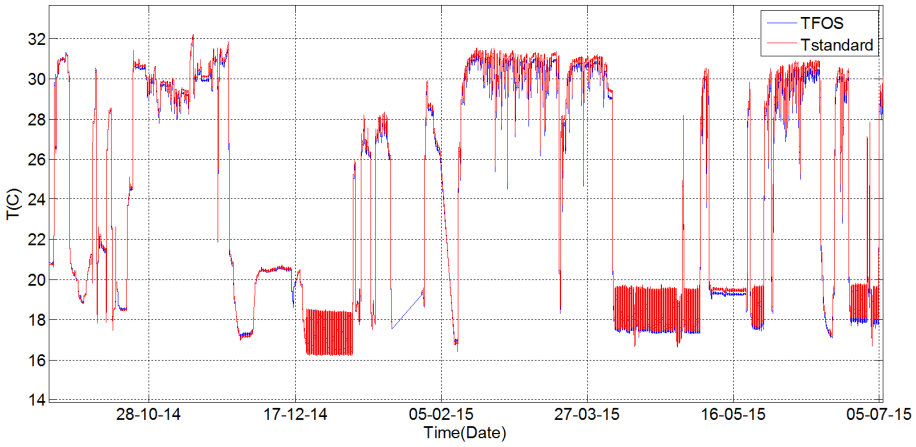

(a)

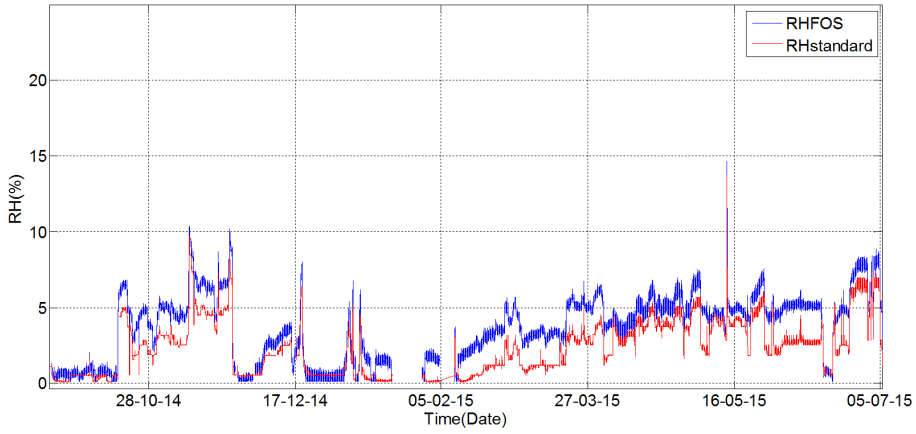

(b)

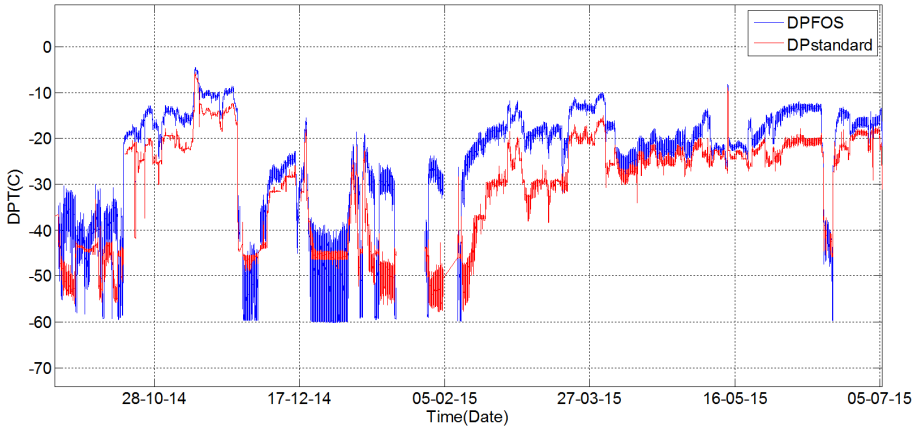

(c)

Figure 4.9: (a) Temperature, (b) relative humidity an (c) dew point reconstruction from the FBG-based thermo-hygrometer installed in position 15 of the schematic in Fig. 4.3a. For comparison the readings from the standard sensor installed in the same position are reported in red

sensor more sensitive to small humidity variations, the difference in the reconstructed dew point temperatures is high, i.e. of the order of 10 °C. In such situations, we are not able to say which one between the two measurements is the most accurate one, as both of the sensors are working outside of the "recommended" operating range; we can only conclude that both the sensors are detecting dry conditions of the air. This is a typical issue shown by the whole class of relative humidity sensors characterized by a quasi-linear calibration: high accuracy measurements are not guaranteed at low humidity, as already mentioned in Section 1.5.

In conclusion, as the sensing performance of both FBG-based sensors and the standard hygrometers available on the market are very similar, the main difference between them is the radiation resistance and this is the key-feature which makes fiber optic-based sensors very appealing for the relative humidity monitoring in the CMS tracker.

Examples of FBG-based thermo-hygrometer coupled only to both T+RH standard sensors and sniffer

In this subsection we provide the results from two FBG-based thermo-hygrometers installed in position 1 of the schematics in Fig. 4.3a and Fig. 4.3b, respectively. These cases are interesting because in the same positions, very close to the optical thermo-hygrometers, we have not only the T+RH standard sensors but also a sniffer pipe, which, as detailed in Section 1.3, extracts air samples from the volume and transfers them to the underground service cavern for the hygrometric analysis.

From Fig. 4.11a and Fig. 4.11b, it is possible to compare the dew point reconstructions from the fiber optic-based sensors (blue line) with the signals provided by both standard sensors (red line) and sniffers (black line) in the last ten months of operation in the experiment.

Also in this case it is possible to appreciate the good agreement, both in shape and measured values, between the optical fiber-based sensors with the standard devices, confirming the reliability of the proposed sensing platform.

Another example of FBG-based thermo-hygrometer coupled to both standard sensors and sniffer pipe is represented by the one installed in position 13 in Fig. 4.3a, in the inner part of the Bulkhead on the Positive side of the experiment.

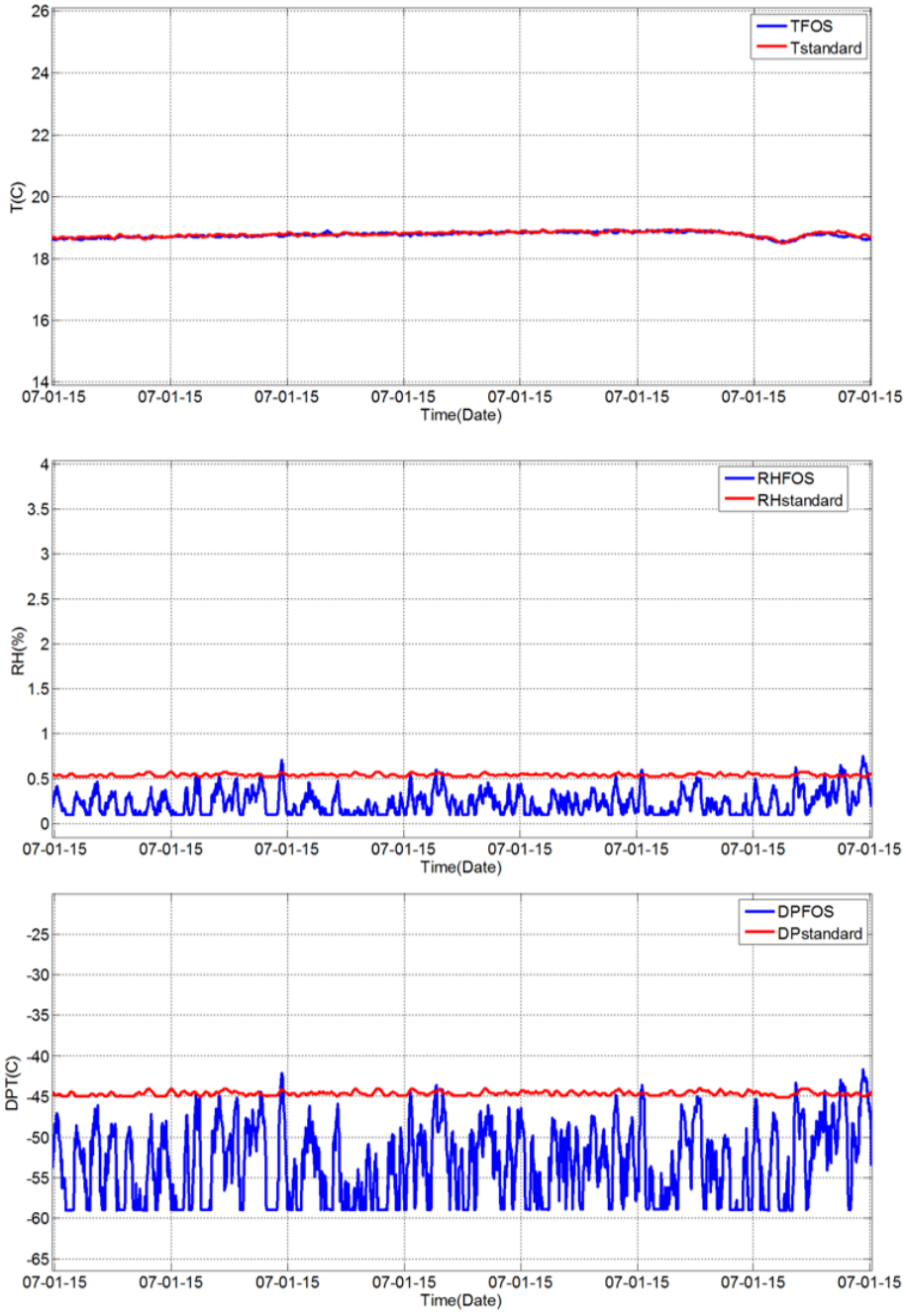

Figure 4.10: Stationary condition reached in the installation point 15 of the schematic in Fig. 4.3a on the 7th of January 2015

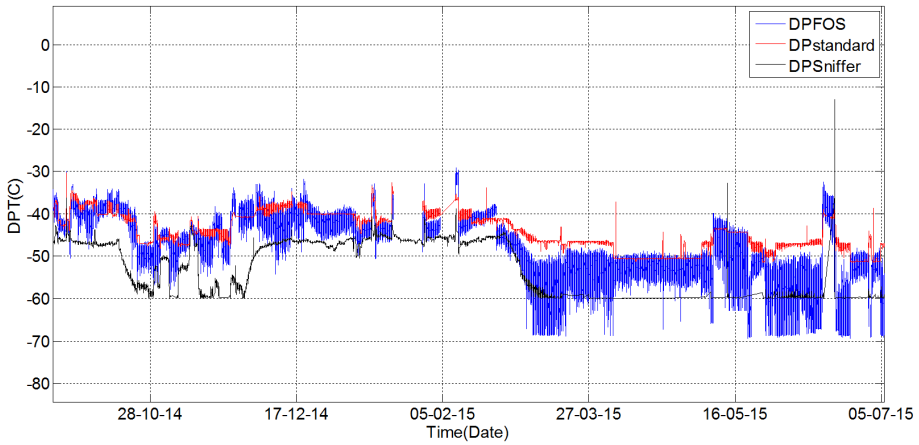

(a)

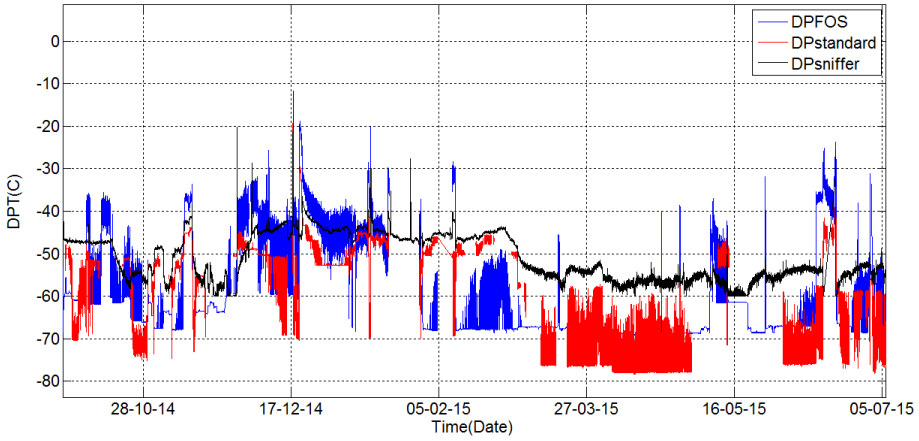

(b)

Figure 4.11: (a) Dew point reconstructions of the FBG-based thermo-hygrometers installed in position 1 on the Positive side (b) and on the Negative side of the CMS experiment (Fig. 4.3a and Fig. 4.3b, respectively). For comparison the readings from the standard sensor and the sniffer available in the same positions are reported in red and black

In particular, Fig. 4.13a, Fig. 4.13b and Fig. 4.13c report the T, RH and DPT reconstructions of the optical sensor, compared to the response of the standard devices, in a particular moment of the life of the experiment represented by the event of the CMS magnet powering. Indeed, as described in Fig. 4.12, the magnet is powered up to a current of 18 kA to reach a 4 Tesla magnetic field and then powered down again.

Even in this case, the FOS readings are in perfect agreement with the measurements of the standard sensors, this confirming that the FBG-based sensors are not sensitive to magnetic field.

On the other hand, it is important to remark that the powering of the magnet, which basically leaves unchanged the temperature level, has an effect on the responses of the relative humidity sensors. As a matter of fact, as soon as the magnet is powered on, both optical and capacitive RH sensors register an increase of the level of humidity. This is consistent with previous observations performed in CMS, suggesting that the movements of the large iron structures under the effect of the strong magnetic fields cause an inflow of humid air from the outside region towards the innermost volume of the detector. Nevertheless, when the current is lowered down, they take some time to reach the same relative humidity value as before the powering.

Finally, considering the dew point temperature reconstruction plot in Fig. 4.13c, it can be observed that the optical sensor shows very similar dynamics to the sniffer's, and their reconstructed values are in a very good agreement, even more than the ones from the standard sensor. [5]

Optical thermo-hygrometers installed on the outer face of the Tracker Bulkhead

As last example of FBG-based thermo-hygrometers in operation in the CMS experiment we report the case of the sensors installed on the outer face of the Tracker Bulkhead of the CMS experiment.

In particular, Fig. 4.14a and Fig. 4.14b report a ten-day period monitoring of temperature and dew point, respectively, recorded by these sensors.

During most of the time window reported, the CMS Tracker is operated with cold fluid at $-15\,^{\circ}\mathrm{C}$ and the external heating foils on the

5 The air sampled by the sniffing lines is directly analyzed by a precision dew point meter (Vaisala *DMT*242) outside of the experiment: only the DPT values are available from these measurements.

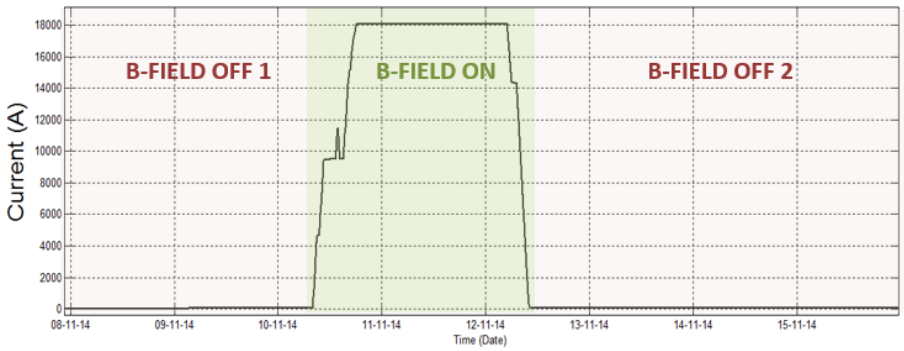

Figure 4.12: Example of ramp-up and ramp-down of the CMS magnet during the experiment life: the magnet is powered up to a current of 18 kA to reach a 4 Tesla magnetic field and then powered down again

surface of the Tracker Bulkhead are active to avoid local condensation problems. For this reason, during operation, the local temperature distribution on the external surface of the Bulkhead shows important spatial variations, depending on the presence of cold pipes in specific regions of the inner surface.

On the right side of the temperature plot of Fig. 4.14a it is very well visible the effect of an intervention requiring the Tracker cooling fluid to be brought at room temperature and the heating foils to be switched off. This causes all the local temperature differences to gradually disappear and the temperature on the Bulkhead surface to become more uniform. Consistently, all the FBG-based temperature sensors tend to converge to a very similar reading.

The black signal visible in the dew point plot in Fig. 4.14b comes from the sniffer sampling in the same volume and for its geometrical position, the sniffer measurement should be compared with the dark blue line corresponding to the FBG measurements.

4.4.1 Long-term hygrometric monitoring with FBG-based sensors

Fig. 4.15 reports, the dew point temperature reconstruction from the FBG-based thermo-hygrometer installed in position 2 of the schematic in Fig. 4.4a, compared to the readings provided by a the sniffer available in the same installation point.

The plot refers to 9 months of operation of the sensor in the experiment and confirms the reliability of this sensing platform. As a matter of fact, a very good agreement, in both shape and amplitude, between the two reported curves can be appreciated within the

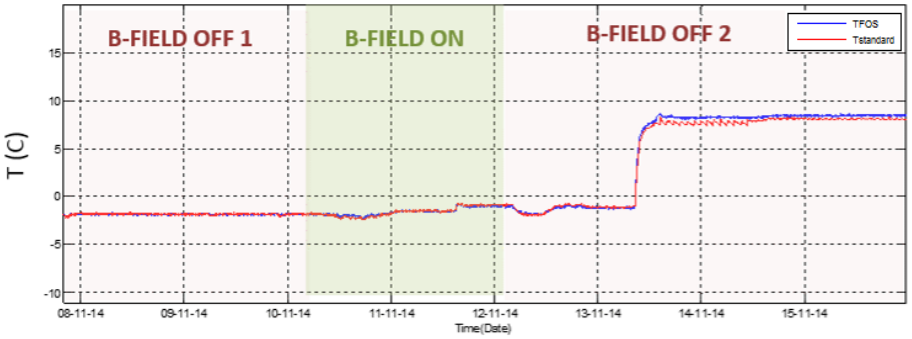

(a)

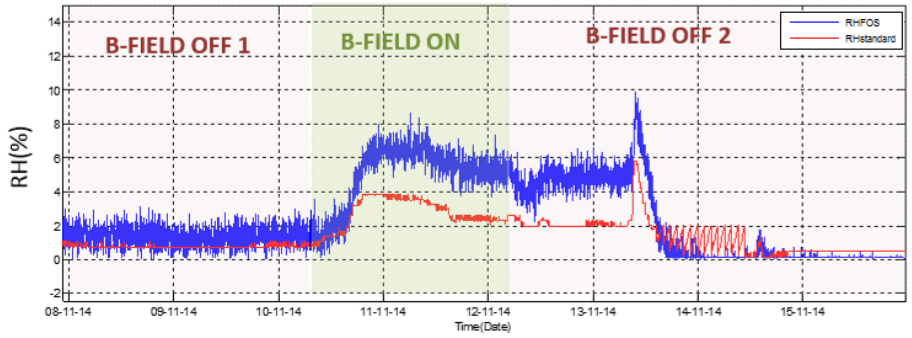

(b)

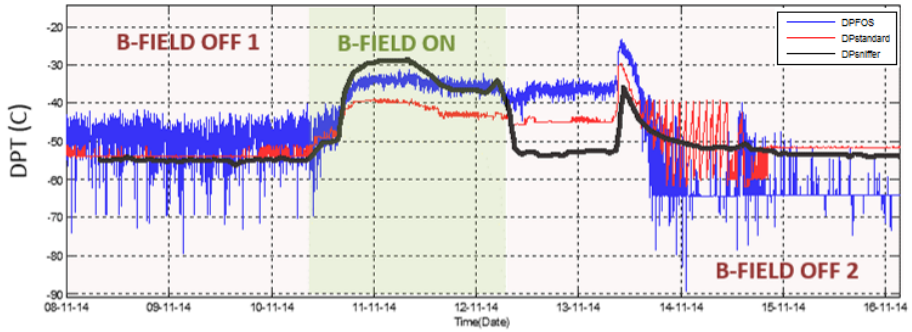

(c)

Figure 4.13: (a) Temperature, (b) relative humidity and (c) dew point reconstructions from a FBG-based thermo-hygrometers during the ramp-up and rump down of the magnet. For comparison the readings from the standard sensors and the sniffer installed in the same position are reported in red and black, respectively

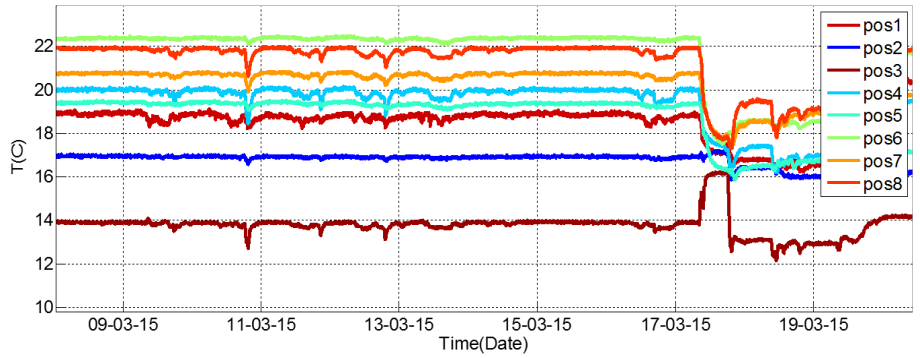

(a)

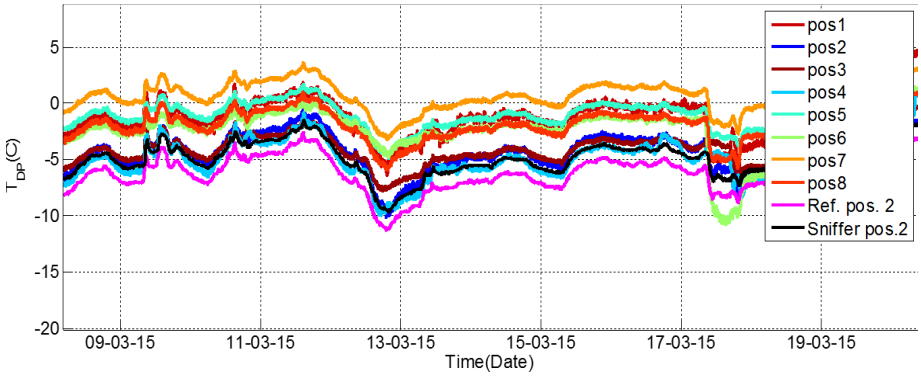

(b)

Figure 4.14: (a) Temperature and (b) dew point reconstructions of the FBG-based thermo-hygrometers installed in the outer face of the Tracker Bulkhead of the CMS experiment. For comparison the readings from the sniffer available in the same positions is reported in black

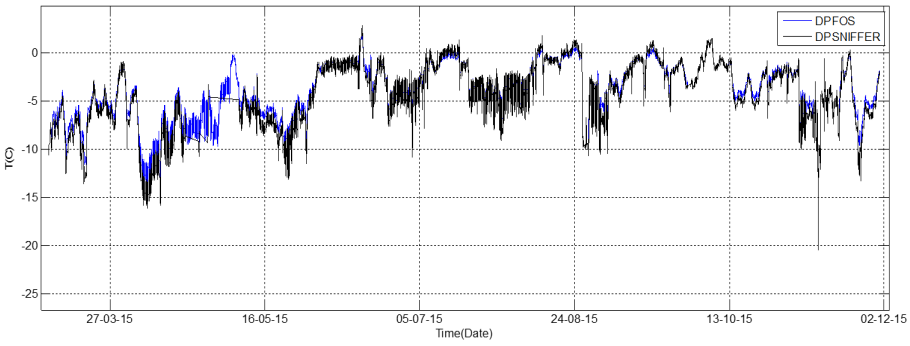

Figure 4.15: Dew point reconstructions from the FBG-based thermo-hygrometer installed in position 2 of the schematic in Fig. 4.4a. For comparison, the readings from the sniffer pipe installed in the same position are reported black

full time window, with a maximum deviation of a 2 °C, in complete respect of the set of requirements from the CMS experiment.

After almost one year of operation, characterized by extreme working conditions such as severe cooling cycles, magnet powering, and with the accelerator working at the full luminosity, we have not registered yet any phenomenon of instability or degradation of the performance of the proposed sensors (e.g due to the aging of polymeric material, as discussed in the next section). However continuous monitoring has to be constantly performed, for a better understanding of the behavior of this innovative class sensors in real environments.

4.4.2 Temperature, relative humidity and dew point mapping

At the end of this section dedicated to the analysis of the data acquired by the optical thermo-hygrometers in the last ten months of operation in the CMS experiment, it is important to remark the strong ability of this technology to correctly work in a such complicated environment, detecting correct values of temperature and humidity.

As a matter of fact, for their characteristic of tolerance to radiations, the proposed FBG-based thermo-hygrometers are at the moment the only devices which can solve the problem of distributed and localized thermal and hygrometric monitoring of the air in front of the Tracker volume.

Indeed, the standard sensors which are now coupled to the optical sensors are expected to be affected by the radiation exposure, thus meaning that soon they will not be able to give any measurement or any correct measurement of humidity in the experiment.

On the other end, the sniffers, which are clearly not affected by radiations, are available only in a few points of the volume and, as consequence, they will only provide a partial indication of the hygrometric conditions of the air in the detector.

To give an idea of the power of the proposed technology, we report in Fig. 4.16a, Fig. 4.16b and Fig. 4.16c a good example of T, RH and DPT mapping which FBG-based thermo-hygrometers are able to provide.

These maps refer to a stationary condition reached in the experiment in March 2015 and they are linked to the eight optical sensors installed on the outer face of the Tracker Bulkhead of the experiment.

Such kind of plots are extremely useful as they provide information about the distribution of temperature, relative humidity and dew

point temperature in the experiment, helping to localize eventual critical spots in the volume.

4.5 ISSUES RELATED TO COATED-FBGS FOR HUMIDITY MONITORING

The first ten months of operation of the optical thermo-hygrometers based on FBG technology in the CMS experiment have confirmed their strong potentiality in the application of relative humidity monitoring in real environments. Collected results are even more interesting if we consider that at the moment the optical fiber-based sensors seem to represent the only producible miniaturized devices satisfying all the requirements from the CMS experiment in terms of reliability, multi-point mapping and tolerance to radiations.

Nevertheless, after four years of research activity dedicated to the exploration of this innovative technology in humidity applications, we found that it is not completely immune from some limitations.

The main issues related to the FBG-based relative humidity sensors, as they have already emerged during the previous dissertations, may be summarized in the following points:

- Coating thickness affecting response time and relative humidity sensitivity

  Confirming the observations found in literature, we found that the choice of the optimal thickness of the sensitive layer must be a compromise between the time response of the sensor and its relative humidity sensitivity. As a matter of fact, increasing the thickness of the layer, we observed higher Bragg wavelength shifts and, consequently, an increase, according to a linear law, of the sensitivity of the sensor, due to higher amount of water molecules absorbed by the coating. At the same time, the increase of the coating thickness has direct repercussions on the time response of the sensor, with the sensor becoming slower if characterized by thicker layers of polyimide. Based on our investigations, we think that the best configuration is represented by a FBG coated with a 10 µm hygroscopic layer, thus guaranteeing a satisfactory time response of a few seconds while still allowing for an acceptable (though low) sensitivity to relative humidity. [48]

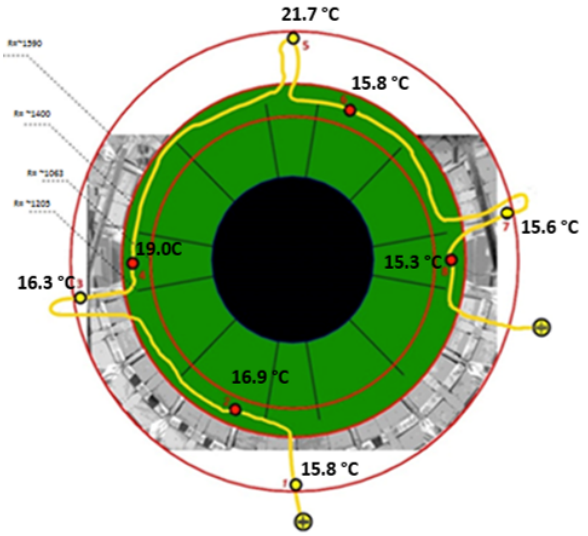

(a)

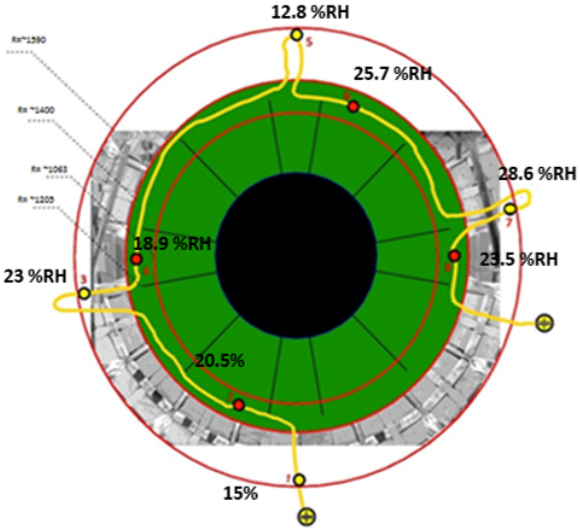

(b)

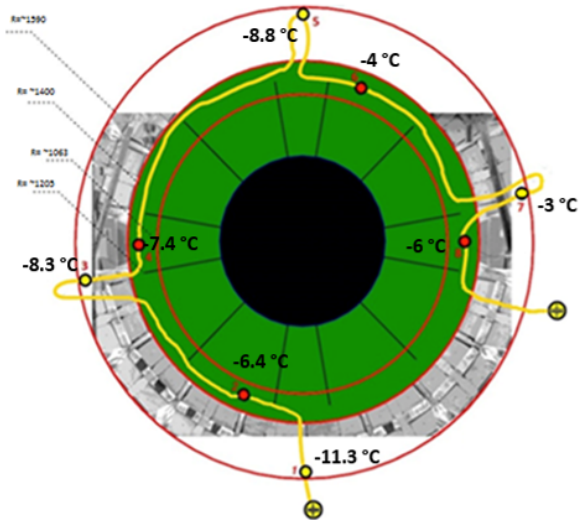

(c)

Figure 4.16: (a) Temperature, (b) relative humidity and (c) dew point mapping with FOS installed on the outer face of the Tracker Bulkhead, on the Positive side of the experiment

- High cross-sensitivity and temperature compensation

  As already discussed in the previous chapter, coated Fiber Bragg Grating-based sensors suffer of the so-called cross-sensitivity problem, as they are sensitive to both temperature and relative humidity changes. The typical value of temperature sensitivity of such devices is of the order of 10 pm/°C, as commonly found in literature, while the sensitivity to relative humidity of a FBG coated with a 10 µm polyimide layer is of the order of 1 pm/%RH . This translates into a typical value of the T/RH sensitivity ratio of around 10 %RH/°C. Therefore, in the application of such devices in real environments, in presence of variations of both temperature and humidity, great care must be taken in the development and application of temperature compensation schemes, in order to correct the relative humidity signal from the temperature effect. For this reason, the solution that we adopted finally consisted in using two FBGs, one coated with hygroscopic material and one uncoated, used as pure thermometer. The temperature measurement provided by the uncoated FBG must have a good accuracy: an error of $\pm$ 1 °C in the temperature reading would typically produce a not acceptable error of $\pm$ 10 %RH in the humidity reading. In order to get precise and reasonable relative humidity reconstructions using FBG-based hygrometers we finally concluded that the accuracy of the optical thermometer should be around $\pm$ 0.1 °C.

- Low accuracy at low relative humidity values

  The sensing properties of the proposed FBG-based sensors were found to be very similar to the ones shown by the traditional hygrometers available on the market. In particular, similarly to all the standard capacitive sensors, the optical sensors based on Fiber Bragg Grating technology cannot guarantee high-precision measurements in the low relative humidity range. This can be considered an issue of the proposed technology in view of the new generation of particles detector planned at CERN for 2020 which will require more challenging temperature of operation and, as consequence, extremely severe requirements in terms of accuracy and precision of relative humidity measurements.

- Aging typical of polymeric materials

  While the hygroscopic nature of the polyimide allows it to be used as moisture sensing element for the development of rel-

ative humidity sensors, at the same time, the presence of water absorbed and desorbed by the polymeric coating can lead to long term reliability problems and chemical instability. [70] Therefore, we are expecting to observe possible aging problems in the sensors responses, after a long-term use, due to the aging of the coating material, although it was proven to be radiation tolerant.

- Free-strain packaging and installation

  The design and engineering of a small, lightweight packaging for the coated FBG-based sensors was another very critical task in this project, as the Fiber Bragg Grating is intrinsically sensitive to strain. In particular the casing for the optical humidity sensors, which was also designed to protect the sensor during its operation in harsh environment such as the CMS experiment, had to provide insensitivity of the light transmission to the fiber bending or strain close to the sensor itself. For the same reason, during the installation of the thermo-hygrometers in CMS, great care was taken in order to place the arrays of FBG-based thermo-hygrometers in a free stress configuration.

- Adhesion of the coating affecting the sensors performance

  The sensing principle of the proposed devices relies on the so-called swelling effect, consisting in the expansion or in the contraction of the hygroscopic coating material due to the absorption or desorption of water molecules. If the deposited coating is not homogeneous along the region of the fiber where the grating is inscribed, the longitudinal strain transmitted to the grating itself may be not homogeneous as well, thus inducing non-linear responses or even not stable and repeatable measurements. As a matter of fact, from our work experience, we can surely assert that custom coated FBG-based sensors, produced in-house with a well controlled process of the coating deposition, are high-performing in terms of linearity, repeatability and stability over the years, compared to the standard sensors produced in batch and in less controlled conditions.

4.6 CONCLUSIONS

A full network of 72 optic fiber-based sensors, each one formed by a FBG temperature sensor and one FBG relative humidity sensor, has been installed from the end of 2013 in the critical areas of the CMS Tracker end-flange for constant distributed thermo-hygrometric monitoring.

During the LS1, the fiber optic-based sensors readings have been constantly compared with the information provided by a network of conventional non-radiation-resistant sensors and also with some punctual dew point measurements provided by a few sniffers, available on the volume. This had allowed for validation of the FBGs measurements in term of both temperature and relative humidity, in a region where the concentration of power cables and cooling pipes creates strong local gradients.

After the CMS closing and even the restarting of the LHC operations in April 2015, the full network of FBG-based thermo-hygrometers installed in the experiment, has been continuing to correctly work, providing continuous distributed monitoring of the environmental conditions in the detector, preventing from the risk of local condensation and ice formation.

After four years of work experience accumulated, we gained confidence on the application of the technology for humidity monitoring, developing an unprecedented wealth of detailed information about the properties, behavior and limits of these innovative sensors.

5 CHARACTERIZATION OF LPG-BASED RELATIVE HUMIDITY SENSORS

In order to overcome the limitations of FBG-based relative humidity sensors, a second generation of optical relative humidity sensors has been launched in 2013, based on the Long Period Grating technology.

In particular, after a deep analysis of the state of art of this kind of devices in literature, we finally decided to focus our investigations on gratings coated with two different metal oxides, titanium dioxide (TiO_2) and tin dioxide (SnO_2), due to their good hygroscopic features and high refractive index.

In the next sections, some details about the fabrication process of TiO_2 and SnO_2-coated LPG sensors are reported, as well as the experimental results obtained during the preliminary test campaigns carried out in the CERN laboratories.

5.1 LPG TECHNOLOGY AND LPG–BASED RELATIVE HUMIDITY SENSORS

LPGs are photonic devices realized by inducing a periodic index modulation of the core of a single mode optical fiber along a few centimeters of its length. The period of the perturbation is longer than the FBG counterpart: it goes typically from 100 to 500 µm and the length of the grating is usually around 2 or 3 cm.

This perturbation allows for the power coupling from the fundamental guided core mode to a discrete number of forward propagating cladding modes. Each coupling happens at a distinct wavelength, where the so-called phase matching condition is satisfied [71]:

$$\lambda_{res,i} = \left(n_{eff,co} - n^{i}_{eff,cl} \right) \Lambda \tag{5.1}$$

where $n_{eff,co}$ and $n^{i}_{eff,cl}$ are the effective refractive indexes of the core and of the i^{th} cladding mode respectively, while Λ is the period of the grating.

A pictorial description of the so-called mode coupling which takes place in a Long Period Grating is given in Fig. 5.1.

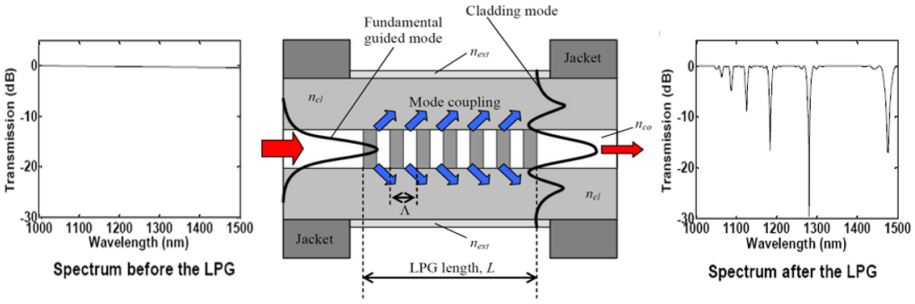

Figure 5.1: Long Period Grating principle of operation

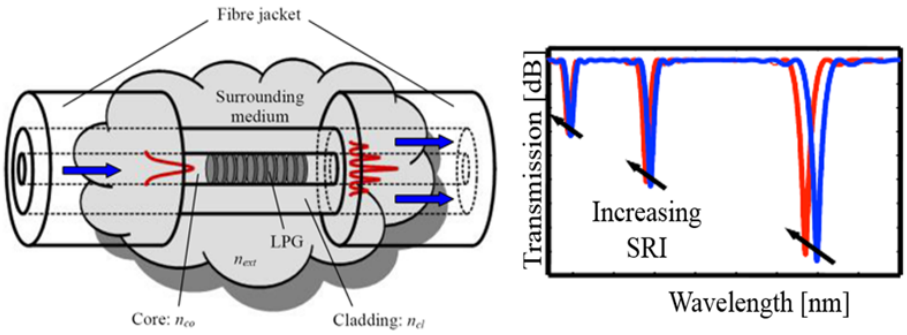

Figure 5.2: Sensitivity of LPG to external surrounding medium

As a result of this coupling, the LPG transmission spectrum shows several attenuation bands or dips related to the different excited optical fields, i.e. to the cladding modes.

A portion of the electromagnetic field of the cladding modes penetrates into the surrounding medium in the form of evanescent wave, thus making $n^{i}_{eff,cl}$ and, consequently, $\lambda_{res,i}$ sensitive to the chemical and physical properties of the surrounding environment, as shown in Fig. 5.2.

Among the different parameters able to influence the spectral features of LPGs, the surrounding refractive index sensitivity can be considered as a key feature, enabling the use of this kind of sensors in chemical and biological sensing applications through the integration of sensitive coatings.[72, 73]

Indeed it was demonstrated in literature that the sensitivity of LPGs to the surrounding refractive index can be greatly optimized for a specific application by acting on the thickness and optical properties of a functional overlay deposited onto the cladding along the grating region. This overlay has higher refractive index than the cladding (which is approximatively around 1.45).[74]

In case of relative humidity sensors based on LPG technology, an appropriate hygrosensitive material has to be selected such that the

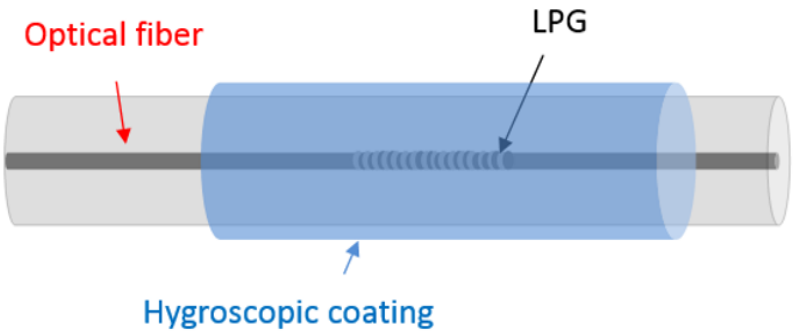

Figure 5.3: Schematization of LPG-coated relative humidity sensors

water absorption/desorption of water by the coating itself modifies its refractive index and/or thickness, thus creating a spectral variation and amplitude change in the LPG attenuation band, independently from the adhesion properties of the coating onto the grating itself.

A simple schematization of a LPG-coated relative humidity sensor is given in Fig. 5.3.

In presence of relative humidity changes (ΔRH), for a "fixed" temperature, the resonance wavelength variation for i^{th} cladding mode, here referred as $\Delta\lambda_{res,i}$, can be expressed as follows [68]:

$$\Delta\lambda_{res,i} = f(\Delta RH) = g\left(\Delta n^{i}_{eff,cl}\right) \tag{5.2}$$

with f and g being typically non-linear functions, generally depending on temperature and relative humidity.

Furthermore, the variations of the refractive index of the cladding related to the i^{th} mode may be expressed as:

$$\Delta n^{i}_{eff,cl} = h(\Delta n_{co}, \Delta x) \tag{5.3}$$

where Δn_{co} and Δx are respectively the variations of the refractive index and of the thickness of the sensitive layer promoted by the water molecules adsorption.

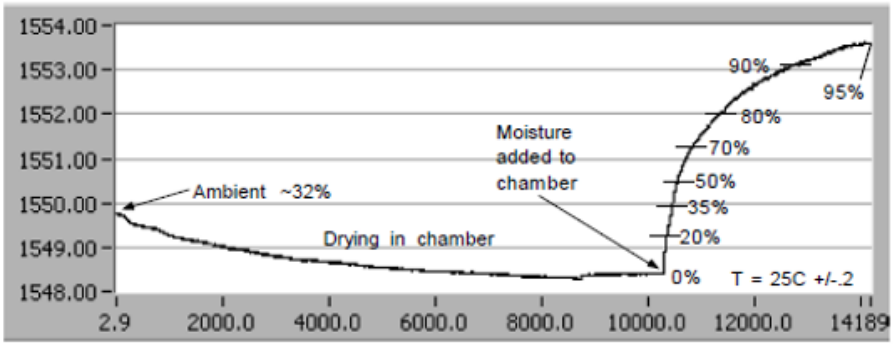

Figure 5.4: Sensing characteristic of carboxymethylcellulose-coated LPG as humidity sensor reported by Luo et al. in [75]

5.2 STATE OF ART OF LPG-BASED RELATIVE HUMIDITY SENSORS

Several kinds of materials have been explored in literature as coating for the development of LPG-based RH sensors.

In particular, the first relevant contribution dates back to 2002, reported by Luo et al. for health monitoring applications in [75]. In the sensor design, carboxymethylcellulose was used as coating of the Long Period Grating. The demonstrated sensor was found to operate well in the range $0-95$ %RH at 25 °C, as shown in Fig. 5.4, with a non-linear response dependency with the humidity change.

A similar LPG-based humidity sensing scheme was demonstrated by Tan et al. using a gelatine coating [76] and by Konstantaki et al. who proposed a LPG humidity sensor utilizing polyethylene oxide/cobalt chloride overlay [77]. In both cases, however, the operating humidity range was found to be limited. As a matter of fact, in case of [76], the tests were conducted in the range $43-99$ %RH at 25 °C but it was found that the gelatin coated LPG-based sensor was more suitable for high RH measurements, as the most significant response was given by the sensor itself for humidity values above 90 %RH, as reported in Fig. 5.5a. Similarly, for the polyethylene oxide/cobalt chloride coated LPG sensors [77], it was concluded that the sensor can detect RH variations with a resolution better of 0.2 % only above 50 %RH (Fig. 5.5b).

Studies conducted by Venugopalan et al. in 2008 have shown the use of polyvinyl alcohol film FBG-based sensors [78, 74] for relative humidity monitoring applications. In this case, the performances of two gratings coated with two different overlay thicknesses (3.6 µm for the first sensor labeled as Sensor 1 and 800 nm for Sensor 2) were eval-

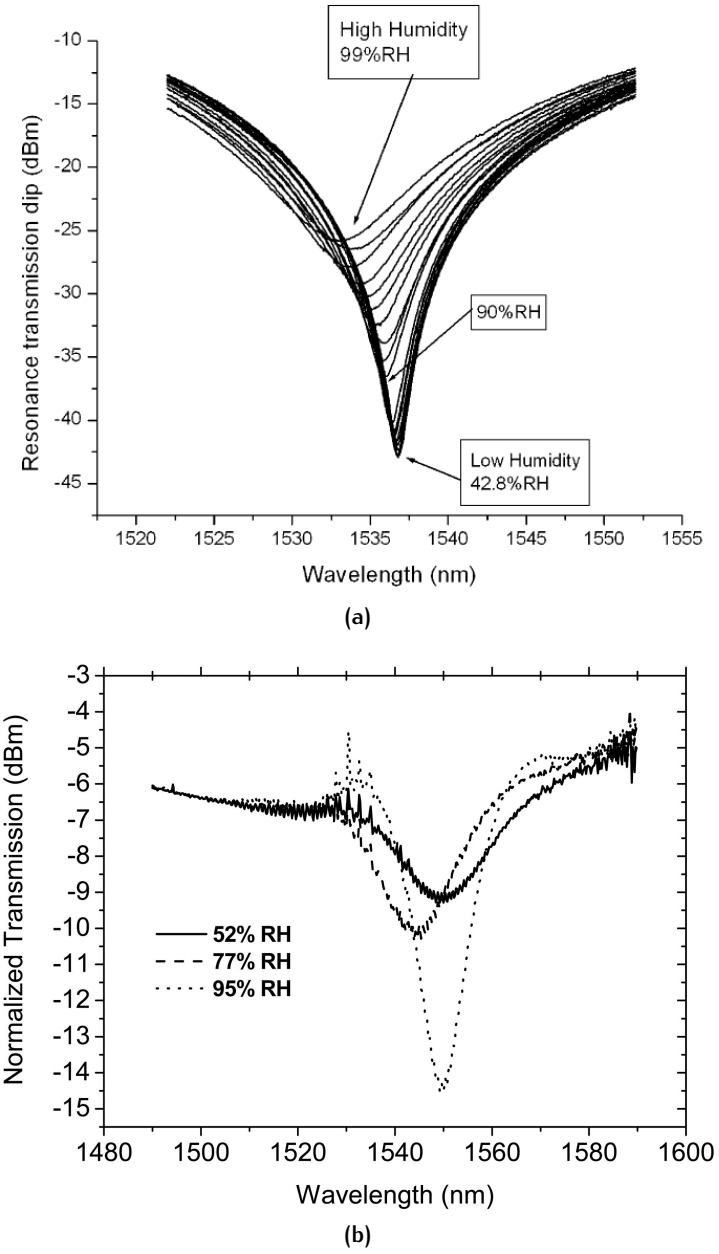

Figure 5.5: (a) Spectrum response to RH changes of gelatine-coated [76] and (b) polyethylene-coated [77] LPG-based relative humidity sensors

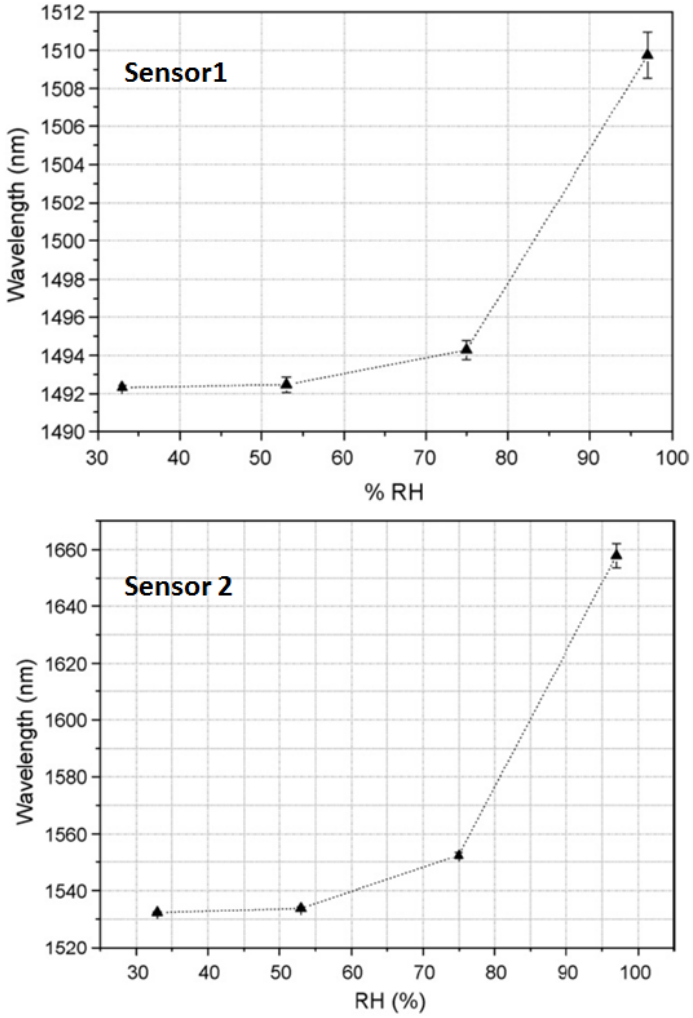

Figure 5.6: Sensing characteristic of polyvinyl alcohol coated LPG as humidity sensors reported by Venugopalan et al. in [74, 78]

uated in the relative humidity range from 33 to 97 %RH at room temperature. The obtained results, here reported in Fig. 5.6, confirmed the non-linear response of both sensor configurations to humidity changes. The sensor sensitivity has been demonstrated to be high, especially in the range 75 −97 %RH ($\sim$ 0.7 nm/%RH for Sensor 1 and $\sim$ 4.5 nm/%RH for Sensor 2), contrary to the case studied in [75], where higher sensitivity is shown at lower relative humidity values. The reported results suggest the possibility to apply this technology in industrial applications requiring humidity measurements.

Tab. 5.1 summarizes the main results available in literature from 2002 to 2011 concerning coated LPG-based sensors for relative humidity monitoring. Blanks in the table represent information not available in the consulted literature.

Table 5.1: Coated LPG-based sensors for relative humidity monitoring proposed in literature from 2002 to 2011

Year	Coating	Thickness nm	RH %	T °C	Ref.
2002	Carboxymethylcellulose	–	0 –95	25	[75]
2005	Gelatin	297.5	43 –99	25	[76]
2006	Cobalt chloride	10^4	38 –97	25	[77]
2007	Hydrogel	–	39 –90	25	[79]
2008	Polyvinyl alcohol	100,800	33 –97	Room	[78]
2011	Silica nanospheres	–	20 –80	25	[80]

It is important to point out that, as already observed for coated FBGs, in literature there is no evidence of the characterization of coated LPGs at low humidity values (below 20 %RH) and temperatures below 15 °C, as evident from Tab. 5.1.

Moreover, while the radiation effects have been investigated in case of bare LPGs up to 1.54 MGy[1] [60, 81], their influence on the sensing performance of coated LPG seems to be completely unexplored.

5.3 IN-HOUSE FABRICATION OF THIN METAL OXIDE-COATED LPGS

Taking in account the novelty and the potential of the Long Period Technology for relative humidity sensing applications, in 2013, we have launched a research and development project based on coated-LPG to be applied in high radiation environments.

In order to avoid possible problems, typical of polymers, related to the aging of the coating material and to its low radiation resistance, we decided to focus our attention on the study of metal oxides-coated LPG-based sensors. As a matter of fact, metal oxides, which are often applied in the development of traditional hygrometers (both capacitive and resistive) [82], have good hygro-sensitive characteristics and they ensure long-term stability. In particular we have concentrated our investigations about TiO_2 and SnO_2. [2]

1 The authors refer to radiation effects up to 1.54 Mrad.

2 Originally we have also proposed Al_2O_3 as coating material but we finally discarded it as the quality of the deposited layer onto the grating was not enough satisfying as in case of TiO_2 and SnO_2.

Different nano-scale metal oxides layers deposition techniques have been reported in literature over the years, including chemical bath deposition [83, 84], spray pyrolysis [85, 86], sol-gel [87, 88, 89], chemical vapor deposition [90, 91] and sputtering [92, 93].

The sol-gel has been finally selected for this work to deposit TiO_2 and SnO_2 onto the Long Period Gratings for its numerous advantages in terms of good optical quality and low loss, ring shaped symmetry, and adequate longitudinal uniformity over the grating length [73]. Furthermore, the sol-gel, which is a low cost deposition method, is characterized by high flexibility, enabling an easy change of the material to deposit on the grating, just applying an appropriate modification of the reagents as well as of the chemical procedure. This is a very useful feature for our application, since it allows the integration of the two selected metal oxides with the grating, without problems connected to contamination of the deposition chamber.

The deposition of the oxides on the Long Period Gratings as well as the optimization of the deposition process have been conducted by the team belonging to the IPCB Insitute and University of Sannio.

A large number of sol-gel solutions have been prepared and experimented for the integration of both titanium and tin dioxide with the grating: some of them were found to be opaque and inhomogeneous, causing macroscopic and non-uniformities into the layers; others were demonstrated to be suitable for depositing high quality layers. [3]

The used deposition procedure mainly consisted of the following four steps:

- sol preparation;
- substrate cleaning;
- dip-coating procedure;
- thermal annealing.

A schematic view of the deposition setup used for the fabrication of coated LPGs, is reported in Fig. 5.7a.

After an accurate cleaning of the substrate, the optical fiber was fixed to a moving arm of the dip coater [4] and then dipped in the ves-

3 It is worth underlining that before integrating the hygrosensitive layers on the Long Period Grating, preliminary tests have been first carried out on glass planar substrates and standard optical fibers (without any grating inscribed) with the aim to assess and optimize the sol-gel preparation process and the integration on the fiber substrates

4 A KSV Nima dip coater, controlled via a PC station was used.

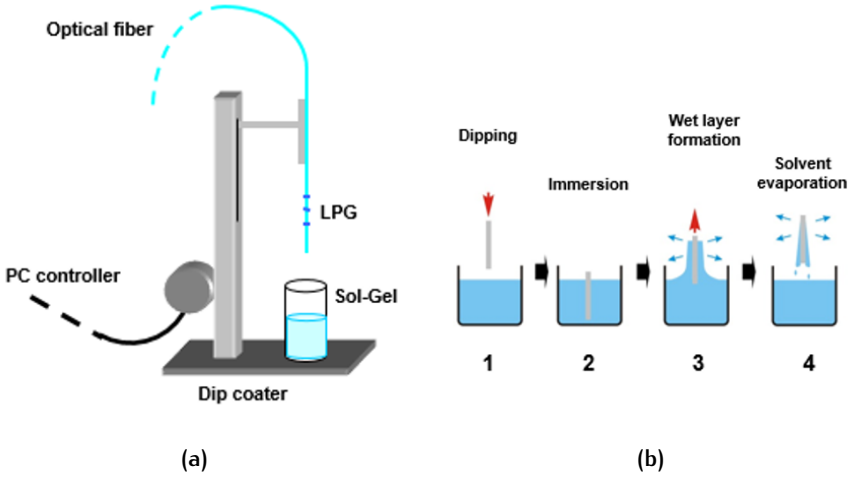

Figure 5.7: (a) Schematic view of the deposition setup; (b) Sol-gel dip coating process

sel with a withdrawal speed of 100 mm/min. As shown in Fig. 5.7b, the substrate was firstly lowered in the sol until it was immersed for the desired length; as soon as the substrate was extracted from the solution, the solvent was starting to evaporate thus promoting the metal oxide layer adhesion to the surface. The complete evaporation of the solvent was reached by thermally annealing the sample in the oven at a temperature of 150 °C for 10 min. [94]

Since this deposition process resulted in very thin overlay deposited on the gratings, multiple depositions had to be performed in order to get the desired thicker final TiO_2 and SnO_2 layers.

5.4 TiO_2-COATED LPG-BASED SENSOR CHARACTERIZATION

The deposition procedure used to fabricate TiO_2-coated LPG RH sensors mainly consisted of the sol-gel preparation,as described in the previous section, using titanium (IV) isopropoxide as titania precursor, followed by a standard dip-coating procedure

Multiple depositions were performed in order to reach the desired layer thickness and several samples with different TiO_2 thicknesses were successfully produced.

Fig. 5.8 reports a 20x optical microscope image of a TiO_2 layer deposited at the end of the sol-gel dip coating process: the layer is ho-

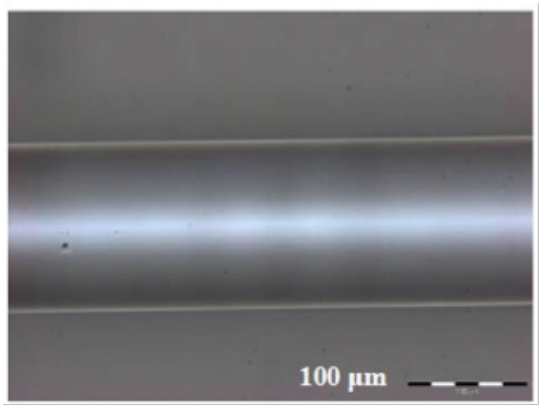

Figure 5.8: 20x optical microscope images of a TiO_2 multi-layered sample

mogeneous, confirming that the selected solution can provide good optical quality and high uniformity.

Here we present results concerning the sample named $LPG1$, characterized by a period of 404 µm and obtained by depositing 6 TiO_2 layers onto the grating for an estimated total coating thickness of around 100 nm.

The spectral response of the sample under investigation before and after the deposition of the oxide onto the grating is reported in Fig. 5.9a. As expected, the spectral response exhibits several resonance dips in the wavelength range from 1200 to 1700 nm.

Considering the operating wavelength range of the optoelectronic interrogator (sm125-500 from Micron Optics, described in Tab. 3.1), already in use in the laboratory at CERN as well as in the CMS experiment for the FBG-based sensors readings , the coated-LPGs have been appropriately designed in order to have attenuation bands, coming from the coupling of the fundamental core mode to higher order modes, centered in the wavelengths between 1510 nm and 1590 nm. Moreover, a proper algorithm has been developed in order to find the the baricentral wavelength of the LPG spectral dips.

In case of $LPG1$, we concentrate our attention on the 5^{th} cladding mode corresponding to the mode characterized by the highest central wavelength.

In particular, it can be seen in Fig. 5.9a that the bare device showed a resonance dip in correspondence to the 5^{th} cladding mode, centered at 1589.0 nm and characterized by a transmitted power of -11.5 dB. The deposition of the TiO_2 layer caused a resonance blue shift of 24.1 nm together with an increase of around 7.5 dB in its depth.

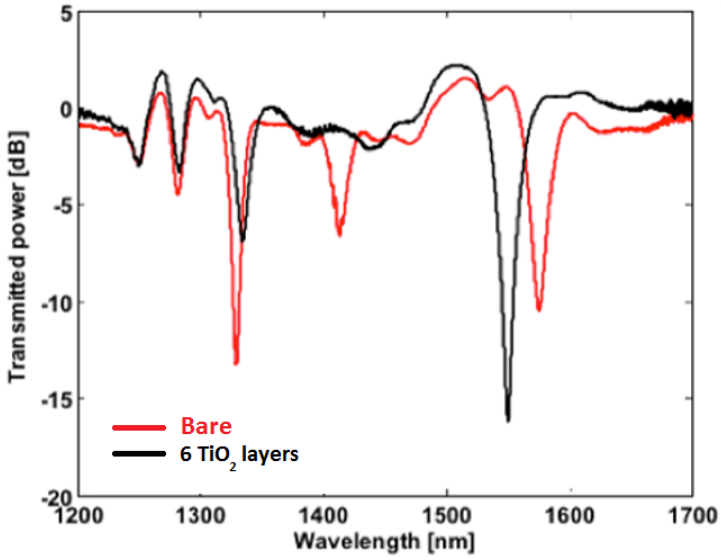

(a)

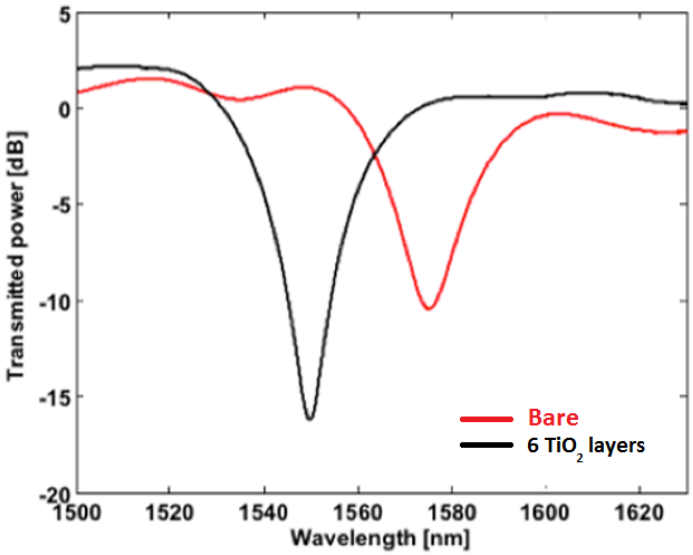

(b)

Figure 5.9: (a) Optical spectra of sample *LPG1*, before and after the TiO_2 overlay deposition; (b) zoom of the 5^{th} cladding mode of the same sample

The first measurement provided evidence of the optical quality of the deposited overlay, indeed, if an optical "lossy" overlay is deposited onto the LPG surface, a decrease in the visibility of the attenuation band combined with a spectral broadening would be expected.[68, 94]

The performances of $LPG1$ were investigated in the relative humidity range from 0 to 75 %RH, at -10, 0, 10 and 25 °C. [68, 94]

Experimental tests were conducted at CERN using the same setup already described in Section 3.3.

Fig. 5.10a shows the $LPG1$ spectral variations during a characterization test carried out at 25 °C.

As theoretically expected, increasing the humidity content inside the test chamber causes a blue shift of the resonance wavelength $\lambda_{res,5}$. This is due to the increase of the TiO_2 coating refractive index, promoted by the higher amount of adsorbed water molecules, which in turn leads to an increase of $n^5_{eff,cl}$. This behavior can also be appreciated in Fig. 5.10b, where the $\lambda_{res,5}$ variations of $LPG1$ during the same characterization test described in Fig. 5.10a are reported. For comparison, the response from the reference humidity sensor is also provided in black.

Moreover, by increasing the relative humidity content in the test chamber, the attenuation band visibility also increases, as results from Fig. 5.10a. This is an important aspect as, in most cases, LPGs coated with "lossy" overlays experience partial or full resonance fading when operating in transition mode [95].

Similar results have also been obtained even at -10, 0 and 10 °C, underlying the capability of the device to work properly also at low temperatures in the full humidity range of interest. [68, 94]

Fig. 5.11 shows the characteristic curves of of the sensor under analysis obtained at the four considered temperatures.

In contrast with what observed in case of polyimide-coated FBGs [68, 94], as explained in the Section 3.4, the calibration curves were found to be non-linear, as a larger shift of the resonance wavelength $\lambda_{res,5}$ was registered at low humidity levels. This corresponds to the most appealing feature of coated LPGs in view of their application for relative humidity monitoring: such non-linear calibration allows to perform high accuracy measurements in the low relative humidity range. This characteristic is also confirmed in Fig. 5.12, where the RH sensitivity curves of $LPG1$ versus the relative humidity variations are plotted.

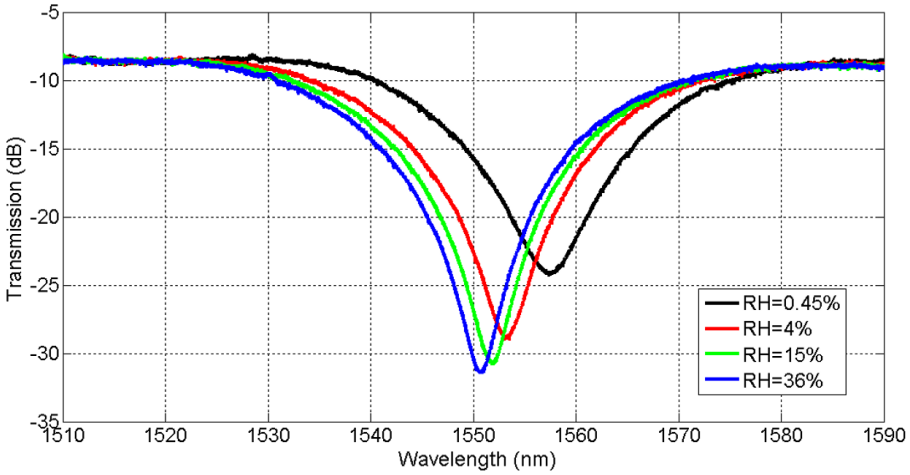

(a)

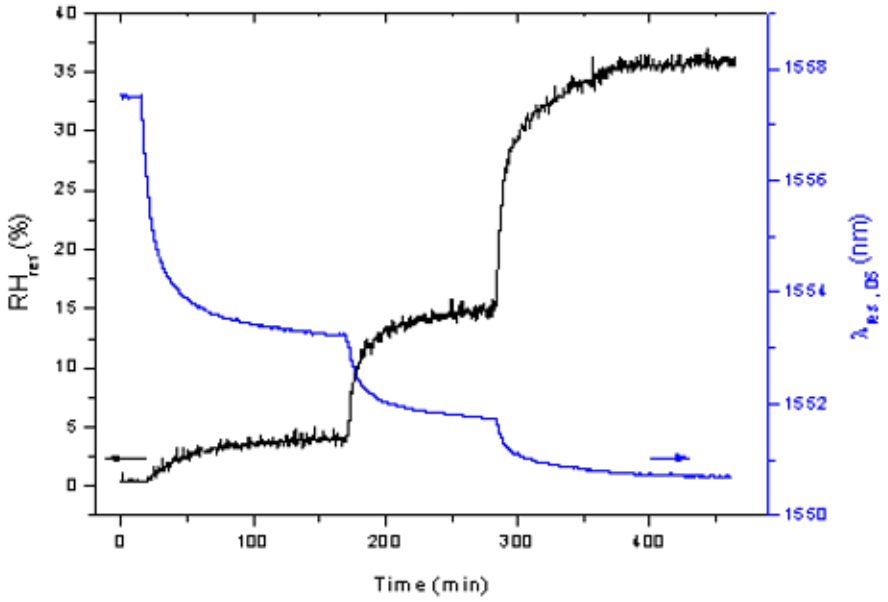

(b)

Figure 5.10: (a) Transmittance spectra of *LPG*1 acquired at different RH values during a test at 25 °C; (b) *LPG*1 response during the same RH characterization

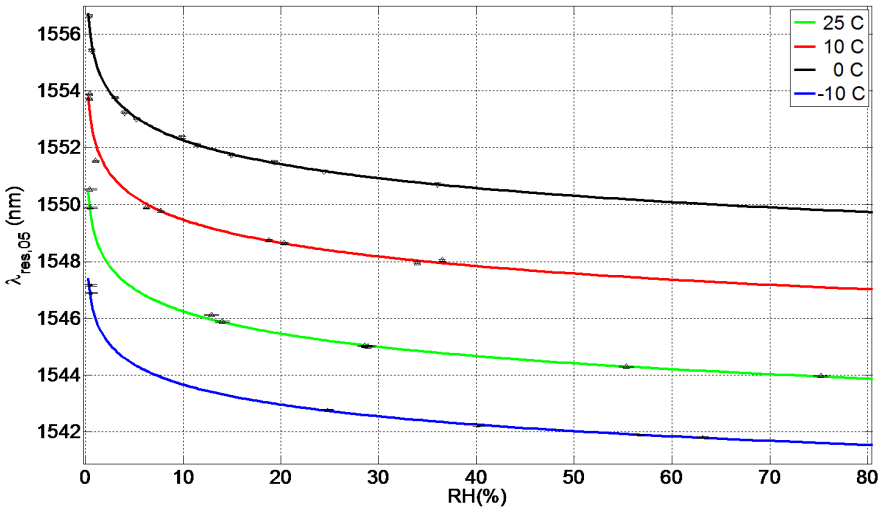

Figure 5.11: Characteristic curves of TiO_2-coated LPG as RH sensor

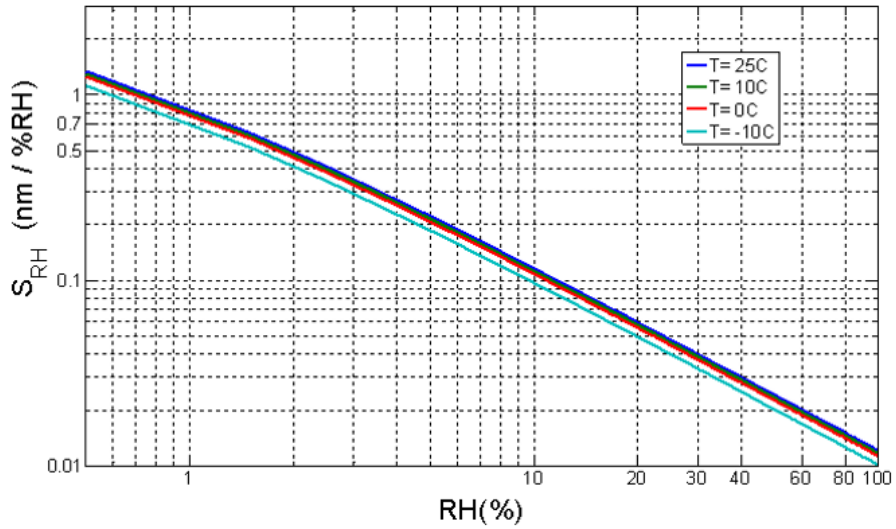

Figure 5.12: *LPG*1 relative humidity sensitivity in function of RH

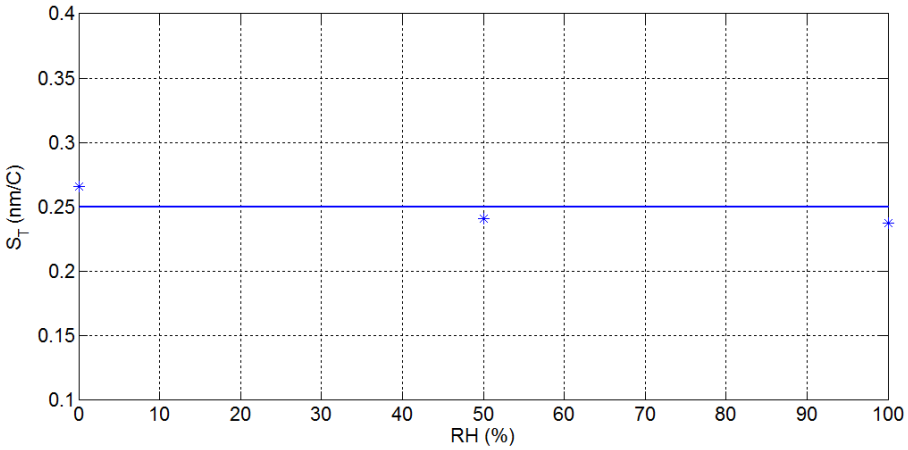

Figure 5.13: *LPG*1 temperature sensitivity in function of RH

At 25 °C, S_{RH} values are between 1.4 nm/%RH and 0.11 nm/%RH in the range 0 − 10 %RH. It then decreases down to 0.01 nm/%RH at higher humidity levels.

This sensitivity has to be compared with a uniform S_{RH} typical of polyimide-coated FBG sensors typically ranged between 1 pm/%RH and 1.5 pm/%RH. [48, 65].

From Fig. 5.12, a slight dependence of S_{RH} on temperature can be also appreciated: as a matter of fact a decrease of the relative humidity sensitivity occurs when temperature decreases, mostly below 0 °C.

Starting from the characteristic curves reported in Fig. 5.11, working at constant humidity, the temperature sensitivity of the sensor $LPG1$ can also be retrieved by differentiating the λ-Tcurves, which were found to be linear, obtained extrapolating the $\lambda_{res,5}$ values for each temperature from the fitting curves.

As a result, the temperature sensitivity values obtained at different humidity levels were found to slightly decrease with RH; however a mean S_T value of around 0.250 ± 0.015 nm/°C was evaluated in the full relative humidity range, as evidenced in Fig. 5.13.

It is worth noticing that also in case of LPG sensors, a temperature compensation scheme is required in order to reduce the cross sensitivity to unavoidable temperature modifications occurring in real applications, as discussed already in case of FBG-based relative humidity sensors. However, in the critical low humidity range, from 0 to 10 $\%RH$, assuming for the Long Period Grating-based sensor a mean value of S_{RH} of around 0.5 nm/%RH, a temperature change of 1 °C (or a similar error in the temperature reading) would induce an error in the relative humidity reading between 0.5 and 1 %RH if no compensation is applied.

This value is significantly better than the thermal cross talk observed in the case of polyimide coated Fiber Bragg Grating for which a typical error of 7 − 10 %RH is registered for a non-compensated temperature change of 1 °C.

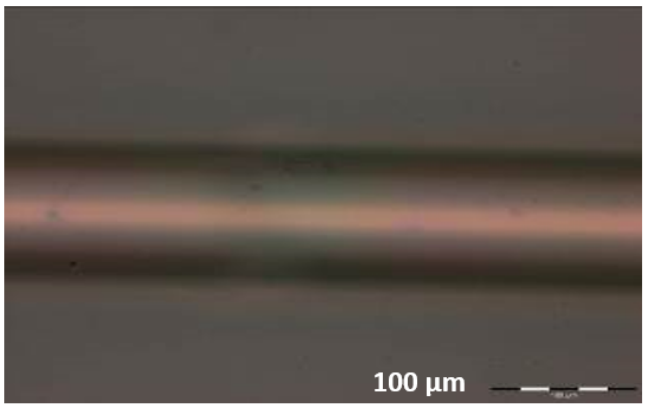

Figure 5.14: 20x optical microscope image of a SnO_2 multi-layered sample

5.5 SnO_2-COATED LPG-BASED SENSOR CHARACTERIZATION

For the SnO_2 solution preparation, tin (IV) tert-butoxide was used as tin oxide precursor and even in this case multiple depositions were performed in order to reach the desired layer thickness.

In Fig. 5.14 a 20x optical microscope image of 10 tin oxide layers deposited on an optical fiber are reported. Also in this case, as observed for the TiO_2 multi-layered sample, the reported images clearly reveal the smoothness and homogeneity of the deposited layer.

Several samples of relative humidity LPG-based sensors, obtained by depositing a different number of SnO_2 layers on the gratings for experimental tests in the laboratory.

Here we concentrate our attention on the sample named $LPG2$, characterized by a period of 410 µm and SnO_2 overlay thickness of around 300 nm, reached through the deposition of six SnO_2 layers onto the grating itself. [68]

The spectral response of the sample under investigation is reported in Fig. 5.15a. As illustrated in Fig. 5.15b, the bare device shows a resonance dip related to the 5^{th} cladding mode which is centered at 1581.5 nm, with a transmitted power of -11.9 dB. After the deposition of six layers of tin dioxide onto the grating, the dip moves to 1563.5 nm, with a power of -8.4 dB. This means that the deposition of the tin oxide layers caused a blue shift of the high wavelength dip of approximately 18 nm, as well as a decrease in its depth of around 3.5 dB.

The sample $LPG2$ has been tested at a constant temperature of 25 °C in the humidity range $0-50$ %RH .

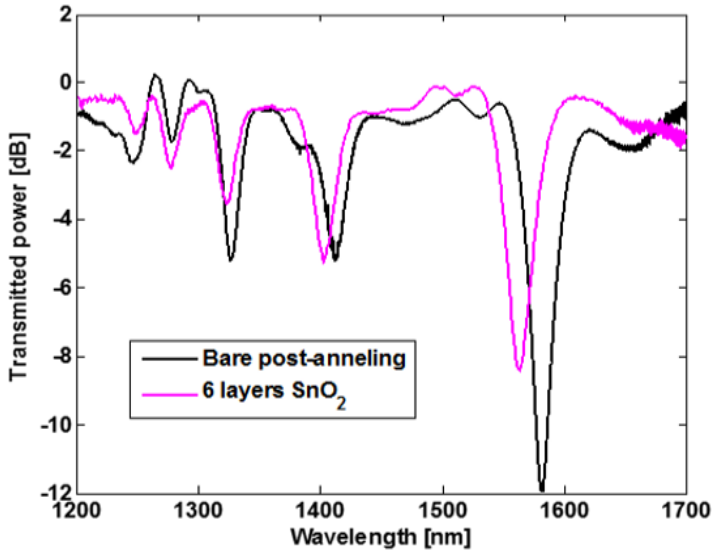

(a)

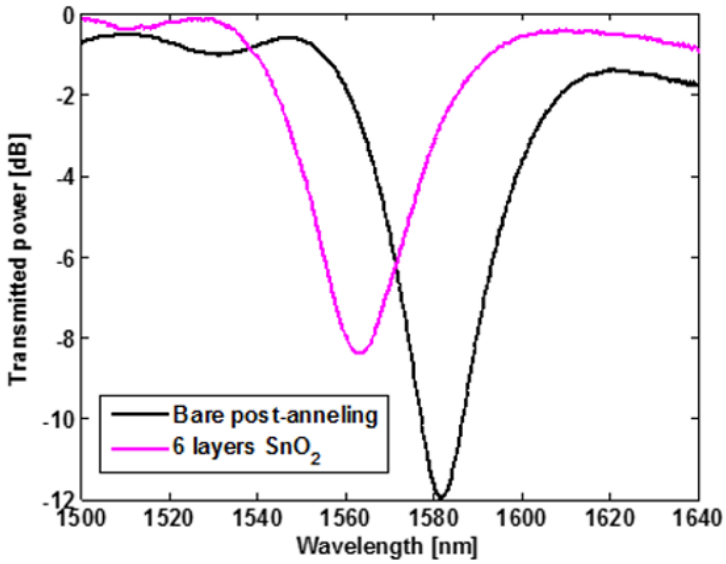

(b)

Figure 5.15: (a) Optical spectra of sample *LPG2*, before and after the SnO_2 overlay deposition; (b) zoom of the 5th cladding mode of the same sample

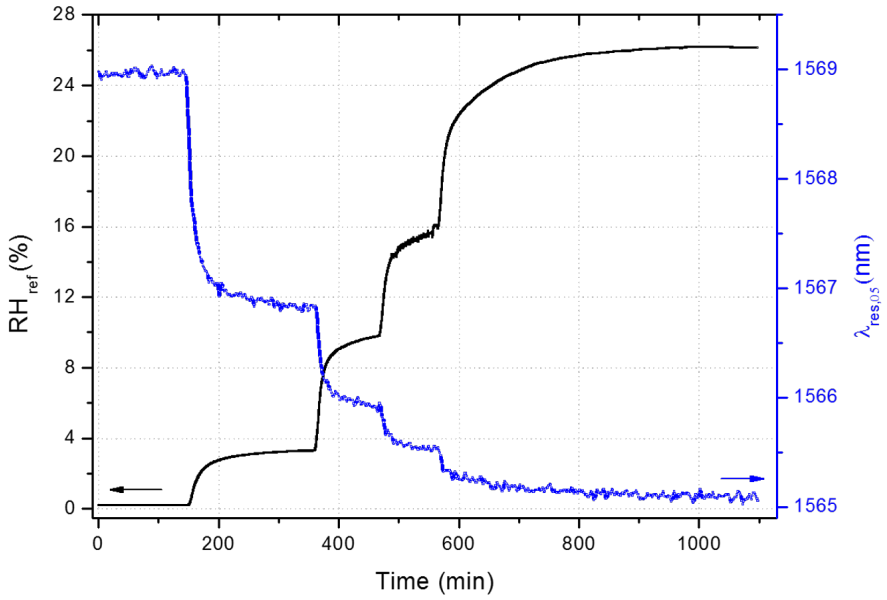

(a)

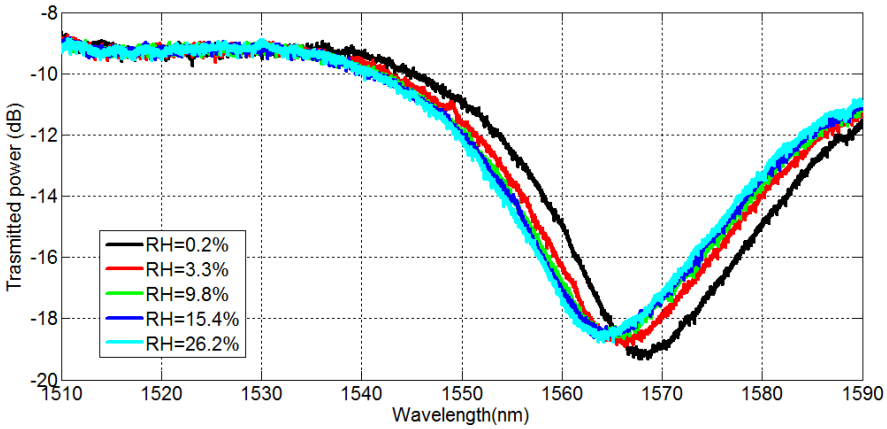

(b)

Figure 5.16: (a) Typical *LPG*2 response during a RH characterization test at 25 °C; (b) Transmittance spectra of *LPG*2 acquired at different RH values during the same test at 25 °C

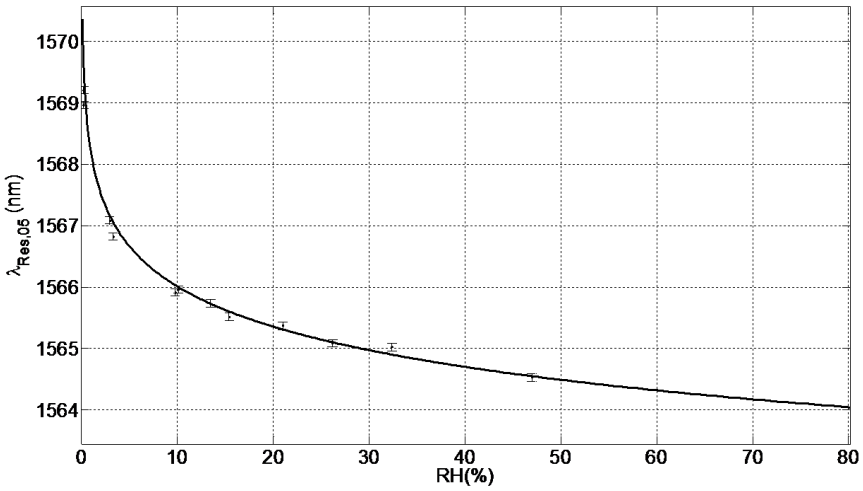

Figure 5.17: *LPG*2 calibration curve at 25 °C

In particular, in Fig. 5.16a the typical variation of the barycentric wavelength of the *LPG*2 resonance dip due to relative humidity changes in the chamber is plotted against time during a test at 25 °C in the range 0 −25 %RH. In the same figure, the readings of the reference device, installed in the same chamber, are available for comparison.

As evident, a blue shift of the $\lambda_{res,5}$ (blue curve) takes place by increasing the level of humidity in the chamber, described by the black curve, due to the SnO_2 coating refractive index increase promoted by the adsorption of moisture. This is also confirmed by the spectral variations registered during the same humidity test at constant temperature, reported in Fig. 5.16b.

Moreover, coherently with what observed for the titanium dioxide-coated LPG sample, the *LPG*2 response towards relative humidity variations was found to be non-linear, as also emphasized by the calibration curve applied to the data sets at 25 °C shown in Fig. 5.17.

Differentiating the fitting curve with respect to RH, the relative humidity sensitivity of the sample *LPG*2 shown in Fig. 5.18 in function of RH was calculated.

In particular, for the six layers SnO_2-coated Long Period Grating under investigation, a maximum sensitivity of around 0.6 nm/%RH at 0.5 %RH was measured while at higher humidity values the sensitivity was found to exponentially decrease against the humidity variations (for example at 50 %RH, the sensor showed a sensitivity of around 0.02 nm/%RH).

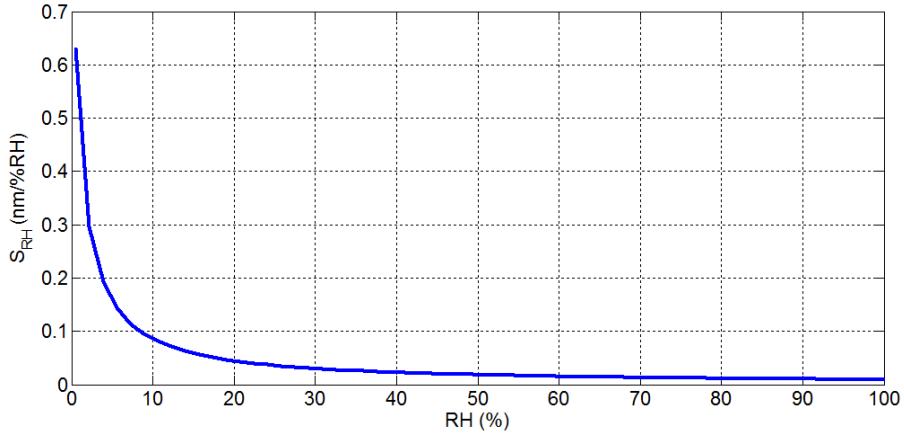

Figure 5.18: Relative humidity sensitivity curve of the *LPG*2 sample

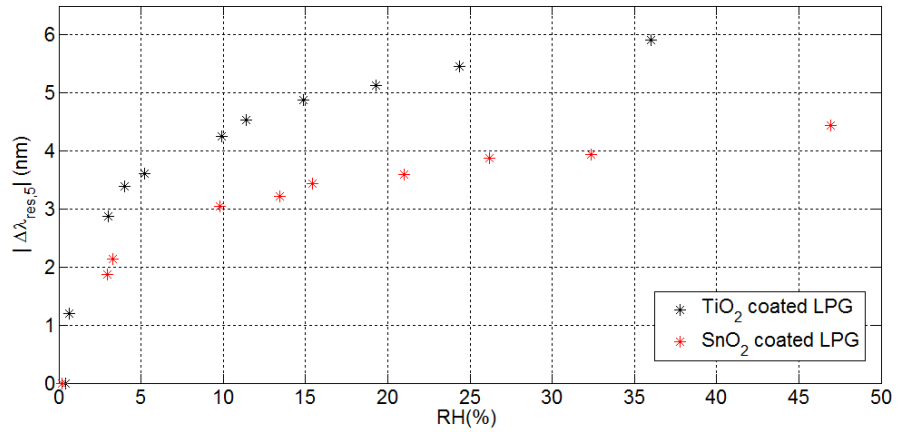

Figure 5.19: Comparison between the resonance wavelength shifts induced by incremental changes of the humidity level in the chamber at constant temperature in case of the the samples *LPG*1 (TiO_2-coated) and *LPG*2 (SnO_2-coated).

5.6 TiO_2 AND SnO_2-COATED LPGS IN COMPARISON

In order to identify which coating material among TiO_2 and SnO_2 is more suitable for the development of high performances relative humidity LPG-based sensors, it is interesting to compare the sensing performances of *LPG*1 and *LPG*2 at 25 °C, presented in sections 5.4 and 5.5, respectively. [68]

To appreciate the main differences in terms of performance between the two investigated samples, it is convenient to refer to Fig. 5.19, where the absolute value of $\Delta\lambda_{res,5}$ (defined as the difference between $\lambda_{res,5\ a\ 10\ kGy}$ and $\lambda_{res,5\ a\ 0\ kGy}$) points versus RH at ambient temperature are plotted.

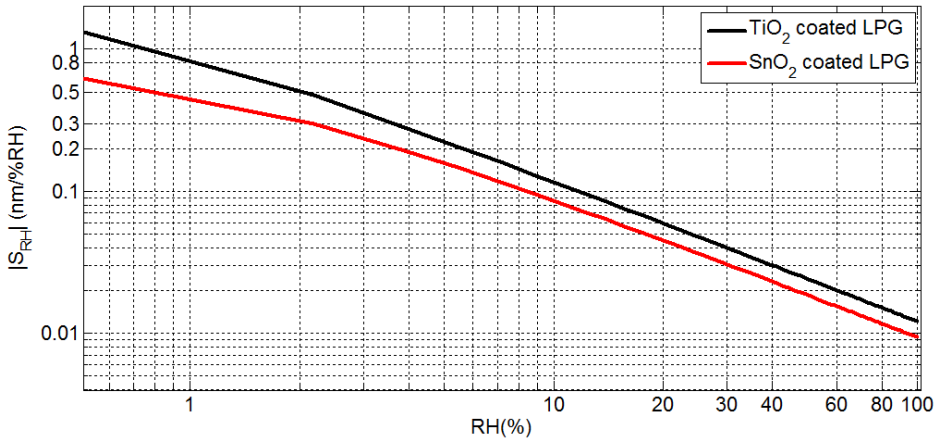

Figure 5.20: TiO_2 and SnO_2-coated LPGs' relative humidity sensitivity in comparison

It turned out that the SnO_2-coated sensor experiences lower resonance wavelength shifts upon the relative humidity level increase if compared to those presented by the TiO_2-coated sample.

Indeed, referring to Fig. 5.19, between 0 and 10 %RH, which is considered as the critical range for our application, the maximum resonance wavelength shifts of TiO_2-coated LPG (black points) resulted to be 4 nm while the one observed for the SnO_2-coated one (red points) was around 3 nm.

In terms of sensitivity to relative humidity variations, the tin dioxide-based hygrometer showed a mean S_{RH} value of around 0.2 nm/%RH against a value of 0.3 nm/%RH obtained with the titanium dioxide-based counterpart, as evidenced in Fig. 5.20.

This behavior is confirmed also at higher humidity values where a smaller sensitivity is obtained for the SnO_2-coated LPG, compared to that provided by the titania-based probe. For example at 40 %RH, the SnO_2-coated LPG-based sensor shows a sensitivity value of around 0.02 nm/%RH in comparison to the 0.03 nm/%RH shown by the TiO_2-coated device.

In addition, the sample $LPG1$ showed higher saturation thresholds with respect to the ones shown by$LPG2$.

For all these reasons, we finally decided to proceed our investigations on the development of TiO_2-coated LPG-based sensors.

5.7 RADIATION TOLERANCE CHARACTERISTIC OF NANO-SCALE COATED LPG-BASED SENSORS

Once completed the characterization of both the TiO_2 and SnO_2-coated LPGs and selected titanium dioxide as the best coating material to use to coat the grating, preliminary irradiation campaigns on the sample $LPG1$ have been conducted, in order to study the effect of radiations on the sensing performance of this device. [68, 94]

In particular the sample $LPG1$ was irradiated at a dose of 10 kGy of γ-ionizing radiation [5] and than re-characterized in the CERN laboratory after the radiation exposure using the same steps and methodologies described in the previous sections.

Preliminary results are shown in Fig. 5.21a, evidencing that a dip wavelength shift of about 4 nm in the range $20-25$ %RH occurs after the radiations exposure.

Even if further irradiation campaigns at progressively higher doses are currently in progress in order to confirm the reported results, it is important to point out that the observed shift is almost in agreement with radiation hardness investigations conducted on different types of bare Long Period Gratings, as found in [60].

In particular, the observed shift is of the same order of magnitude of the shift observed with bare chiral Long Period Gratings discussed in [60] and also very similar to that recorded after a dose of 6 kGy with low order modes (8th, 9th and 10th) in case of a bare turnaround point LPG written in a B/Ge doped fiber, as documented in [96].

In Fig. 5.21b the absolute value of $\lambda_{res,5}$ versus RH at 25 °C of the sample $LPG1$ before (black curve) and after (red curve) the irradiation campaign, is depicted.

Interestingly, the TiO_2-coated LPG sensor does not lose its excellent capability to respond to RH changes and, apart some variations, its characteristic curve after the 10 kGy exposure still exhibits the same behavior shown before irradiation.

The obtained results suggest the necessity of taking in account the γ-ionizing radiation effects on the response of the LPG-based sensor in order to fully exploit the extremely sensitivity of these devices in high radiations applications.

5 The irradiation process was performed in an external company using a Cobalt-60 source.

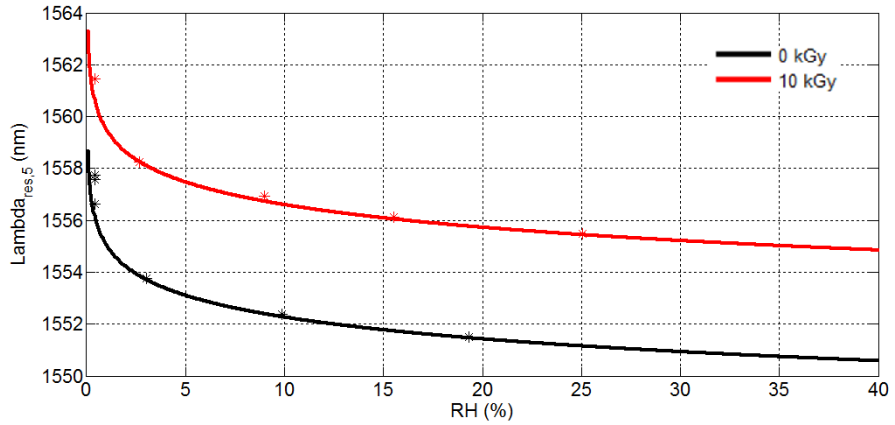

(a)

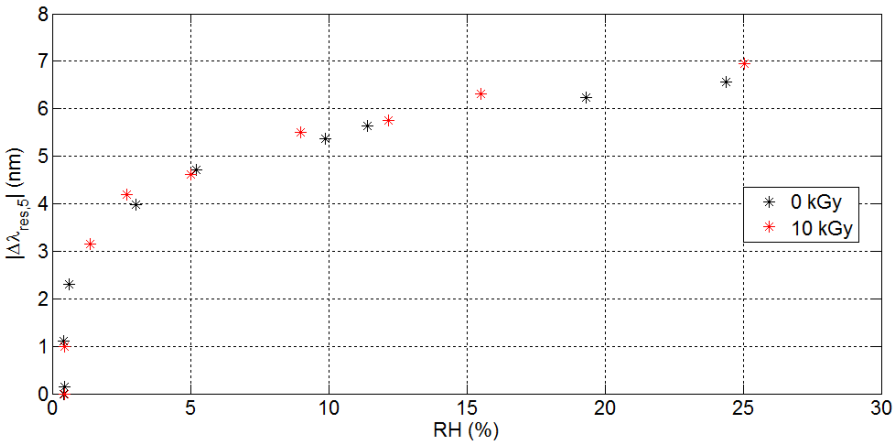

(b)

Figure 5.21: (a) $\lambda_{res,5}$ versus RH and (b) $|\Delta\lambda_{res,5}|$ (defined as the absolute value of the difference between $\lambda_{res,5\ a\ 10\ kGy}$ and $\lambda_{res,5\ a\ 0\ kGy}$) versus RH at 25 °C for the sample $LPG1$ before (black points) and after (red points) 10 kGy γ-ionizing radiation dose exposure

5.8 CONCLUSIONS

In this chapter we reported results concerning the development and the first experimental demonstration of high-sensitivity TiO_2-coated LPG sensors for humidity monitoring at temperatures below 0 °C as well as after high γ-ionizing radiation dose exposures.

The results obtained are very encouraging and demonstrate the capability of coated LPG sensors to provide very high RH sensitivity, up to 1.4 nm/%RH in correspondence to very low humidity values, which turned out to be one to three orders of magnitude higher than those exhibited by FBG sensors coated by micrometer-thin polyimide overlays.

In addition, from the first irradiation campaign performed at a γ-ionizing radiation dose of 10 kGy, we found that TiO_2-coated LPG sensors have a good resistance to radiations and that the sensing performances of these devices in terms of relative humidity sensitivity are not affected by radiations. As a matter of fact, as already observed for the polyimide coated FBG-based sensors, only a radiation-induced shift has been registered after the dose exposure. More investigations at higher doses have to be performed in order to understand the saturation properties of this shift.

Overall, the results collected demonstrate the strong potential of the proposed technology with regard to its future exploitation as a robust and valid alternative for high energy physics applications to both the commercial hygrometers and polyimide coated Fiber Bragg Gratings.

6 FINAL REMARKS AND CONCLUSIONS

In the context of this work, two technological solutions related to the problem of relative humidity monitoring in high-radiation environments were developed and studied.

The main results and perspectives can be summarized as follows.

FBG-based relative humidity sensors

The R&D project concerning the development and testing of relative humidity sensors based on fiber Bragg grating technology started at CERN in 2011 in collaboration with University of Sannio and the Institute for Polymers Composite and Biomaterials (CNR Naples).

Our investigations gave for the first time the experimental demonstration of the possibility to use them at low temperature, in the relative humidity range $0-75\,\%$RH. In particular we found that the response of polyimmide coated FBGs to relative humidity variations is linear, even after high radiations exposure, and that the sensitivity to relative humidity changes of these devices is not affected by radiations. Only a pre-irradiation step before the installation of these sensors in high radiation environments is suggested in order to guarantee negligible radiation-induced signal shifts.

Many efforts have been dedicated to the development of a mathematical model to translate the wavelength readings from the FBGs in temperature, relative humidity and dew point values.

From December 2013, a full network of 72 FBG-based thermo-hygro meters, each consisting of two FBGs, one coated with polyimide and one uncoated for temperature measurements, have been installed in the CMS experiment for the temperature and relative humidity monitoring of the air in cold areas in front of the tracker. Before the installation, the sensors have been pre-irradiated at 210 kGy.

Off-line remote monitoring of the FBG-based temperature and relative humidity sensors readout has been daily performed and the correct operation of the sensors in the cavern has been constantly verified.

After ten months of operation, results provided by the FBG-based thermo-hygrometers are very encouraging as the reconstructions from

fiber optic sensors are in agreement with the readings of temporary reference sensors installed in the cavern.

The results are even more interesting if we think that the installation of FBG-based thermo-hygrometers in the CMS experiment represents the very first application of this technology in real environment, outside the controlled laboratory conditions.

LPG-based relative humidity sensors

In 2013 our research group has launched a second R&D project at CERN concerning the development of a second generation of fiber optic sensors for humidity sensing application based on the LPG technology.

In particular, in-house fabricated prototypes of LPG humidity sensors, manufactured at University of Sannio in collaboration with the Institute for Polymers Composite and Biomaterials, using several thin hygrosensitive metal oxide coatings of different materials (such as SnO_2 and TiO_2) and thickness (between $100-200$ nm) have been tested in the facility available in the CERN lab.

A careful analysis of the behavior of all the fabricated samples has been conducted in the range $0-65$ %RH at different temperature values between -10 and $25\,^{\circ}$C, in order to understand the response of this innovative class of sensors in terms of relative humidity and temperature variations as well as to assess their stability, accuracy, and repeatability features.

We finally decided to focus our research on TiO_2-coated LPG sensors, which were found to operate with a higher sensitivity over a wide humidity range and with good hygroscopic characteristics.

Preliminary results evidenced the very high sensitivity of the fabricated devices, especially in the low relative humidity range (e.g. $0-10$ %RH), where it reaches values thousands of times higher than that achieved with the FBG technology.

A study on the effects of ionizing radiation on the sensing performance was also started and we found that the excellent sensing characteristics of these devices are not affected by the irradiation up to doses of 10 kGy . Exposures to progressively higher doses of radiations are currently in progress in order to define the applicability limits.

However the collected results indicate good perspectives for an effective exploitation of the LPG technology for humidity monitoring in high radiations experiments detectors at CERN.

Relative humidity FBG and LPG-based sensors in comparison

Our investigations filled the gaps in the state of the art of coated FBGs and LPGs relative humidity sensors literature demonstrating that both the two proposed technologies can correctly work at temperature below 0 °C and have good radiation tolerant characteristics.

We also point out that there are some aspects which have to be taken into account in order to understand which technology is more or less suitable for specific applications.

To this aim, in Fig. 6.1 the main features of polyimide-coated FBGs and metal oxide-coated LPG sensors for relative humidity monitoring in high radiation environments are schematically summarized. [68]

In particular, the choice of using LPGs instead of FBGs-based sensors can be advantageous in some cases, mostly linked to their high relative humidity sensitivity, especially at very low humidity values.

This is a very relevant feature of LPG technology which opens new scenarios for its possible future application for relative humidity monitoring in the new generation of particles detectors at CERN.

For example, the High Luminosity LHC project, which has formally been approved by the CERN Council in 2014, foresees, around 2020, a major upgrade of the accelerator in order to increase its luminosity by a factor of ten beyond the original design value (from 300 to 3000 fb^{-1}). [97] This means that the level of radiations due to the particles collisions in the experiments will become extremely high, and to mitigate the effect of radiations on the silicon tracker sensors, the temperature of operation of the detectors will be lowered.

In these conditions, a correct and reliable thermal and hygrometric control of the air in the experiments will be extremely important, and better accuracy of relative humidity sensors, mostly in the low humidity range, will be requested by the experiments.

For their enhanced sensitivity to relative humidity, even at low relative humidity values, oxide-coated LPG-based sensors seem to be very recommended in this kind of applications, compared to the FBGs.

On the other hand, LPGs suffer from limitations to the level of multiplexing, mainly due to limitations in terms of available bandwidth with respect to the FBGs. For this reason, in case of applications requesting dense multiplexing without any urgent requirement in terms of high relative humidity accuracy measurements, the use of FBG is generally suggested.

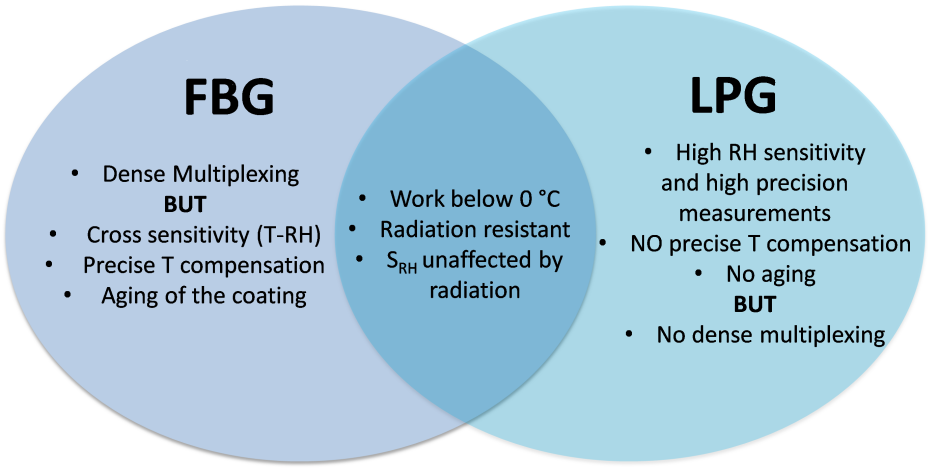

Figure 6.1: Main features of polyimide coated FBGs and thin oxide coated LPGs sensors proposed for relative humidity monitoring in high radiation environments

Potential applications of optical FBG and LPG-based relative humidity sensors outside high energy physics environments are primarily connected to fields confronted with the need of local distributed RH monitoring in hostile environments (in particular – but not limited to – due to the presence of radiation).

Some examples may be represented by nuclear reactors, food packaging and production plants, chemical plants and sterilization plants for medical applications.

However, other potential applications can be found in fields where highly distributed monitoring over very large volumes or surfaces can be significantly simplified by the natural attitude of optical fiber sensors to reliably transmit over very long distances multi-point information encoded on a single fiber.

In this sense, optical relative humidity sensors could help in different fields such as weather forecasting, controlled manufacturing processes, air quality monitoring and assessment.

The main "obstacle" in the spread of this novel technologies in the market, anyway, seems to be related to the external perception of optical fiber sensors as "exotic" products, difficult to use and extremely fragile. This is more a psychological effect, but it is the main factor which is still slowing down the expansion of fiber optic sensor based techniques on the commercial, together with the absence of a clear existing standard.

GLOSSARY

ALICE A Large Ion Collider Experiment

ATLAS A Toroidal LHC Apparatus

CERN European Organization for Nuclear Research

CMS Compact Muon Solenoid

CNR National Research Council

FBG Fiber Bragg Grating

FOS Fiber Optic Sensor

HL-LHC High Luminosity Large Hadron Collider

LHC Large Hadron Collider

LHCb Large Hadron Collider beauty

LHCf Large Hadron Collider forward

LPG Long Period Grating

LS1 First Long Shutdown

MoEDAL Monopole and Exotics Detector

RIA Radiation Induced Attenuation

SRI Surrounding Refractive Index

TOTEM TOTal Elastic and diffractive cross section Measurement

USC Underground Service Cavern

BIBLIOGRAPHY

[1] *CERN web page*. URL: http://goo.gl/LxcZj5.

[2] O. Brüning et al. "LHC design report". In: *Reports- CERN* (2004). URL: http://goo.gl/hd6X6h.

[3] *CMS web page*. URL: http://goo.gl/ZtPsYI.

[4] D. Lincoln. *The Large Hadron Collider: the extraordinary story of the Higgs Boson and other stuff that will blow your mind*. Johns Hopkins University Press, 2014.

[5] CMS collaboration and others. "The CMS experiment at the CERN LHC". In: *JINST 3 S08004* (2008), pp. 1748–0221. URL: http://goo.gl/BT5Poc.

[6] L. R. Evans. *The Large Hadron Collider: a marvel of technology*. EPFL Press, 2009.

[7] CMS collaboration and others. *The CMS Tracker*. Tech. rep. CMS NOTE 2007/000. CERN, Oct. 2, 2007.

[8] J. Daguin et al. "Evaporative CO 2 cooling system for the upgrade of the CMS pixel detector at CERN". In: *Thermal and Thermomechanical Phenomena in Electronic Systems (ITherm), 2012 13th IEEE Intersociety Conference on*. IEEE. 2012, pp. 723–731. URL: http://goo.gl/Q6cxiX.

[9] M. Schwerin et al. *The humidity sensors for the CMS Tracker*. Tech. rep. CMS NOTE 2005/000. CERN, Feb. 14, 2005. URL: http://goo.gl/AJm6lg.

[10] Z. Rittersma. "Recent achievements in miniaturised humidity sensors—a review of transduction techniques". In: *Sensors and Actuators A: Physical* 96.2 (2002), pp. 196–210. URL: http://goo.gl/gWgrYh.

[11] *HIH-3610 Series*. URL: http://goo.gl/h2Dj76.

[12] *HIH-4010/4020/4021 Series-Humidity Sensors*. URL: http://goo.gl/ay6g6K.

[13] URL: https://goo.gl/EvX0P0.

[14] E. M. Butz. *CMS Strip Detector: Operational Experience and Run1 to Run2 Transition*. Tech. rep. CMS-CR-2014-390. CERN, Nov. 2014. URL: https://goo.gl/56cdda.

[15] M. Fossa and P. Petagna. *Use and calibration of capacitive RH sensors for the hygrometric control of the CMS tracker*. Tech. rep. CMS NOTE 2003/024. Sept. 2003. URL: http://goo.gl/nAwFGe.

[16] M. Fossa and P. Petagna. *Temperature influence on humidity measurements for CMS tracker control*. Tech. rep. CMS IN 2006/03. Jan. 2006.

[17] *Data sheet Hs-2000V*. URL: http://goo.gl/yky7w9.

[18] M. Loeschner, A. Tsirou, and P. Verdini. *The Dewpoint sensors at the Tracker bulkheads*. Tech. rep. CMS IN -2012/009. Aug. 2012. URL: http://goo.gl/nAwFGe.

[19] *Vaisala DRYCAP Dewpoint Transmitter DMT242- USER'S GUIDE*. URL: http://goo.gl/GsZ6T3.

[20] M. Fossa and P. Petagna. *Humidity measurements inside ATLAS and CMS:notes on sensor calibration*. Tech. rep. Apr. 2004. URL: http://goo.gl/pG8hSd.

[21] *SHT2x Digital Humidity and Temperature Sensor*. URL: http://goo.gl/wEcg91.

[22] *BME280*. URL: http://goo.gl/NKaV84.

[23] U. Sharma and X. Wei. "Fiber Optic Interferometric Devices". In: *Fiber Optic Sensing and Imaging*. Springer, 2013, pp. 29–53.

[24] *Fiber Optic Sensors:Global Market*. June 2014. URL: http://goo.gl/oB7GBQ.

[25] G. Rajan. *Optical Fiber Sensors: Advanced Techniques and Applications*. Vol. 36. CRC Press, 2015.

[26] K. Grattan and T. Sun. "Fiber optic sensor technology: overview". In: *Sensors and Actuators A: Physical* 82.1 (2000), pp. 40–61. URL: http://goo.gl/MkeI3X.

[27] T. Yeo, T. Sun, and K. Grattan. "Fibre-optic sensor technologies for humidity and moisture measurement". In: *Sensors and Actuators A: Physical* 144.2 (2008), pp. 280–295. URL: http://goo.gl/vRvX6J.

[28] L. Alwis, T. Sun, and K. Grattan. "Optical fibre-based sensor technology for humidity and moisture measurement: Review of recent progress". In: *Measurement* 46.10 (2013), pp. 4052–4074. URL: http://goo.gl/zZpi7X.

[29] J. M. Corres, I. R. Matias, and F. J. Arregui. "Optical Fibre Humidity Sensors Using Nano-films". In: *Sensors*. Springer, 2008, pp. 153–177. URL: http://goo.gl/KAVHgf.

[30] S. A. Kolpakov et al. “Toward a New Generation of Photonic Humidity Sensors”. In: *Sensors* 14.3 (2014), pp. 3986–4013. URL: http://goo.gl/3rGVNv.

[31] F. Boltinghouse and K. Abel. “Development of an optical relative humidity sensor. Cobalt chloride optical absorbency sensor study”. In: *Analytical Chemistry* 61.17 (1989), pp. 1863–1866. URL: http://goo.gl/1NL8l3.

[32] M. Ando, T. Kobayashi, and M. Haruta. “Humidity-sensitive optical absorption of Co 3 O 4 film”. In: *Sensors and Actuators B: Chemical* 32.2 (1996), pp. 157–160. URL: http://goo.gl/JfTxU2.

[33] S. Otsuki, K. Adachi, and T. Taguchi. “A novel fiber-optic gas sensing arrangement based on an air gap design and an application to optical detection of humidity”. In: *Analytical sciences* 14 (1998), pp. 633–636. URL: https://goo.gl/EqupYw.

[34] J. M. Corres, F. J. Arregui, and I. R. Matías. “Sensitivity optimization of tapered optical fiber humidity sensors by means of tuning the thickness of nanostructured sensitive coatings”. In: *Sensors and Actuators B: Chemical* 122.2 (2007), pp. 442–449. URL: http://goo.gl/538uxh.

[35] F. Mitschke. “Fiber-optic sensor for humidity”. In: *Optics letters* 14.17 (1989), pp. 967–969. URL: https://goo.gl/MM7ZPF.

[36] M. Consales et al. “Fiber optic humidity sensors for high-energy physics applications at CERN”. In: *Sensors and Actuators B: Chemical* 159.1 (2011), pp. 66–74. URL: http://goo.gl/BCK3Xc.

[37] K. O. Hill and G. Meltz. “Fiber Bragg grating technology fundamentals and overview”. In: *Journal of lightwave technology* 15.8 (1997), pp. 1263–1276. URL: http://goo.gl/J6HWv7.

[38] Y.-J. Rao. “In-fibre Bragg grating sensors”. In: *Measurement science and technology* 8.4 (1997), p. 355. URL: http://goo.gl/l3Xjl1.

[39] A. D. Kersey et al. “Fiber grating sensors”. In: *Journal of lightwave technology* 15.8 (1997), pp. 1442–1463. URL: http://goo.gl/g2TXIm.

[40] A. Cusano, A. Cutolo, and J. Albert. *Fiber Bragg grating sensors: recent advancements, industrial applications and market exploitation*. Bentham Science Publishers, 2011.

[41] W. W. Morey, G. Meltz, and W. H. Glenn. "Fiber optic Bragg grating sensors". In: *OE/FIBERS'89*. International Society for Optics and Photonics. 1990, pp. 98–107. URL: http://goo.gl/szwbQg.

[42] J. W. Miller and A. Méndez. "Fiber Bragg Grating Sensors: Market Overview and New Perspectives". In: *Fiber Bragg Grating Sensors: Recent Advancements, Industrial Applications and Market Exploitation* (2011), p. 313. URL: http://goo.gl/hdO9hI.

[43] Z. Szillási et al. "One Year of FOS Measurements in CMS Experiment at CERN". In: *Physics Procedia* 37 (2012), pp. 79–84. URL: http://goo.gl/Uj22bc.

[44] A. Cusano et al. "Fiber optic sensors for CMS-CERN". In: *Fourth European Workshop on Optical Fibre Sensors*. International Society for Optics and Photonics. 2010, 76533G–76533G. URL: http://goo.gl/uuQxMG.

[45] S. Buontempo. *FOS in CMS detector at CERN*. Tech. rep. CERN-CMS-CR-2010-100, 2010. URL: http://goo.gl/R84DWN.

[46] P. Kronenberg et al. "Relative humidity sensor with optical fiber Bragg gratings". In: *Optics letters* 27.16 (2002), pp. 1385–1387. URL: https://goo.gl/fqQeiO.

[47] G. Berruti et al. "Radiation hard humidity sensors for high energy physics applications using polymide-coated Fiber Bragg Gratings sensors". In: *IEEE Sensors 2011 Conference Proceedings*. IEEE. 2011. URL: http://goo.gl/wMu5Tl.

[48] G. Berruti et al. "Radiation hard humidity sensors for high energy physics applications using polyimide-coated fiber Bragg gratings sensors". In: *Sensors and Actuators B: Chemical* 177 (2013), pp. 94–102. URL: http://goo.gl/C2KUcF.

[49] O. Frazão et al. "Applications of fiber optic grating technology to multi-parameter measurement". In: *Fiber and integrated optics* 24.3-4 (2005), pp. 227–244. URL: http://goo.gl/G8qkar.

[50] P. Giaccari, H. Limberger, and P. Kronenberg. "Influence of humidity and temperature on polyimide-coated fiber Bragg gratings". In: *Proceedings of Bragg Gratings, Photosensitivity, and Poling in Glass Fibers and Waveguides* (2001). URL: http://goo.gl/CGcZMP.

[51] T. Yeo et al. “Characterisation of a polymer-coated fibre Bragg grating sensor for relative humidity sensing”. In: *Sensors and Actuators B: Chemical* 110.1 (2005), pp. 148–156. URL: http://goo.gl/Exdxxk.

[52] T. L. Yeo et al. “Polymer-coated fiber Bragg grating for relative humidity sensing”. In: *Sensors Journal, IEEE* 5.5 (2005), pp. 1082–1089. URL: http://goo.gl/rNjmRr.

[53] T. Venugopalan et al. “Evaluation and calibration of FBG-based relative humidity sensor designed for structural health monitoring”. In: *20th International Conference on Optical Fibre Sensors*. International Society for Optics and Photonics. 2009, pp. 750310–750310. URL: http://goo.gl/591zdn.

[54] F. Ding et al. “Experimental study on humidity sensing using a FBG sensor with polyimide coating”. In: *Asia Communications and Photonics Conference and Exhibition*. International Society for Optics and Photonics. 2010, pp. 79900C–79900C. URL: http://goo.gl/60d4Fw.

[55] W. Kunzler, S. G. Calvert, and M. Laylor. “Measuring humidity and moisture with fiber optic sensors”. In: *Sixth Pacific Northwest Fiber Optic Sensor Workshop*. International Society for Optics and Photonics. 2003, pp. 86–93. URL: http://goo.gl/mHkPvH.

[56] T. Yeo et al. “Optical fiber sensors for monitoring ingress of moisture in structural concrete”. In: *Review of scientific instruments* 77.5 (2006), p. 055108. URL: http://goo.gl/qPYvF8.

[57] B. G. Risch et al. “Optical fibre and cable reliability for high radiation environments”. In: *Proceedings of the 61st IWCS/IICIT, Rhode Island, USA* (2012). URL: http://goo.gl/yjghgJ.

[58] M. Van Uffelen et al. “Long-term prediction of radiation induced losses in single mode optical fibers exposed to gamma rays using a pragmatic approach”. In: *Radiation Effects Data Workshop, 2000*. IEEE. 2000, pp. 80–84. URL: http://goo.gl/E3Y8J3.

[59] J. Troska et al. “Radiation effects in commercial off-the-shelf single-mode optical fibers”. In: *SPIE’s International Symposium on Optical Science, Engineering, and Instrumentation*. International Society for Optics and Photonics. 1998, pp. 112–119. URL: http://goo.gl/yJU1QX.

[60] A. Gusarov and S. K. Hoeffgen. "Radiation effects on fiber gratings". In: *IEEE Trans. Nucl. Sci* 60.3 (2013), pp. 2037–2053. URL: http://goo.gl/Kr90As.

[61] H. Henschel et al. "Influence of fiber composition and grating fabrication on the radiation sensitivity of fiber Bragg gratings". In: *Radiation and Its Effects on Components and Systems, 2007. RADECS 2007. 9th European Conference on*. IEEE. 2007, pp. 1–8. URL: http://goo.gl/5htdg7.

[62] *Dew Master CHiller Mirror Hygrometer*. URL: http://goo.gl/ZeCS4d.

[63] *HIH-4000 Series*. URL: http://goo.gl/q33xFt.

[64] *Optical Sensing Interrogator-sm125*. URL: http://goo.gl/AOjkWt.

[65] A. Makovec et al. "Radiation hard polyimide-coated FBG optical sensors for relative humidity monitoring in the CMS experiment at CERN". In: *Journal of Instrumentation* 9.03 (2014), p. C03040. URL: http://goo.gl/nLcy0Q.

[66] *Non-metallic Temperature Sensor os4300*. URL: http://goo.gl/DFJgS4.

[67] A. Gusarov et al. "High total dose radiation effects on temperature sensing fiber Bragg gratings". In: *Photonics Technology Letters, IEEE* 11.9 (1999), pp. 1159–1161. URL: http://goo.gl/i9FzOZ.

[68] G. Berruti et al. "A Comparative Study of Radiation-Tolerant Fiber Optic Sensors for Relative Humidity Monitoring in High-Radiation Environments at CERN". In: *Photonics Journal, IEEE* 6.6 (2014), pp. 1–15. URL: http://goo.gl/KOhWKy.

[69] A. Saccomanno et al. "Long-term temperature monitoring in CMS using fiber optic sensors". In: *Sensors Journal, IEEE* 12.12 (2012), pp. 3392–3398. URL: http://goo.gl/f3QRVB.

[70] M. C. Buncick and D. D. Denton. "Effects of aging on polyimide: a study of bulk and interface chemistry". In: *Journal of applied polymer science* 46.2 (1992), pp. 271–280. URL: http://goo.gl/T1MG9L.

[71] S. W. James, R. P. Tatam, et al. "Optical fibre long-period grating sensors: characteristics and application". In: *Measurement science and technology* 14.5 (2003), R49–R61. URL: http://goo.gl/iBPZDF.

[72] I. D. Villar et al. “Optimization of sensitivity in long period fiber gratings with overlay deposition”. In: *Optics Express* 13.1 (2005), pp. 56–69. URL: https://goo.gl/L26CpQ.

[73] A. Cusano et al. “Mode transition in high refractive index coated long period gratings”. In: *Optics Express* 14.1 (2006), pp. 19–34. URL: https://goo.gl/h9bkpR.

[74] T. Venugopalan et al. “LPG-based PVA coated sensor for relative humidity measurement”. In: *Sensors Journal, IEEE* 8.7 (2008), pp. 1093–1098. URL: http://goo.gl/Udp36r.

[75] S. Luo et al. “Applications of LPG fiber optical sensors for relative humidity and chemical-warfare-agents monitoring”. In: *Photonics Asia 2002*. International Society for Optics and Photonics. 2002, pp. 193–204. URL: http://goo.gl/1r7y03.

[76] K. M. Tan et al. “High relative humidity measurements using gelatin coated long-period grating sensors”. In: *Sensors and Actuators B: Chemical* 110.2 (2005), pp. 335–341. URL: http://goo.gl/8NPSiF.

[77] M. Konstantaki et al. “Optical fiber long-period grating humidity sensor with poly (ethylene oxide)/cobalt chloride coating”. In: *Applied optics* 45.19 (2006), pp. 4567–4571. URL: http://goo.gl/IhC7Zt.

[78] T. Venugopalan, T. Sun, and K. Grattan. “Long period grating-based humidity sensor for potential structural health monitoring”. In: *Sensors and Actuators A: Physical* 148.1 (2008), pp. 57–62. URL: http://goo.gl/tHPDIJ.

[79] Y. Liu et al. “Long-period grating relative humidity sensor with hydrogel coating”. In: *Photonics Technology Letters, IEEE* 19.12 (2007), pp. 880–882. URL: http://goo.gl/w9u8AG.

[80] D. Viegas et al. “Simultaneous measurement of humidity and temperature based on an SiO-nanospheres film deposited on a long-period grating in-line with a fiber Bragg grating”. In: *Sensors Journal, IEEE* 11.1 (2011), pp. 162–166. URL: http://goo.gl/XWBsNi.

[81] S. Kher et al. “Measurement of-Radiation Induced Refractive Index Changes in B/Ge Doped Fiber Using LPGs”. In: *Photonics Technology Letters, IEEE* 25.21 (2013), pp. 2070–2073. URL: http://goo.gl/03iUAb.

[82] G. Montesperelli et al. “Sol-gel processed TiO 2-based thin films as innovative humidity sensors”. In: *Sensors and Actuators B: Chemical* 25.1 (1995), pp. 705–709. URL: http://goo.gl/ska3Y5.

[83] K. Von Rottkay and M. Rubin. “Optical indices of pyrolytic tin-oxide glass”. In: *MRS Proceedings*. Vol. 426. Cambridge Univ Press. 1996, p. 449. URL: http://goo.gl/tHHdj6.

[84] H. Igwe, O. Ekpe, and E. Ugwu. “Effects of thermal annealing on the optical properties of titanium oxide thin films prepared by chemical bath deposition technique”. In: *Research Journal of Applied Sciences, Engineering and Technology* 2.5 (2010), pp. 447–451. URL: http://goo.gl/uj2Gaj.

[85] J. Manifacier et al. “Optical and electrical properties of SnO 2 thin films in relation to their stoichiometric deviation and their crystalline structure”. In: *Thin Solid Films* 41.2 (1977), pp. 127–135. URL: http://goo.gl/Ny99ty.

[86] A. Buosciolo et al. “Fiber-Optic Near-Field Chemical Sensors Based on Wavelength Scale Tin Dioxide Particle Layers”. In: *Journal of Lightwave Technology* 26.20 (2008), pp. 3468–3475. URL: http://goo.gl/kAb91N.

[87] C. Cobianu et al. “Tin dioxide sol-gel derived thin films deposited on porous silicon”. In: *Sensors and Actuators B: Chemical* 43.1 (1997), pp. 114–120. URL: http://goo.gl/e03JLE.

[88] R. Rella et al. “Tin oxide-based gas sensors prepared by the sol-gel process”. In: *Sensors and Actuators B: Chemical* 44.1 (1997), pp. 462–467. URL: http://goo.gl/bTTzfR.

[89] Y. U. Ahn et al. “Variation of structural and optical properties of sol-gel TiO2 thin films with catalyst concentration and calcination temperature”. In: *Materials Letters* 57.30 (2003), pp. 4660–4666. URL: http://goo.gl/W7lMlK.

[90] v. A. Mol. “Chemical vapour deposition of tin oxide thin films”. PhD thesis. Technische Universiteit Eindhoven, 2003. URL: http://goo.gl/LIqFVZ.

[91] S. A. O’Neill et al. “Atmospheric pressure chemical vapour deposition of titanium dioxide coatings on glass”. In: *Journal of Materials Chemistry* 13.1 (2003), pp. 56–60. URL: http://goo.gl/XuRd5x.

[92] A. Chowdhuri et al. "H2S gas sensing mechanism of SnO2 films with ultrathin CuO dotted islands". In: *Journal of applied physics* 92.4 (2002), pp. 2172–2180. URL: http://goo.gl/PLhcWb.

[93] J. M. Bennett et al. "Comparison of the properties of titanium dioxide films prepared by various techniques". In: *Applied optics* 28.16 (1989), pp. 3303–3317. URL: https://goo.gl/cBoCgq.

[94] M. Consales et al. "Nanoscale TiO 2-coated LPGs as radiation-tolerant humidity sensors for high-energy physics applications". In: *Optics letters* 39.14 (2014), pp. 4128–4131. URL: https://goo.gl/N2dncl.

[95] I. D. Villar et al. "Nanodeposition of materials with complex refractive index in long-period fiber gratings". In: *Journal of lightwave technology* 23.12 (2005), p. 4192. URL: http://goo.gl/Ckp3Xb.

[96] S. Kher et al. "Turnaround-point long-period fiber gratings (TAP-LPGs) as high-radiation-dose sensors". In: *Photonics Technology Letters, IEEE* 24.9 (2012), pp. 742–744. URL: http://goo.gl/WYZVzA.

[97] *High Luminosity upgrade for the LHC*. URL: http://goo.gl/LvDvmt.

LIST OF PUBLICATIONS

CONFERENCES AND WORKSHOPS

• *"MULTIFUNCTIONAL FIBER OPTIC SENSORS FOR HIGH ENERGY PHYSICS EXPERIMENTS AT CERN"*

(INVITED PRESENTATION)

FRONTIERS IN OPTICS- OSA'S 97TH ANNUAL MEETING, SESSION FIO5: OPTICAL FIBER SENSING

ORLANDO - FLORIDA, 6-10 OCTOBER 2013.

• *"RADIATION TOLERANT HIGH SENSITIVITY TiO_2-COATED LONG PERIOD GRATING SENSORS FOR HUMIDITY MONITORING IN HIGH-ENERGY PHYSICS APPLICATIONS"*

(ORAL PRESENTATION)

SPIE PHOTONICS EUROPE, SESSION 8: OPTICAL FIBER-BASED SENSORS III

BRUSSELS- BELGIUM, 14-17 APRIL 2014.

• *"RADIATION TOLERANT FIBER OPTIC SENSORS FOR RELATIVE HUMIDITY DETECTION IN THE CMS EXPERIMENT AT CERN"*

(ORAL PRESENTATION)

THIRD MEDITERRANEAN PHOTONICS CONFERENCE, 1ST SESSION: PHOTONIC SENSORS

TRANI- ITALY, 7-9 MAY 2014.

• *"RADIATION TOLERANT HUMIDITY SENSORS BASED ON NANO-SCALE TIO2-COATED LPGS FOR HIGH-ENERGY PHYSICS APPLICATIONS"*

(ORAL PRESENTATION)

THIRD MEDITERRANEAN PHOTONICS CONFERENCE, 1ST SESSION: PHOTONIC SENSORS

TRANI- ITALY, 7-9 MAY 2014.

• *"RADIATION TOLERANT FIBER OPTIC SENSORS FOR RELATIVE HUMIDITY DETECTION IN HIGH ENERGY PHYSICS APPLICATIONS"*

(ORAL PRESENTATION)

FOTONICA 2014 AEIT, SESSIONE C1: PHYSICAL AND CHEMICAL SENSORS

NAPOLI- ITALY, 12-14 MAY 2014.

• *"Radiation tolerant Fiber Optic Thermo-Hygrometers for Aerospace Applications"*

(ORAL PRESENTATION)

IEEE International Workshop on Metrology for Aerospace, Session SS10: Photonic Sensors for Aerospace

Benevento- Italy, 29- 30 May 2014

• *"Radiation tolerant Fiber Optic Thermo-Hygrometers for Relative Humidity Detection in the CMS Experiment at CERN"*

(POSTER)

23rd International Conference on Optical Fiber Sensors

Santander-Cantabria-Spain, 2-6 June 2014.

• "High-sensitivity humidity sensors based on TiO2-coated long period fiber grating for high-energy physics application"

(ORAL PRESENTATION)

23rd International Conference on Optical Fiber Sensors

Santander-Cantabria-Spain, 2-6 June 2014.

• "Radiation tolerant Fiber Optic Humidity Sensors for High-Energy Physics Applications"

(ORAL PRESENTATION)

7th European Workshop on Structural Monitoring, Session WECT1: Fiber Optics II

La Cite', Nantes, France, 8-11 July 2014

• "Radiation tolerant Fiber Optic Sensors for Relative Humidity monitoring for experiments running at CERN"

(POSTER)

Gruppo Elettronica 2014

Cagliari, Italia, 16-20 June 2014

• "Radiation tolerant fiber optic sensors for long term humidity monitoring in the CMS experiment"

(ORAL PRESENTATION)

Forum on Tracking Detector Mechanics 2015

Nikhef, Amsterdam, Netherlands, 15-17 June 2015

JOURNALS

• *"RADIATION HARD HUMIDITY SENSORS FOR HIGH ENERGY PHYSICS APPLICATIONS USING POLYIMIDE-COATED FIBER BRAGG GRATINGS SENSORS"*

G. BERRUTI, M. CONSALES, M. GIORDANO, L. SANSONE, P. PETAGNA, S. BUONTEMPO, G. BREGLIO, A. CUSANO

IN **SENSORS AND ACTUATORS B**: CHEMICAL, VOLUME 177, PAGES 94-102, ISSN 0925-4005, (2013)

• *"RADIATION HARD POLYIMIDE-COATED FBG OPTICAL SENSORS FOR RELATIVE HUMIDITY MONITORING IN THE CMS EXPERIMENT AT CERN"*

A. MAKOVEC, G. BERRUTI, M. CONSALES, M. GIORDANO, P. PETAGNA, S. BUONTEMPO, G. BREGLIO, Z. SZILLASI, N. BENI, A. CUSANO

IN **JOURNAL OF INSTRUMENTATIONS**, 9, C03040 (2014).

• *"NANOSCALE TIO_2-COATED LPGS AS RADIATION-TOLERANT HUMIDITY SENSORS FOR HIGH-ENERGY PHYSICS APPLICATIONS"*

M. CONSALES, G. BERRUTI, A. BORRIELLO, M. GIORDANO, S. BUONTEMPO, G. BREGLIO, A. MAKOVEC, P. PETAGNA AND A. CUSANO

IN **OPTICS LETTERS**, 39, 14 (2014)

• *"A COMPARATIVE STUDY OF RADIATION TOLERANT FIBER OPTIC SENSORS FOR RELATIVE HUMIDITY MONITORING IN HIGH RADIATION ENVIRONMENTS AT CERN"*

G. BERRUTI, M. CONSALES, A. BORRIELLO, M. GIORDANO, S. BUONTEMPO, A. MAKOVEC, G. BREGLIO, P. PETAGNA, AND A. CUSANO

IN **IEEE PHOTONICS JOURNAL**, 6(6), 1-15, (2014).

• *"ONE YEAR OF FBG-BASED THERMO-HYGROMETERS IN OPERATION IN THE CMS EXPERIMENT AT CERN"*

G. BERRUTI, P. PETAGNA, S. BUONTEMPO, A. MAKOVEC, Z. SZILLASI, N. BENI, M. CONSALES AND A. CUSANO

IN **JOURNAL OF INSTRUMENTATION**, UNDER REVIEW